JOURNAL OF THE AERONAUTICAL SCIENCES

VOLUME 16 SEPTEMBER, 1949 NUMBER 9

Interaction Between Parallel Streams of Subsonic and Supersonic Velocities*

H. S. TSIEN† AND M. FINSTON‡

Massachusetts Institute of Technology

SUMMARY

An essential feature of the interaction phenomena between the compression shock and the boundary layer is the coexistence of parallel streams of subsonic and supersonic velocities. The compression disturbance of the shock is propagated "ahead" of the shock through the subsonic portion of the boundary layer, and "softening" of the shock takes place. It is the purpose of the present paper to demonstrate definitely this essential feature of boundary layer-shock interaction by using a simplified model. The boundary layer is replaced by a uniform subsonic stream of finite width, bounded on one side by the solid wall and on the other side by the interface with the uniform supersonic stream of infinite extent. The flow fields of two cases are analyzed in detail: (a) a compression wave in the supersonic stream incident upon the subsonic layer, and (b) outgoing compression waves generated by a sudden change in the slope of the solid wall. Both types of disturbances are assumed to be small, so that linearization of the differential equations is possible. A general result is that the distance of upstream propagation is directly proportional to the width of the subsonic layer. Therefore, when the boundary layer is turbulent and the subsonic layer is extremely thin, there is negligible softening of the shock.

INTRODUCTION

THE PHENOMENON OF INTERACTION between the shock and the boundary layer in supersonic flow over a solid surface, as first explicitly demonstrated by Ackeret, Feldmann, and Rott,[1] and then by Liepmann,[2] has aroused great interest among the investigators of fluid mechanics. However, because of the great complexity of the phenomenon that involves both viscous heat-conducting effects and the effects of compressibility, it has not been possible to give a complete account based upon the first principles. The above-cited authors themselves have tried to elucidate some features of their experimental observations. A more conscientious effort on the qualitative relations in the interaction of shock and boundary layer is that of Lees.[3] Lagerstrom[4] introduced the effects of viscosity and heat-conduction into the discussion of general compressible flow outside of the boundary layer. However, in order to make the mathematics involved tractable, he limits himself to the consideration of small disturbances and is thus able to linearize the differential equations. Under this assumption, the velocity at every point of the flow field has to be extremely close to the free-stream velocity—i.e., the flow is completely supersonic. On the other hand, it is the general belief of the investigators of the interaction phenomenon that one of the essential features is the coexistence of subsonic velocities in the boundary layer with the supersonic velocities in the main stream. This important fact is most clearly demonstrated by Howarth in a recent paper.[5] Howarth considers the problem of effects of a disturbance generated in a uniform supersonic stream that is bounded on one side by an interface with a uniform subsonic stream. Both regions are thus of semi-infinite extent. By assuming small disturbances and a perfect compressible fluid, he shows that the disturbances are propagated upstream through the subsonic region and that there is a region of expansion immediately behind the point of incidence of a compression wave in the interface.

Howarth's results are in general agreement with experimental observations on the shock and boundary-layer interaction. Thus the concept that at least one of the essential features of this phenomenon is the coexistence of subsonic flow with supersonic flow is proved quantitatively. The purpose of the present paper is to continue this line of attack and to improve Howarth's model for the real flow. The boundary layer is simulated by a uniform subsonic stream of finite width bounded on one side by a solid wall and on the

Presented at the Fluid Mechanics Session, Seventeenth Annual Meeting, I.A.S., New York, January 24–27, 1949.

* This paper is based on work supported in part by the Bureau of Ordnance, U.S. Navy.

† Professor of Aerodynamics.

‡ Staff Member, Supersonic Laboratory.

other side by the interface with a uniform supersonic stream of semi-infinite extent. The fluid is assumed to be nonviscous and nonheat-conducting and the disturbances are assumed to be small. Two cases will be considered. First, the case of an incident compression wave from the supersonic stream on the interface will be studied. Second, the wall is assumed to have a break with a small constant slope after the break. For both cases, the pressure distribution at the interface and at the wall will be calculated. The results can then be used to interpret the experiments on the interaction of shock and the boundary layer.

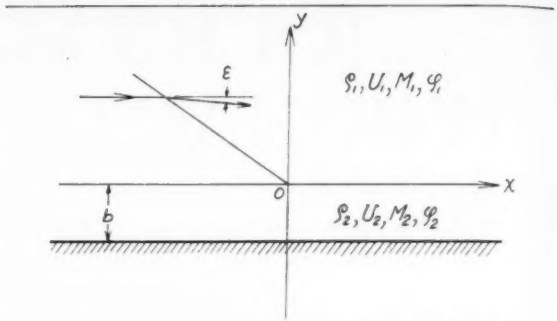

FIG. 1. Compression wave with deflection angle ϵ incident upon the interface of parallel subsonic and supersonic streams.

INCIDENT WAVE

Let the x-axis be parallel to the undisturbed flows and coincide with the undisturbed interface (Fig. 1). For $y > 0$, the flow is supersonic, and quantities there will be denoted by the subscript 1. Let the line $y = -b$ represent the solid wall. For $-b < y < 0$, the flow is subsonic, and quantities there will be denoted by the subscript 2. Furthermore, the pressure, the density, and the Mach Number will be denoted by p, ρ, and M, respectively. Then $M_1 > 1$ and $M_2 < 1$. The linearized differential equation for the disturbance velocity potential φ_1 in the supersonic stream is

$$(M_1^2 - 1)(\partial^2\varphi_1/\partial x^2) - (\partial^2\varphi_1/\partial y^2) = 0 \qquad (1)$$

The general solution of this equation can be written as

$$\varphi_1 = f(x + \sqrt{M_1^2 - 1}\, y) + g(x - \sqrt{M_1^2 - 1}\, y) \qquad (2)$$

where f and g are arbitrary functions. If the undisturbed flow is in the positive x-direction, then waves represented by the first term on the right of Eq. (2) are the incoming waves. The second term represents the outgoing waves originating from the interface.

To fix ideas, the form of the function f will now be specialized. Let

$$\left.\begin{aligned} f(x + \sqrt{M^2 - 1}\, y) &= U_1 \epsilon \frac{1}{\beta\sqrt{M_1^2 - 1}} \\ & e^{-\beta(x + \sqrt{M_1^2 - 1}\, y)}, \quad \text{for } x + \sqrt{M_1^2 - 1}\, y > 0 \\ f(x + \sqrt{M_1^2 - 1}\, y) &= 0, \text{ for } x + \\ & \sqrt{M_1^2 - 1}\, y < 0 \end{aligned}\right\} \qquad (3)$$

where U_1 is the undisturbed velocity in the supersonic stream, and ϵ, β are constants. The reason for choosing this form for f will be clear presently. By differentiating the potential φ_1 with respect to x and y, one obtains the x and y components u_1 and v_1 of the disturbance velocity in the supersonic stream. Therefore, the disturbance velocities of the incoming waves in the x and y directions are

$$-U_1 \epsilon(1/\sqrt{M_1^2 - 1})\, e^{-\beta(x + \sqrt{M_1^2 - 1}\, y)}$$

and

$$-U_1 \epsilon\, e^{-\beta(x + \sqrt{M_1^2 - 1}\, y)}, \quad \text{for } x + \sqrt{M_1^2 - 1}\, y > 0$$

For $x + \sqrt{M_1^2 - 1}\, y < 0$ there is no disturbance. By making $\beta \to 0$, the incoming waves then degenerate into a single compression wave with a deflection angle equal to ϵ, and the origin of the x, y plane is the point of incidence of this compression wave with the interface of supersonic and subsonic streams.

For convenience of calculation, the discontinuous form of the disturbance velocities due to incoming waves can be written in the equivalent Fourier-integral form. This is possible by noting that

$$\left.\begin{aligned} e^{-\beta z}, & \; z > 0 \\ 0, & \; z < 0 \end{aligned}\right\} = \frac{1}{\pi}\int_0^\infty \left\{\frac{\beta}{\beta^2 + \lambda^2}\cos \lambda z + \frac{\lambda}{\beta^2 + \lambda^2}\sin \lambda z\right\} d\lambda \qquad (4)$$

Then the potential of the outgoing wave should be also written in the form of a Fourier-integral. Thus,

$$g(x - \sqrt{M_1^2 - 1}\, y) = U_1 \int_0^\infty \left\{A_1(\lambda)\, \sin\, \lambda(x - \sqrt{M_1^2 - 1}\, y) + B_1(\lambda)\cos \lambda(x - \sqrt{M_1^2 - 1}\, y)\right\} d\lambda \qquad (5)$$

where $A_1(\lambda)$ and $B_1(\lambda)$ are the undetermined Fourier coefficients. As will be shown, the quantities of particular interest are the disturbance velocities at the interface. These can be obtained from Eqs. (3) and (5) with the aid of Eq. (4). Thus,

$$u_{1\,y=+0} = U_1\Big[-\frac{\epsilon}{\pi\sqrt{M_1^2-1}}\int_0^\infty\Big\{\frac{\beta}{\beta^2+\lambda^2}\cos\lambda x+\frac{\lambda}{\beta^2+\lambda^2}\sin\lambda x\Big\}d\lambda+$$
$$\int_0^\infty\{\lambda A_1(\lambda)\cos\lambda x-\lambda B_1(\lambda)\sin\lambda x\}d\lambda\Big] \quad (6)$$

$$v_{1\,y=+0} = U_1\Big[-\frac{\epsilon}{\pi}\int_0^\infty\Big\{\frac{\beta}{\beta^2+\lambda^2}\cos\lambda x+\frac{\lambda}{\beta^2+\lambda^2}\sin\lambda x\Big\}d\lambda-$$
$$\sqrt{M_1^2-1}\int_0^\infty\{\lambda A_1(\lambda)\cos\lambda x-\lambda B_1(\lambda)\sin\lambda x\}d\lambda\Big] \quad (7)$$

The linearized differential equation for the disturbance velocity potential φ_2 in the subsonic stream is

$$(1-M_2^2)(\partial^2\varphi_2/\partial x^2)+(\partial^2\varphi_2/\partial y^2)=0 \quad (8)$$

The appropriate form of solution for the case concerned is

$$\varphi_2 = U_2\int_0^\infty\cosh\lambda\sqrt{1-M_2^2}(y+b)\{A_2(\lambda)\sin\lambda x+B_2(\lambda)\cos\lambda x\}d\lambda \quad (9)$$

where $A_2(\lambda)$ and $B_2(\lambda)$ are again the undetermined Fourier coefficients. That this form of φ_2 satisfies the differential equation can be easily verified. The boundary condition on the wall is

$$v_{2\,y=-b}=0 \quad (10)$$

This condition is satisfied also by φ_2 specified by Eq. (9). At the interface, $y=0$, the disturbance velocities of the subsonic side are thus

$$u_{2\,y=-0} = U_2\int_0^\infty\cosh\lambda\sqrt{1-M_2^2}b\{\lambda A_2(\lambda)\cos\lambda x-\lambda B_2(\lambda)\sin\lambda x\}d\lambda \quad (11)$$

and

$$v_{2\,y=-0} = U_2\sqrt{1-M_2^2}\int_0^\infty\sinh\lambda\sqrt{1-M_2^2}b\{\lambda A_2(\lambda)\sin\lambda x+\lambda B_2(\lambda)\cos\lambda x\}d\lambda \quad (12)$$

In the solutions for supersonic stream and subsonic stream, there are four unknowns A_1, A_2, B_1, and B_2. These have to be determined by the conditions at the interface. Since the disturbances are assumed to be small, the values of quantities at the interface can be always taken at $y=0$, the undisturbed interface. The physical conditions to be satisfied at the interface are equal static pressure and equal inclination of the flow. Since under undisturbed conditions the static pressures in the supersonic stream must be equal to the static pressure in the subsonic stream, only the change in static pressure due to the disturbance velocities needs to be considered. The change in static pressure is equal to $-\rho Uu$ under the assumption of small disturbances; thus

$$-\rho_1U_1u_{1\,y=+0} = -\rho_2U_2u_{2\,y=-0} \quad (13)$$

The condition for equal flow inclination at the interface is, similarly,

$$v_{1\,y=+0}/U_1 = v_{2\,y=-0}/U_2 \quad (14)$$

Eqs. (13) and (14) are then the required conditions at the interface.

By substituting Eqs. (6), (7), (11), and (12) into Eqs. (13) and (14), one can then equate the corresponding Fourier coefficients on the two sides of these boundary equations. With some reductions, the resulting equations from Eq. (13) are

$$A_1(\lambda)-\frac{M_2^2}{M_1^2}\cosh(\lambda b\sqrt{1-M_2^2})A_2(\lambda) = \frac{\epsilon}{\pi\sqrt{M_1^2-1}}\Big[\frac{\beta}{\lambda(\beta^2+\lambda^2)}\Big] \quad (15)$$

$$B_1(\lambda)-\frac{M_2^2}{M_1^2}\cosh(\lambda b\sqrt{1-M_2^2})B_2(\lambda) = -\frac{\epsilon}{\pi\sqrt{M_1^2-1}}\Big[\frac{1}{\beta^2+\lambda^2}\Big] \quad (16)$$

Similarly, from Eq. (14) one has

$$A_1(\lambda)+\frac{\sqrt{1-M_2^2}}{\sqrt{M_1^2-1}}\sinh(\lambda b\sqrt{1-M_2^2})B_2(\lambda) = -\frac{\epsilon}{\pi\sqrt{M_1^2-1}}\Big[\frac{\beta}{\lambda(\beta^2+\lambda^2)}\Big] \quad (17)$$

$$B_1(\lambda)-\frac{\sqrt{1-M_2^2}}{\sqrt{M_1^2-1}}\sinh(\lambda b\sqrt{1-M_2^2})A_2(\lambda) = \frac{\epsilon}{\pi\sqrt{M_1^2-1}}\Big(\frac{1}{\beta^2+\lambda^2}\Big) \quad (18)$$

Eqs. (15) to (18) are the four equations for the four unknowns A_1, A_2, B_1, and B_2. Solution of these equations then determines the four quantities. For instance,

$$\left[\left(\frac{M_2^2}{M_1^2}\right)^2 \cosh^2(\lambda b\sqrt{1-M_2^2}) + \left(\frac{1-M_2^2}{M_1^2-1}\right)\sinh^2(\lambda b\sqrt{1-M_2^2})\right]A_2\lambda = -\frac{2\epsilon}{\pi\sqrt{M_1^2-1}(\beta^2+\lambda^2)} \times \left[\frac{\beta}{\lambda}\left(\frac{M_2^2}{M_1^2}\right)\cosh(\lambda b\sqrt{1-M_2^2}) + \sqrt{\frac{1-M_2^2}{M_1^2-1}}\sinh(\lambda b\sqrt{1-M_2^2})\right] \quad (19)$$

$$\left[\left(\frac{M_2^2}{M_1^2}\right)^2 \cosh^2(\lambda b\sqrt{1-M_2^2}) + \left(\frac{1-M_2^2}{M_1^2-1}\right)\sinh^2(\lambda b\sqrt{1-M_2^2})\right]B_2(\lambda) = \frac{2\epsilon}{\pi\sqrt{1-M_2^2}(\beta^2+\lambda^2)} \times \left[\left(\frac{M_2^2}{M_1^2}\right)\cosh(\lambda b\sqrt{1-M_2^2}) - \frac{\beta}{\lambda}\sqrt{\frac{1-M_2^2}{M_1^2-1}}\sinh(\lambda b\sqrt{1-M_2^2})\right] \quad (20)$$

There are similar expressions for A_1 and B_1. With the Fourier coefficients so determined, the solution of the problem is then complete.

However, the quantities that are of particular interest are the pressure distributions along the interface and along the solid wall. If Δp is the change in pressure from the undisturbed value, then $\Delta p = -\rho U u$. At the interface, let the change in pressure be denoted by $(\Delta p)_i$; then Eq. (11) gives

$$(\Delta p)_i = -\rho_2 U_2^2 \int_0^\infty \cosh(\lambda\sqrt{1-M_2^2}b)\{\lambda A_2(\lambda)\cos\lambda x - \lambda B_2(\lambda)\sin\lambda x\}d\lambda \quad (21)$$

The integral can be evaluated after the A_2 and B_2 from Eqs. (19) and (20) are substituted into the integrand. To simplify the resultant expression, it is convenient to introduce the following notations:

$$\cos\theta = \left[\left(\frac{M_2^2}{M_1^2}\right)^2 - \left(\frac{1-M_2^2}{M_1^2-1}\right)\right]\Big/\left[\left(\frac{M_2^2}{M_1^2}\right)^2 + \left(\frac{1-M_2^2}{M_1^2-1}\right)\right] \quad (22)$$

with

$$\sin\frac{\theta}{2} = \sqrt{\left(\frac{1-M_2^2}{M_1^2-1}\right)\Big/\left[\left(\frac{M_2^2}{M_1^2}\right)^2 + \frac{1-M_2^2}{M_1^2-1}\right]} \quad (23)$$

and

$$\cos\frac{\theta}{2} = \left(\frac{M_2^2}{M_1^2}\right)\Big/\sqrt{\left(\frac{M_2^2}{M_1^2}\right)^2 + \frac{1-M_2^2}{M_1^2-1}} \quad (24)$$

Then Eq. (21) can be written as

$$\frac{(\Delta p)_i}{(1/2)\rho_1 U_1^2} = \frac{4\epsilon}{\pi\sqrt{M_1^2-1}}\left[\cos^2\frac{\theta}{2}\int_0^\infty\left\{\frac{\beta}{\beta^2+\lambda^2}\cos\lambda x + \frac{\lambda}{\beta^2+\lambda^2}\sin\lambda x\right\}d\lambda + \frac{1}{2}\sin^2\theta \times \int_0^\infty \frac{(\beta\cos\lambda x + \lambda\sin\lambda x)d\lambda}{(\beta^2+\lambda^2)[\cosh(2b\sqrt{1-M_2^2}\lambda) + \cos\theta]} + \frac{1}{2}\sin\theta \times \int_0^\infty \frac{\{\lambda\sinh(2b\sqrt{1-M_2^2}\lambda)\cos\lambda x - \beta\sinh(2b\sqrt{1-M_2^2}\lambda)\sin\lambda x\}d\lambda}{(\beta^2+\lambda^2)[\cosh(2b\sqrt{1-M_2^2}\lambda) + \cos\theta]}\right] \quad (25)$$

Now the problem can be greatly simplified by making $\beta \to 0$—i.e., the incoming waves are finally reduced to a simple compression wave with a deflection angle ϵ. At this limit, the first integral of Eq. (25) becomes the unit step function $1(x)$—i.e.,

$$\left.\begin{aligned} 1(x) &= 1, \quad x > 0 \\ &= 0, \quad x < 0 \end{aligned}\right\} \quad (26)$$

By the substitution $\lambda/\beta = z$, the first part of the second integral is

$$\lim_{\beta\to 0}\int_0^\infty \frac{\beta\cos\lambda x d\lambda}{(\beta^2+\lambda^2)[\cosh(2b\sqrt{1-M_2^2}\lambda) + \cos\theta]} = \lim_{\beta\to 0}\int_0^\infty \frac{\cos(\beta x z)dz}{(z^2+1)[\cosh(2b\sqrt{1-M_2^2}\beta z) + \cos\theta]} = \frac{1}{1+\cos\theta}\int_0^\infty \frac{dz}{z^2+1} = \frac{\pi}{2(1+\cos\theta)} = \frac{\pi}{4\cos^2(\theta/2)}$$

Denoting the limiting value of $(\Delta p)_i$ by $(\Delta p)_i^*$,

$$\frac{(\Delta p)_i^*}{(1/2)\rho_1 U_1^2} = \frac{4\epsilon}{\sqrt{M_1^2 - 1}}\left[\cos^2\frac{\theta}{2}\,1(\xi) + \frac{1}{2}\sin^2\frac{\theta}{2} + \frac{1}{2\pi}\sin^2\theta\int_0^\infty \frac{\sin(S\xi/\pi)dS}{S[\cosh S + \cos\theta]} + \frac{1}{2\pi}\sin\theta\int_0^\infty \frac{\sinh S\cos(S\xi/\pi)dS}{S[\cosh S + \cos\theta]}\right] \quad (27)$$

where

$$S = 2b\lambda\sqrt{1 - M_2^2} \quad (28)$$

$$\xi = \pi x/2b\sqrt{1 - M_2^2} \quad (29)$$

ξ is thus the characteristic nondimensional distance parameter. The first integral in Eq. (27) is an odd function of ξ, while the second integral is an even function of ξ. As shown in the Appendix, for *positive values of* ξ, these integrals have the following values:

$$\frac{1}{2\pi}\int_0^\infty \frac{\sin(S\xi/\pi)dS}{S[\cosh S + \cos\theta]} = \frac{1}{8\cos^2(\theta/2)} + \frac{1}{2\pi\sin\theta}\sum_{n=0}^{\infty} e^{-(2n+1)\xi}\left\{\frac{e^{-(\theta/\pi)\xi}}{2n + 1 + (\theta/\pi)} - \frac{e^{(\theta/\pi)\xi}}{2n + 1 - (\theta/\pi)}\right\} \quad (30)$$

and

$$\frac{1}{2\pi}\int_0^\infty \frac{\sinh S\cos(S\xi/\pi)dS}{S[\cosh S + \cos\theta]} = \frac{1}{2\pi}\sum_{n=0}^{\infty} e^{-(2n+1)\xi}\left\{\frac{e^{-(\theta/\pi)\xi}}{2n + 1 + (\theta/\pi)} + \frac{e^{(\theta/\pi)\xi}}{2n + 1 - (\theta/\pi)}\right\} \quad (31)$$

By substituting the values of these integrals into Eq. (27), the pressure distribution at the interface for positive ξ is, finally,

$$\frac{(\Delta p)_i^*}{(1/2)\rho_1 U_1^2} = \frac{4\epsilon}{\sqrt{M_1^2 - 1}}\,[1 + \sin\theta F_1(\xi;\theta)],\quad \xi > 0 \quad (32)$$

where the function $F_1(\xi;\theta)$ is

$$F_1(\xi;\theta) = \frac{1}{\pi}\sum_{n=0}^{\infty}\frac{e^{-[2n+1+(\theta/\pi)]|\xi|}}{2n + 1 + (\theta/\pi)} \quad (33)$$

By observing the proper symmetry of the integrals in Eq. (27), one can easily obtain the pressure distribution for negative values of ξ:

$$\frac{(\Delta p)_i^*}{(1/2)\rho_1 U_1^2} = \frac{4\epsilon}{\sqrt{M_1^2 - 1}}\sin\theta F_2(\xi;\theta),\quad \xi < 0 \quad (34)$$

where

$$F_2(\xi;\theta) = \frac{1}{\pi}\sum_{n=0}^{\infty}\frac{e^{-[2n+1-(\theta/\pi)]|\xi|}}{2n + 1 - (\theta/\pi)} \quad (35)$$

To determine the pressure distribution along the wall, one obtains first, from Eq. (9), the x-component of disturbance velocity u_2 at $y = -b$, the wall. Thus with values of A_2 and B_2 from Eqs. (19) and (20),

$$u_{2\,y=-b} = U_2\int_0^\infty \{\lambda A_2(\lambda)\cos\lambda x - \lambda B_2(\lambda)\sin\lambda x\}d\lambda$$

The pressure change at the wall $(\Delta p)_w$ can then be calculated as $-\rho_2 U_2 u_2\,(y = -b)$. Now let $\beta \to 0$ so as to obtain the value $(\Delta p)_w^*$ for a single compression wave of deflection ϵ. The procedure of calculation is similar to that for the pressure distribution along the interface. The final result is

$$\frac{(\Delta p)_w^*}{(1/2)\rho_1 U_1^2} = \frac{4\epsilon}{\sqrt{M_1^2 - 1}}\left[\frac{1}{2} + \cos^2\frac{\theta}{2}\left(\frac{2}{\pi}\right)\int_0^\infty \frac{\cosh\frac{S}{2}\sin\frac{S\xi}{\pi}\,dS}{S[\cosh S + \cos\theta]} + \sin\frac{\theta}{2}\cos\frac{\theta}{2}\left(\frac{2}{\pi}\right)\int_0^\infty \frac{\sinh\frac{S}{2}\cos\frac{S\xi}{\pi}\,ds}{S[\cosh S + \cos\theta]}\right] \quad (36)$$

The first integral in Eq. (36) is again an odd function of ξ and the second integral is an even function of ξ. As given in the Appendix, for *positive values of* ξ, these integrals can be evaluated as follows:

$$\frac{2}{\pi}\int_0^\infty \frac{\cosh\frac{S}{2}\sin\frac{S\xi}{\pi}\,dS}{S[\cosh S + \cos\theta]} = \frac{1}{2\cos^2\frac{\theta}{2}} - \frac{1}{\pi\cos\frac{\theta}{2}}\sum_{n=0}^{\infty}(-1)^n e^{-(2n+1)\xi}\left\{\frac{e^{-(\theta/\pi)\xi}}{2n + 1 + \frac{\theta}{\pi}} + \frac{e^{(\theta/\pi)\xi}}{2n + 1 - \frac{\theta}{\pi}}\right\} \quad (37)$$

for $\xi > 0$.

$$\frac{2}{\pi}\int_0^\infty \frac{\sinh\frac{S}{2}\cos\frac{S\xi}{2}\,dS}{S[\cosh S+\cos\theta]} = -\frac{1}{\pi\sin\frac{\theta}{2}}\sum_{n=0}^{\infty}(-1)^n e^{-(2n+1)\xi}\left\{\frac{e^{-(\theta/\pi)\xi}}{2n+1+\frac{\theta}{\pi}}-\frac{e^{(\theta/\pi)\xi}}{2n+1-\frac{\theta}{\pi}}\right\} \tag{38}$$

for $\xi > 0$. Then, for positive values of ξ, the pressure distribution can be written as

$$\frac{(\Delta p)_w^*}{(1/2)\rho_1 U_1^2} = \frac{4\epsilon}{\sqrt{M_1^2-1}}\left[1-2\cos\frac{\theta}{2}F_3(\xi;\theta)\right], \quad \xi > 0 \tag{39}$$

where

$$F_3(\xi;\theta) = \frac{1}{\pi}\sum_{n=0}^{\infty}(-1)^n\frac{e^{-[2n+1+(\theta/\pi)]|\xi|}}{2n+1+(\theta/\pi)} \tag{40}$$

By utilizing the symmetry properties of the integrals in Eq. (36), one can immediately write down the expression for the pressure distribution along the wall for negative values of ξ:

$$\frac{(\Delta p)_w^*}{(1/2)\rho_1 U_1^2} = \frac{4\epsilon}{\sqrt{M_1^2-1}}\,2\cos\frac{\theta}{2}F_4(\xi;\theta), \quad \xi < 0 \tag{41}$$

where

$$F_4(\xi;\theta) = \frac{1}{\pi}\sum_{n=0}^{\infty}(-1)^n\frac{e^{-[2n+1-(\theta/\pi)]|\xi|}}{2n+1-(\theta/\pi)} \tag{42}$$

Eqs. (32), (34), (39), and (41) then give the formulas for computing the pressure distributions of interest.

For comparison with experimental observations on the shock-boundary layer interaction, it is of interest to determine the position of the displaced interface between the supersonic and the subsonic flows. Let the displacement from the undisturbed position be denoted by η. The slope $d\eta/dx$ of the disturbed interface is found by substituting Eqs. (19) and (20) into Eq. (12) so that

$$\frac{d\eta}{dx} = \frac{V_{2y=-0}}{U_2} = -\frac{2\epsilon\sqrt{\frac{1-M_2^2}{M_1^2-1}}}{\pi\left[\left(\frac{M_2^2}{M_1^2}\right)^2+\frac{1-M_2^2}{M_1^2-1}\right]}\times$$

$$\left[\int_0^\infty \frac{\left\{\beta\left(\frac{M_2^2}{M_1^2}\right)\sinh(2\lambda b\sqrt{1-M_2^2})+\lambda\sqrt{\frac{1-M_2^2}{M_1^2-1}}\left(-\frac{1}{2}+\frac{1}{2}\cosh(2\lambda b\sqrt{1-M_2^2})\right)\right\}\sin\lambda x\,d\lambda}{(\beta^2+\lambda^2)\{\cosh(2\lambda b\sqrt{1-M_2^2})+\cos\theta\}}-\right.$$

$$\left.\int_0^\infty \frac{\left\{\lambda\left(\frac{M_2^2}{M_1^2}\right)\sinh(2\lambda b\sqrt{1-M_2^2})-\beta\sqrt{\frac{1-M_2^2}{M_1^2-1}}\left[-\frac{1}{2}+\frac{1}{2}\cosh(2\lambda b\sqrt{1-M_2^2})\right]\right\}\cos\lambda x\,d\lambda}{(\beta^2+\lambda^2)\{\cosh(2\lambda b\sqrt{1-M_2^2})+\cos\theta\}}\right]$$

Introducing ξ, S and pa ssing to the limit $\beta \to 0$, as above

$$\frac{d\eta}{dx} = -\frac{2\epsilon}{\pi}\sin\frac{\theta}{2}\left[\sin\frac{\theta}{2}\left\{\int_0^\infty\frac{\cosh S\sin\frac{S\xi}{\pi}\,dS}{S[\cosh S+\cos\theta]}-\int_0^\infty\frac{\sin\frac{S\xi}{\pi}\,dS}{S[\cosh S+\cos\theta]}\right\}-\cos\frac{\theta}{2}\int_0^\infty\frac{\sinh S\cos\frac{S\xi}{\pi}\,dS}{S[\cosh S+\cos\theta]}\right]$$

It can be shown that, for $\xi > 0$,

$$I(\xi) = \int_0^\infty\frac{\cosh S\sin(S\xi/\pi)dS}{S[\cosh S+\cos\theta]} = \frac{\pi}{2(1+\cos\theta)}-\pi\cot\theta\,[F_1(\xi;\theta)-F_2(\xi;\theta)]$$

With Eqs. (30) and (31) and $I(-\xi) = -I(\xi)$,

$$\begin{aligned} d\eta/dx &= 2\epsilon\sin\theta\,F_1(\xi;\theta), \quad \xi > 0 \\ &= 2\epsilon\sin\theta\,F_2(\xi;\theta), \quad \xi < 0 \end{aligned} \tag{43}$$

Noting that the displacement vanishes far ahead of the disturbance, integration, with respect to ξ, of these results gives

$$\left.\begin{aligned}\frac{\pi}{2b\sqrt{1-M_2^2}}[\eta(\xi;\theta)] &= 2\epsilon\sin\theta\,\frac{1}{\pi}\sum_{n=0}^{\infty}\frac{e^{-[2n+1-(\theta/\pi)]|\xi|}}{\left(2n+1-\frac{\theta}{\pi}\right)^2}, \quad \xi<0\\ &= 2\epsilon\sin\theta\,\frac{1}{\pi}\sum_{n=0}^{\infty}\left\{\frac{1}{\left(2n+1-\frac{\theta}{\pi}\right)^2}+\frac{1}{\left(2n+1+\frac{\theta}{\pi}\right)^2}-\frac{e^{-[2n+1+(\theta/\pi)]|\xi|}}{\left(2n+1+\frac{\theta}{\pi}\right)^2}\right\}, \quad \xi>0\end{aligned}\right\} \tag{44}$$

Since $F_1, F_2 \to +\infty$ as $\xi \to 0$, the interface slope is infinite at the point of incidence of the compression wave in the interface. However, it is easy to show that, where δ is a positive quantity,

$$\left(\frac{d\eta}{dx}\right)_{\xi=+\delta}-\left(\frac{d\eta}{dx}\right)_{\xi=-\delta}=4\epsilon\sin\theta\,\frac{1}{\pi}\sum_{n=0}^{\infty}\frac{e^{-(2n+1)\delta}\left\{-(2n+1)\sinh\frac{\theta\delta}{\pi}-\frac{\theta}{\pi}\cosh\frac{\theta\delta}{\pi}\right\}}{(2n+1)^2-(\theta/\pi)^2}$$

Then, the limit as $\delta \to 0$ is

$$\left(\frac{d\eta}{dx}\right)_{\xi=+0}-\left(\frac{d\eta}{dx}\right)_{\xi=-0}=-4\epsilon\sin\theta\left(\frac{\theta}{\pi^2}\right)\sum_{n=0}^{\infty}\frac{1}{(2n+1)^2-(\theta/\pi)^2} \tag{45}$$

This is a negative quantity. The significance of these calculations will be discussed in a later section, together with the numerical results.

Inclined Wall

In the problem of the inclined wall, the solid wall is assumed to have a small inclination ϵ for $x > 0$. For $x < 0$, the wall is parallel to the undisturbed streams of supersonic and subsonic velocities (Fig. 2). The x-axis is again the undisturbed interface between the semi-infinite uniform supersonic stream of Mach Number M_1 and the uniform subsonic stream of width b and Mach Number M_2. Since now the disturbances all originate from the inclined wall, there are no incoming waves from the supersonic stream. The appropriate disturbance velocity potential φ_1 for the supersonic region is then

$$\varphi_1 = U_1\int_0^{\infty}\{a_1(\lambda)\sin\lambda(x-\sqrt{M_1^2-1}\,y)+b_1(\lambda)\cos\lambda(x-\sqrt{M_1^2-1}\,y)\}d\lambda \tag{46}$$

where a_1 and b_1 are again the undetermined Fourier coefficients. For the disturbance velocity potential φ_2 in the subsonic region, one can take

$$\varphi_2 = U_2\left[\frac{\epsilon}{\pi\sqrt{1-M_2^2}}\int_0^{\infty}\frac{\sinh\lambda\sqrt{1-M_2^2}(y+b)}{\lambda}\left\{\frac{\beta}{\beta^2+\lambda^2}\cos\lambda x+\frac{\lambda}{\beta^2+\lambda^2}\sin\lambda x\right\}d\lambda+\int_0^{\infty}\cosh\lambda\sqrt{1-M_2^2}(y+b)\{a_2(\lambda)\sin\lambda x+b_2(\lambda)\cos\lambda x\}d\lambda\right] \tag{47}$$

where a_2 and b_2 are the Fourier coefficients to be determined. The y-component v_2 of the disturbance velocity at the wall, obtained by differentiating the expression in Eq. (47) with respect to y and then setting $y = -b$, is solely due to the first integral. Then, if $\beta \to 0$, one has

$$\begin{aligned}v_{2y=-b} &= U_2\epsilon, \quad x>0\\ &= 0, \quad x<0\end{aligned}$$

This means that for $x > 0$ the wall is inclined at a small angle ϵ from the free stream. Therefore the boundary condition at the wall is satisfied by choosing φ_2 as given by Eq. (47).

To determine the Fourier coefficients a_1, a_2, b_1, and b_2, the physical conditions at the interface as expressed by Eqs. (13) and (14) again have to be used. In other words, the velocity components at the interface from the supersonic side and from the subsonic side must be first obtained from the expressions for φ_1 and φ_2, and then these values are substituted into Eqs. (13) and (14). By equating the corresponding Fourier terms, the following equations for the unknowns a_1, a_2, b_1, and b_2 are obtained:

$$a_1(\lambda)-\frac{M_2^2}{M_1^2}\cosh(\lambda\sqrt{1-M_2^2}b)[a_2(\lambda)]=\frac{M_2^2\epsilon\sinh(\lambda\sqrt{1-M_2^2}b)}{M_1^2\pi\sqrt{1-M_2^2}}\left(\frac{1}{\beta^2+\lambda^2}\right) \tag{48}$$

$$b_1(\lambda) - \frac{M_2^2}{M_1^2}\cosh(\lambda\sqrt{1-M_2^2}b)\,[b_2(\lambda)] = \frac{M_2^2}{M_1^2}\frac{\epsilon\sinh(\lambda\sqrt{1-M_2^2}b)}{\pi\sqrt{1-M_2^2}}\left[\frac{\beta}{\lambda(\beta^2+\lambda^2)}\right] \tag{49}$$

$$a_1(\lambda) + \sqrt{\frac{1-M_2^2}{M_1^2-1}}\sinh(\lambda\sqrt{1-M_2^2}b)\,[b_2(\lambda)] = -\frac{\epsilon\cosh(\lambda\sqrt{1-M_2^2}b)}{\pi\sqrt{M_1^2-1}}\left[\frac{\beta}{\lambda(\beta^2+\lambda^2)}\right] \tag{50}$$

$$b_1(\lambda) - \sqrt{\frac{1-M_2^2}{M_1^2-1}}\sinh(\lambda\sqrt{1-M_2^2}b)[a_2(\lambda)] = \frac{\epsilon\cosh(\lambda\sqrt{1-M_2^2}b)}{\pi\sqrt{M_1^2-1}}\left(\frac{1}{\beta^2+\lambda^2}\right) \tag{51}$$

The solution of these equations yields the values for a_2 and b_2 given by the following expressions:

$$\left[\left(\frac{M_2^2}{M_1^2}\right)^2\cosh^2(\lambda b\sqrt{1-M_2^2}) + \frac{1-M_2^2}{M_1^2-1}\sinh^2(\lambda b\sqrt{1-M_2^2})\right]a_2(\lambda) =$$

$$-\frac{\epsilon}{\pi\sqrt{M_1^2-1}(\beta^2+\lambda^2)}\left[\frac{\beta}{\lambda}\left(\frac{M_2^2}{M_1^2}\right) + \frac{1}{2}\sqrt{\frac{M_1^2-1}{1-M_2^2}}\left\{\left(\frac{M_2^2}{M_1^2}\right)^2 + \frac{1-M_2^2}{M_1^2-1}\right\}\sinh(2\lambda b\sqrt{1-M_2^2})\right] \tag{52}$$

$$\left[\left(\frac{M_2^2}{M_1^2}\right)^2\cosh^2(\lambda b\sqrt{1-M_2^2}) + \frac{1-M_2^2}{M_1^2-1}\sinh^2(\lambda b\sqrt{1-M_2^2})\right]b_2(\lambda) =$$

$$-\frac{\epsilon}{\pi\sqrt{M_1^2-1}(\beta^2+\lambda^2)}\left[-\frac{M_2^2}{M_1^2} + \frac{1}{2}\sqrt{\frac{M_1^2-1}{1-M_2^2}}\left\{\left(\frac{M_2^2}{M_1^2}\right)^2 + \frac{1-M_2^2}{M_1^2-1}\right\}\sinh(2\lambda b\sqrt{1-M_2^2})\right] \tag{53}$$

Similar expressions for a_1 and b_1 can be also computed.

With the Fourier coefficients so determined, the desired pressure distributions along the interface and the wall can be easily calculated by following exactly the procedure outlined in the problem of an incident wave. No details of calculation will be given here but only the final results. For the pressure distribution along the interface ($\beta \to 0$),

$$\frac{(\Delta p)_i^*}{(1/2)\rho_1 U_1^2} = \frac{2\epsilon}{\sqrt{M_1^2-1}}\left[1 - \frac{1}{2}\frac{\cot(\theta/2)}{\sin(\theta/2)}F_4(\xi;\theta) - \frac{1}{2}\cos\frac{\theta}{2}\left(3-\cot^2\frac{\theta}{2}\right)F_3(\xi;\theta)\right], \quad \xi > 0 \tag{54}$$

and

$$\frac{(\Delta p)_i^*}{(1/2)\rho_1 U_1^2} = \frac{2\epsilon}{\sqrt{M_1^2-1}}\left[\frac{1}{2}\cos\frac{\theta}{2}\left(3-\cot^2\frac{\theta}{2}\right)F_4(\xi;\theta) + \frac{1}{2}\frac{\cot(\theta/2)}{\sin(\theta/2)}F_3(\xi;\theta)\right], \quad \xi < 0 \tag{55}$$

The pressure distribution along the wall is given by ($\beta \to 0$)

$$\frac{(\Delta p)_w^*}{(1/2)\rho_1 U_1^2} = \frac{2\epsilon}{\sqrt{M_1^2-1}}\left[1 + 2\cot\frac{\theta}{2}F_1(\xi;\theta)\right], \quad \xi > 0 \tag{56}$$

and

$$\frac{(\Delta p)_w^*}{(1/2)\rho_1 U_1^2} = \frac{2\epsilon}{\sqrt{M_1^2-1}}\,2\cot\frac{\theta}{2}F_2(\xi;\theta), \quad \xi < 0 \tag{57}$$

In Eqs. (54) to (57), the functions F_1, F_2, F_3, and F_4 are functions defined by Eqs. (33), (35), (40), and (42). The variable θ is connected with the Mach Numbers M_1 and M_2 as specified by Eqs. (22) to (24). These equations then supply the desired information for the problem of an inclined wall. The numerical results and the discussions of the results will be presented in the next section.

Numerical Results and Discussion

The parameter θ occurs in all expressions for the pressure distributions. As shown by Eq. (22), it is connected with the Mach Numbers M_1 and M_2 and can be taken to have the range from 0 to π. When $0 < M_2 < 1$, the value of θ increases to π when the ratio M_2/M_1 tends to zero. When $M_1 > 1$ but finite, θ tends to 0 when M_2 tends to 1. The general relationships between θ and M_1, M_2 are given by Fig. 3. It is seen that, if the representative Mach Numbers for the boundary-layer flow and the free stream are taken to be 0.8 and 2, then the corresponding value of θ in the flow model is approximately $3\pi/4$. This fact should be kept in mind when the theoretical results are compared with the experiments on the shock and boundary-layer interactions.

The series for the functions F_1, F_2, F_3, and F_4 as given by Eqs. (33), (35), (40), and (42) are suitable for numerical computation when ξ is large, since the convergence is then extremely rapid. For small values of ξ, modified series as given in the Appendix is more appropriate. F_1 and F_2 have a logarithmic infinity at $\xi = 0$, but F_3 and F_4 are finite at $\xi = 0$. Table 1 gives the tabulated values for these functions.

The results of computation for the case of an incoming compression wave are shown in Figs. 4, 5, 6, and 7. In these graphs, the abscissas are the characteristic nondimensional length ξ along the streams defined by Eq. (29). The physical distance x for any value of ξ is thus proportional to $b\sqrt{1 - M_2^2}$. The width b of the undisturbed subsonic stream is then the measure of length in the problems concerned. The ordinates of these graphs are

$$[\Delta p/(1/2)\rho_1 U_1^2]/(2\epsilon/\sqrt{M_1^2 - 1})$$

Since, under the general assumption of small disturbances, a compression wave of ϵ deflection is associated with a pressure rise equal to

$$(1/2)\rho_1 U_1^2(2\epsilon/\sqrt{M_1^2 - 1})$$

the ordinates of these graphs are then the ratio of pressure rise to the pressure rise caused by the simple incoming compression wave. It is then immediately seen that the pressure rise far downstream of the point of incidence of the wave on the interface is twice as large as the pressure rise for a simple compression wave. When an incoming compression wave is incident upon a solid wall, the compression wave is reflected as a compression wave, and the pressure rise after the reflection is twice as large as the pressure rise before the reflection. Therefore, except for the local interaction, the incoming compression wave is reflected as if by a solid wall without the subsonic stream.

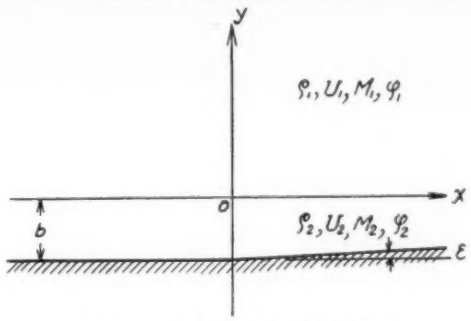

FIG. 2. Inclined wall with angle ϵ.

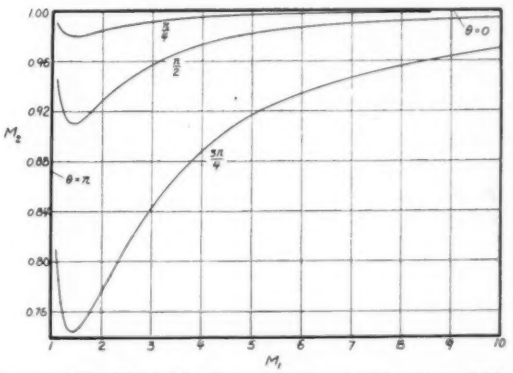

FIG. 3. The Mach Number parameter θ as function of Mach Numbers M_1 and M_2 in the supersonic and the subsonic streams, respectively.

Another feature of these graphs is that the pressure distribution along the interface has a peak at the point of incidence ($\xi = 0$) of the compression wave. There-

TABLE 1

	$\theta = 0$				$\theta = \pi/4$			
ξ	F_1	F_2	F_3	F_4	F_1	F_2	F_3	F_4
0	∞	∞	0.2512	0.2512	∞	∞	0.1940	0.3496
0.05	0.5927	0.5927	0.2431	0.2431	0.5090	0.6761	0.1858	0.3416
0.10	0.4825	0.4825	0.2343	0.2343	0.4010	0.5716	0.1771	0.3328
0.25	0.3369	0.3369	0.2107	0.2107	0.2616	0.4335	0.1542	0.3079
0.40	0.2629	0.2629	0.1887	0.1887	0.1942	0.3611	0.1334	0.2835
0.50	0.2275	0.2275	0.1735	0.1735	9.1627	0.3251	0.1204	0.2674
0.75	0.1649	0.1649	0.1391	0.1391	0.1104	0.2580	0.0907	0.2291
1.00	0.1246	0.1246	0.1121	0.1121	0.0783	0.2094	0.0693	0.1932
1.75	0.0561	0.0561	0.0548	0.0548	0.0290	0.1157	0.0282	0.1135
2.50	0.0266	0.0266	0.0260	0.0260	0.0118	0.0656	0.0112	0.0646
4.00	0.0059	0.0059			0.0018	0.0213		0.0212
	$\theta = \pi/2$				$\theta = 3\pi/4$			
ξ	F_1	F_2	F_3	F_4	F_1	F_2	F_3	F_4
0	∞	∞	0.1569	0.5538	∞	∞	0.1312	1.1776
0.05	0.4520	0.9461	0.1486	0.5457	0.4092	1.6056	0.1229	1.1698
0.10	0.3459	0.8278	0.1401	0.5340	0.3050	1.4895	0.1144	1.1608
0.25	0.2111	0.6803	0.1175	0.5147	0.1762	1.3252	0.0930	1.1338
0.40	0.1498	0.5869	0.0988	0.4836	0.1189	1.2321	0.0756	1.1050
0.50	0.1217	0.5444	0.0872	0.4654	0.0935	1.1802	0.0651	1.0817
0.75	0.0771	0.4620	0.0631	0.4202	0.0552	1.0872	0.0445	1.0323
1.00	0.0513	0.3993	0.0448	0.3766	0.0345	1.0125	0.0298	0.9777
1.75	0.0156	0.2676	0.0152	0.2640	0.0087	0.8256	0.0084	0.8200
2.50	0.0054	0.1821	0.0049	0.1815	0.0028	0.6820	0.0023	0.6804
4.00	0.0006	0.0864		0.0864	0.0002	0.4688		0.4688

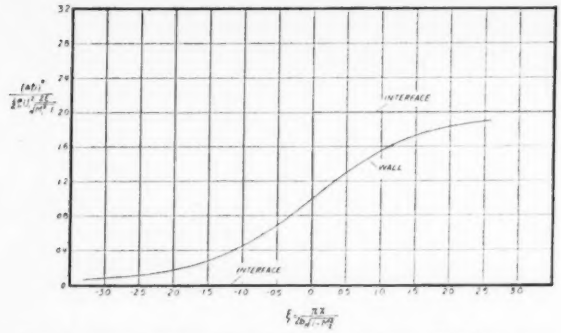

FIG. 4. Pressure increment $(\Delta p)^*$ for the case of incident wave plotted against the distance x from the point of incidence of the wave upon the interface. $\theta = 0$.

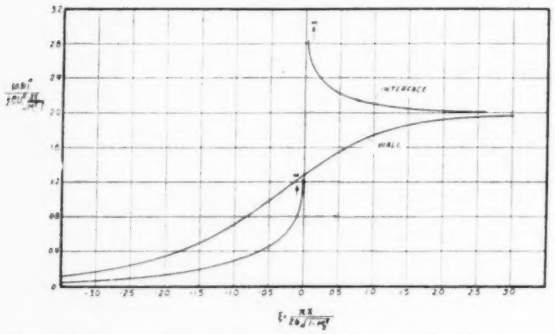

FIG. 5. Pressure increment $(\Delta p)^*$ for the case of incident wave plotted against the distance x from the point of incidence of the wave upon the interface. $\theta = \pi/4$.

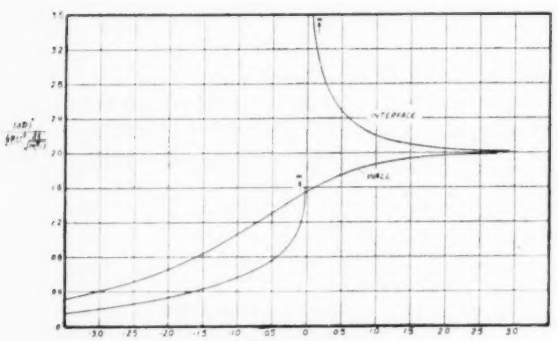

FIG. 6. Pressure increment $(\Delta p)^*$ for the case of incident wave plotted against the distance x from the point of incidence of the wave upon the interface. $\theta = \pi/2$.

fore before the point of incidence the flow is compressed, but after the point of incidence the flow is expanded. In the supersonic stream then, there is a series of compression wavelets sloping downstream, ahead of the incoming compression wave. After the incident compression wave, there is an expansion region. The pressure distribution along the wall has no peak and is a smooth rising curve. Most of the pressure rise along the wall occurs, however, before the point of incidence of the compression wave. In fact for all points ahead

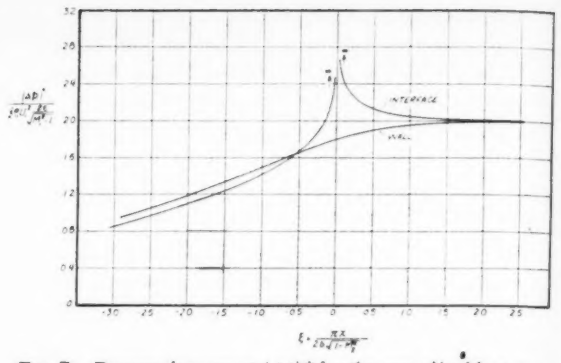

FIG. 7. Pressure increment $(\Delta p)^*$ for the case of incident wave plotted against the distance x from the point of incidence of the wave upon the interface. $\theta = 3\pi/4$.

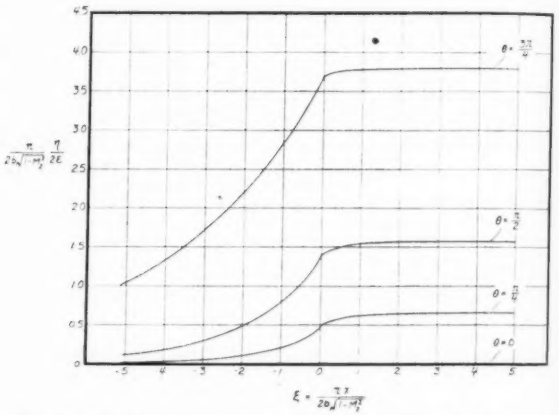

FIG. 8. Incident wave case, the displacement η of the interface (or increment of the thickness of the subsonic stream) plotted against the distance x from the point of incidence of wave upon the interface.

of the point of incidence, the wall pressure is higher than the pressure at the interface. The region where there is strong interaction between the supersonic stream and the subsonic stream is of the order of tens of widths b of the subsonic stream. The length of this region is increased as θ approaches π.

Fig. 8 shows the results of computations for the interface displacement. A noticeable feature of these curves is the rapid change from an infinite slope at $\xi = 0$ to small values at $\xi \neq 0$. This is especially marked for $\xi > 0$. Eq. (45) shows that the slope for positive x is less than the slope for negative x. Therefore, as far as the subsonic flow is concerned, the corner at the point of incidence of the compression wave is a compression corner. This result agrees with computations for $(\Delta p)_i^*$, inasmuch as it implies compression upstream of $\xi = 0$, an infinite rise in pressure at $\xi = 0$, and expansion downstream of $\xi = 0$. It is also seen that the displacement increases as θ increases. Recalling that $\theta \to \pi$ as $M_2/M_1 \to 0$, for $0 < M_2 < 1$, this means the displacement increases as M_2 decreases—i.e., as the disturbance propagates upstream with greater strength (see Figs. 4–7), as would be expected.

One further comparison with the pressure calculations may be made. For $\xi < 0$, the wall pressure exceeds interface pressure except in an extremely small region about the singularity. The pressure gradient is such, then, as to be consistent with an increasing interface slope as $\xi \to 0$. For $\xi > 0$ the gradient is from the interface to the wall, consistent with a decreasing slope as ξ increases.

When a shock occurs over a laminar boundary layer, the case of the so-called λ-shock (Fig. 9), experiments show that there is a compression region in the free supersonic stream ahead of the shock and an expansion region after the shock. Furthermore, the pressure rise along the wall is known to be continuous. These features of the λ-shock are then completely demonstrated by the incident wave case discussed above. It is evident that the analysis presented is not a quantitative explanation of λ-shock, since the shock is a rather strong disturbance, while small disturbances and linearization of the differential equation are the basis of the present analysis. Furthermore, in the analysis, the viscous and the heat-conducting effects are completely neglected. Perhaps a more important omission is the velocity gradient in the boundary layer. The theoretical calculation assumes uniform supersonic and subsonic streams, and therefore the vorticity is concentrated at the interface instead of distributed throughout the subsonic layer, as is the case for the boundary layer. However, the close qualitative agreement between the theory and the experimental observations on the λ-shock indicates the importance of the effects of interaction between the supersonic and the subsonic region in the shock-boundary-layer phenomenon.

One might now ask: Why is the interaction between the shock and a turbulent boundary layer different from that of the λ-shock? In the case of a turbulent boundary layer, one does not observe the extended compression region before the shock and the expansion region after the shock. If the theory presented is of any real value, it must explain this case also. The authors believe the solution of this paradox lies in the thickness of the subsonic layer in case of turbulent boundary layer. Because of the much steeper velocity gradient resulting from the extremely intensive turbulent flow exchange, the subsonic part of the turbulent boundary layer is generally extremely thin. For usual dimensions the subsonic layer in a turbulent boundary layer is only of the order of hundreths of an inch thick, while the subsonic layer in a laminar boundary layer is of the order of tenths of an inch thick. Therefore, the characteristic interaction effect between the subsonic and the supersonic flows, if it occurs, will be limited to a region of only a few tenths of an inch for the turbulent boundary layer. This would be difficult to observe, especially if, as is usually the case, the shock is not stationary but oscillates slightly in position. Furthermore, the large velocity gradient in the turbulent layer will certainly modify the flow considerably from that

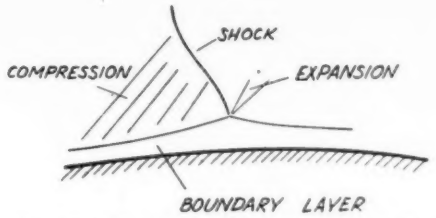

FIG. 9. Flow pattern of a λ-shock. Interaction of shock and laminar boundary layer.

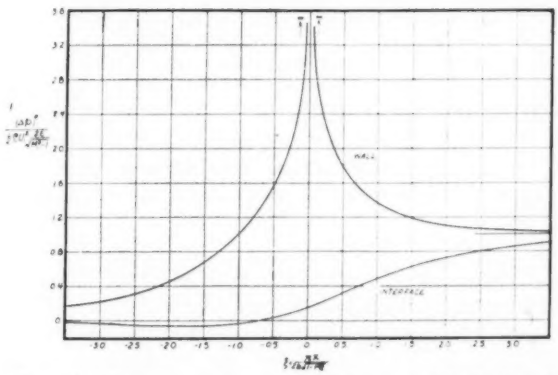

FIG. 10. Pressure increment $(\Delta p)^*$ for case of inclined wall plotted against the distance x from the break in the wall. $\theta = \pi/4$.

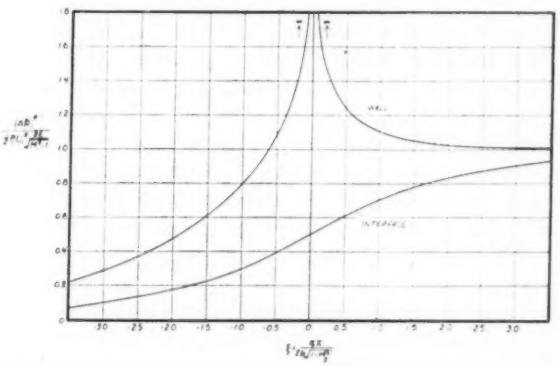

FIG. 11. Pressure increment $(\Delta p)^*$ for case of inclined wall plotted against the distance x from the break in the wall. $\theta = \pi/2$.

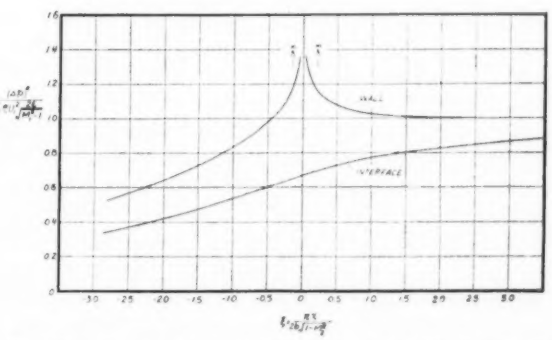

FIG. 12. Pressure increment $(\Delta p)^*$ for case of inclined wall plotted against the distance x from the break in the wall. $\theta = 3\pi/4$.

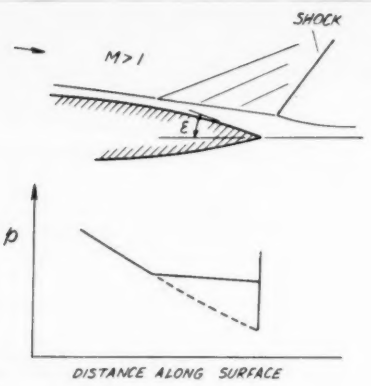

FIG. 13. Flow pattern near the trailing edge of a supersonic airfoil.

calculated theoretically, both because of the strong influence of vorticity and because of the effects of viscosity and heat-conductance. Therefore, while the theory presented cannot give a clear explanation for the interaction between shock and the turbulent boundary layer, the theory and the experiments are not contradictory.

The numerical results for the second problem of the inclined wall are presented in Figs. 10, 11, and 12. Here the general features of the pressure distributions are the same as for the problem of the incident wave. Only now the role of the wall and the interface is changed. The pressure distribution along the wall now has a peak at the starting point of the inclination, while the pressure at the interface rises steadily. At distances far downstream of the break in the wall, the pressure is equal to that due to a wedge of vertex ϵ, the angle of inclination of the wall. This is, of course, expected. But the important result is the rather large compression ahead of the change in flow direction caused by the inclination. One can compare these calculated results with the measured pressure distribution over the upper surface near the trailing edge of an airfoil in a supersonic stream (Fig. 13). At the trailing edge, the flow has to turn through an angle so that compatibility conditions for the flows along the upper surface and the flow along the lower surface can be satisfied. This change in the direction of flow is the same as that caused by the inclination of wall shown in Fig. 2. Therefore, from the results of the calculations, one can expect a rise of pressure over the surface of airfoil ahead of the trailing edge above that predicted by a theory without taking into account the effects of the boundary layer. This is actually observed.[6] Of course, when the boundary layer near the trailing edge is turbulent instead of laminar, the subsonic layer will be so thin as to cause negligible forward propagation of pressure. Then the pressure rise before the trailing edge will be greatly reduced, and the simple classical theory for pressure distribution over a supersonic airfoil will be more accurate.

REFERENCES

[1] Ackeret, J., Feldmann, F., and Rott, N., *Untersuchungen an Verdichtungsstossen und Grenzschichten in schnell bewegten Gasen*, Mitteilungen aus dem Institut fur Aerodynamik, E. T. H., No. 10 (1946); or N.A.C.A. T.M. No. 1113, 1947.

[2] Liepmann, H. W., *The Interaction Between Boundary Layer and Shock Waves in Transonic Flow*, Journal of the Aeronautical Sciences, Vol. 13, pp. 623–637, 1946.

[3] Lees, L., *Remarks on the Interaction Between Shock Wave and Boundary Layer in Transonic and Supersonic Flow*, Report No. 120, Aeronautical Engineering Laboratory, Princeton University (Project Squid), 1947.

[4] Lagerstrom, P. A., Cole, J. D., and Trilling, L., *Viscous Effects in Compressible Flow*, Paper presented at the Institute on Heat Transfer and Fluid Mechanics, June 23, 1948.

[5] Howarth, L., *The Propagation of Steady Disturbances in a Supersonic Stream Bounded on One Side by a Parallel Subsonic Stream*, Proc. Cambridge Philosophical Society, Vol. 44, pp. 380–390, 1948.

[6] Ferri, A., *Experimental Results with Airfoils Tested in the High Speed Tunnel at Guidonia*, N.A.C.A. T.M. No. 946, 1940.

Appendix

(I) EVALUATION OF INTEGRALS

The infinite integrals in the expressions for the pressure distributions can be evaluated by contour integration. For instance,

$$\frac{1}{2\pi}\int_0^\infty \frac{\sin\frac{S\xi}{\pi}\,dS}{S[\cosh S+\cos\theta]} = \frac{1}{4\pi}\int_{-\infty}^{\infty} \frac{\sin\frac{S\xi}{\pi}\,ds}{S[\cosh S+\cos\theta]} = \frac{1}{4\pi i}\int_{-\infty}^{\infty} \frac{e^{iS\xi/\pi}\,ds}{S[\cosh S+\cos\theta]}$$

Now consider S as a complex variable and take the contour as (1) the real axis indented at the origin, and (2) semicircle in the upper-half of the complex plane with infinite radius. It is easy to show that the contribution to the contour integral along the semicircle is zero. The contour encloses the following simple poles:

$$S = i[(2n+1)\pi \pm \theta], \quad n = 1, 2, 3, \ldots$$

Thus,

$$\frac{1}{2\pi}\int_0^\infty \frac{\sin\frac{S\xi}{\pi}\,ds}{S[\cosh S+\cos\theta]} = \frac{1}{2}\left[\frac{1}{2(1+\cos\theta)} + \sum_{n=0}^{\infty}\frac{e^{-[2n+1+(\theta/\pi)]\xi}}{i[(2n+1)\pi+\theta]\sinh i\,[(2n+1)\pi+\theta]} + \sum_{n=0}^{\infty}\frac{e^{-[2n+1-(\theta/\pi)]\xi}}{i[(2n+1)\pi-\theta]\sinh i\,[(2n+1)\pi-\theta]}\right] =$$

(*Formula continued at top of facing page*)

$$\frac{1}{8\cos^2(\theta/2)} + \frac{1}{2\pi \sin\theta} \sum_{n=0}^{\infty} e^{-(2n+1)\xi} \times \left\{ \frac{e^{(\theta/\pi)\xi}}{2n+1+(\theta/\pi)} - \frac{e^{-(\theta/\pi)\xi}}{2n+1-(\theta/\pi)} \right\}, \quad \xi > 0$$

This is the result given in Eq. (30).

The other integrals can be evaluated in a similar way. The results are already given in Eqs. (31), (37), and (38).

(II) Continuity of Wall Pressure

From the computed results it appears that the wall pressure is continuous for the incident wave case and the interface pressure is continuous for the inclined wall case. From Eqs. (39), (41) and (50), (52), it is seen that this condition implies that

$$F_3(0;\theta) + F_4(0;\theta) = (1/2)\sec(\theta/2) \qquad \text{(A)}$$

This may be verified in several ways. The simplest seems to be the following:

$$\frac{dF_3}{d\xi} = -\frac{1}{\pi}\sum_{n=0}^{\infty}(-1)^n e^{-[2n+1+(\theta/\pi)]\xi} = -\frac{1}{\pi}\frac{e^{-[1+(\theta/\pi)]\xi}}{1+e^{-2\xi}}$$

$$\frac{dF_4}{d\xi} = -\frac{1}{\pi}\frac{e^{-[1-(\theta/\pi)]\xi}}{1+e^{-2\xi}}$$

Now $F_3(\infty;\theta) = F_4(\infty;\theta) = 0$, so

$$F_3(\xi;\theta) + F_4(\xi;\theta) = \frac{1}{\pi}\int_{\xi}^{\infty} \frac{e^{-[1+(\theta/\pi)]t} + e^{-[1-(\theta/\pi)]t}}{1+e^{-2t}}\,dt$$

and

$$F_3(0;\theta) + F_4(0;\theta) = \frac{1}{\pi}\int_0^{\infty} \frac{\cosh(\theta/\pi)t}{\cosh t}\,dt$$

Finally,

$$F_3(0;\theta) + F_4(0;\theta) = \frac{1}{2\pi}\int_{-\infty}^{\infty} \frac{\cosh(\theta/\pi)t}{\cosh t}\,dt$$

Now consider t as a complex quantity and integrate $\cosh(\theta/\pi)t/\cosh t$ around a rectangular contour (1) along the real axis from $(-R, 0)$ to $(R, 0)$, (2) normal to the real axis along $(R, 0)$ to (R, π) and $(-R, \pi)$ to $(-R, 0)$, and (3) parallel to the real axis from (R, π) to $(-R, \pi)$. The only pole enclosed is at $(t + is) = i(\pi/2)$ and the residue is $-i\cos(\theta/2)$. By making $R \to \infty$, Eq. (A) can be shown to be true.

(III) Series for Computing F-Functions at Small Values of Argument

The series for F_1, F_2, F_3, and F_4 as given by Eqs. (33), (35), (40), and (42) are suitable for numerical computation only when $|\xi|$ is large. When $|\xi|$ is small, the convergence of these series is slow and computation tedious. On the other hand, the physical problem requires the values of these functions at small values of $|\xi|$. The following series for these functions are thus more convenient.

For $\xi > 0$

$$F_1(\xi;\theta) = \frac{1}{\pi}\sum_{n=0}^{\infty}\frac{e^{-[2n+1+(\theta/\pi)]\xi}}{2n+1+(\theta/\pi)}$$

Thus

$$\frac{dF_1}{d\xi} = -\frac{1}{\pi}\sum_{n=0}^{\infty} e^{-[2n+1+(\theta/\pi)]\xi} = -e^{-[1+(\theta/\pi)]\xi}\sum_{n=0}^{\infty}(e^{-2\xi})^n = -\frac{1}{\pi}\frac{e^{-[1+(\theta/\pi)]\xi}}{1-e^{-2\xi}}$$

Since $F_1(\infty;\theta) = 0$,

$$F_1(\xi;\theta) = \frac{1}{\pi}\int_{\xi}^{\infty}\frac{e^{-[1+(\theta/\pi)]t}}{1-e^{-2t}}\,dt$$

Now let

$$e^{-2t} = S$$

Then

$$F_1 = \frac{1}{2\pi}\int_{\eta}^{\cdot}\frac{dS}{S^k(1-S)}$$

where $\eta = e^{-2\xi}$ and $k = (1/2) - (\theta/2\pi)$. For θ such that $0 \le \theta \le \pi$, $0 \le k \le 1/2$. Also, $0 \le \eta \le 1$.

Now

$$F_1 = \frac{1}{2\pi}\int_0^{\eta}\frac{[(1-S)+S]\,dS}{S^k(1-S)} = \frac{1}{2\pi}\int_0^{\eta}\frac{dS}{S^k} + \frac{1}{2\pi}\int_0^{\eta}\frac{S^{(1-k)}\,dS}{1-S}$$

Thus

$$2\pi F_1 = \frac{\eta^{(1-k)}}{1-k} - [S^{(1-k)}\log(1-S)]_0^{\eta} + (1-k)\int_0^{\eta}\frac{\log(1-S)}{S^k}\,dS$$

The remaining integration may be effected by a further change of variable. Let $1 - S = z$. Then one has to evaluate

$$\int_{(1-\eta)}^{1}\frac{\log z}{(1-z)^k}\,dz = \sum_{n=0}^{\infty}(-1)^n\binom{-k}{n}\times\int_{1-\eta}^{1} z^n\log z\,dz$$

$$= -\sum_{n=0}^{\infty}(-1)^n\binom{-k}{n}\times\left\{\frac{(1-\eta)^{n+1}}{n+1}\log(1-\eta) - \frac{1}{(n+1)^2}[(1-\eta)^{n+1}-1]\right\}$$

where $\binom{-k}{n}$ is the binomial coefficient:

$$\binom{-k}{n} = \frac{(-k)(-k-1)\ldots(-k-n+1)}{n!}$$

Finally,

$$2\pi F_1 = \eta^{(1-k)}\left\{\frac{1}{1-k} - \log(1-\eta)\right\} - \sum_{n=0}^{\infty}(-1)^n\binom{-k}{n}\left\{\frac{(1-\eta)^{n+1}}{n+1}\log(1\eta) - \frac{1}{(n+1)^2}[(1-\eta)^{n+1}-1]\right\}$$

a form that is convenient for evaluation at small values of ξ.

In similar fashion modified series for F_2, F_3, and F_4 may be determined. Then,

$$2\pi F_4 = \eta^{(1-k)}\left\{\frac{1}{1-k} - \log(1+\eta)\right\} + (1-k)\times \sum_{n=1}^{\infty}(-1)^{n+1}\frac{\eta^{(n+1-k)}}{n(n+1-k)}$$

where η, k are as above. $2\pi F_2$, $2\pi F_3$ have the same forms as $2\pi F_1$, $2\pi F_4$, respectively, except that $k = (1/2) + (\theta/2\pi)$.

Important Notice

Papers for Presentation at Eighteenth Annual Meeting

Outlines or abstracts of papers to be considered by the Meetings Committee for presentation at the Eighteenth Annual Meeting in January, 1950, must be submitted no later than September 30.

Send to: The Secretary, Institute of the Aeronautical Sciences, 2 East 64th Street, New York 21, N.Y.

Notice to Contributors

Manuscripts submitted for publication *must* be double- or triple-spaced originals. There should be wide margins on both sides of the sheets and triple spacing around formulas to allow for the marking of directions for the printer.

Original drawings (jet black India ink on white paper or tracing cloth) should accompany the manuscript. (*Blueprints are not acceptable.*) Photographs *must* be on glossy white paper.

Only the simplest formulas should be typewritten; all others should be carefully written in pen and ink. The difference between capital and lower-case letters and Greek symbols should be clearly distinguished.

See page 576 of this issue for further details.

Theory and Tests on the Plastic Stability of Plates and Shells*

P. P. BIJLAARD†
Cornell University

SUMMARY

Buckling of plates and shells superimposes an additional state of stress on the original one. Assuming that plastic deformation is governed only by the amount of elastic shearing energy at the point in question, it is shown that the assumption of "plastic deformation" leads to smaller buckling stresses than that of "plastic flow." Using the assumption of "plastic deformation," it is found that the theory is in good agreement with tests by Kollbrunner and by the N.A.C.A. It is found that the ratio between plastic and elastic buckling stress is highest when the proportions of the deviator components, as superimposed by buckling, differ most from the proportions of the original deviator components. The stress-strain relations are derived by writing the infinitely small excess strains as total differentials and computing the partial derivatives of the strains with respect to the stresses. The differential equation for plate buckling is derived, and results of its application to several kinds of loading and boundary conditions are tabulated. The theory for the buckling of shells is also given. The author presents a comparison of his theory with the theories of Ilyushin, Stowell, and Handelman and Prager.

INTRODUCTION

A COMPLETE THEORY of the plastic stability of plates was given by the author in 1938. It appears, from several American publications after World War II which deal only with special cases, that this theory is not well known in America. Its results are in accord with tests by Kollbrunner,[30] especially with regard to the buckle length. They are also in accord with tests conducted by the N.A.C.A.[41–46]

FLOW LINES IN WIDE PLATES

In the author's theory it is assumed that plastic deformations are governed by the elastic shearing energy. Previously it was thought (for example, by Bierett[1] and others) that with inhomogeneous stress distribution the yield stress depends not only on the state of stress at the point involved but also on the stress distribution in the adjacent material, both in the elastic domain. It is shown by the author's theory of local plastic deformations[2] that plastic deformation is always governed by the amount of elastic shearing energy at the proper point and that apparent raising of the yield stress at points of stress concentration is caused by a change of the state of stress in consequence of minor plastic deformations.[3,4] In this way the direction of flow lines in wide steel plates[5] and thick bars[6] was explained as was also the difference between upper and lower yield stress in thick steel bars.[6] In wide plates subjected to pure tension or pure compression, these flow lines form angles of 55° with the direction of the force.

The latter may be easily explained as follows. If, for example, in a plate that is sufficiently buckling-proof a flow line should occur perpendicularly to the direction of the compressive force (Fig. 1), the flow in the longitudinal direction (x-direction) would cause an expansion of the material within the flow lines in the lateral direction (y-direction). This would, however, be impeded by the adjacent elastic material, so that excess stresses σ_y' would be superimposed. According to Fig. 2, representing all states of stress situated at the yield point, this would involve a shifting of the representative point of the state of stress from $\sigma_x = \sigma_f$, $\sigma_y = 0$ to $\sigma_x = \sigma_f + \sigma_x'$, $\sigma_y = \sigma_y'$, so that the appearance of such a flow line would require a higher stress than the yield stress σ_f for pure compression. Only when the flow lines embrace an angle of 55° with the direction of the compressive force does the plastic strain in the longitudinal direction of the flow lines happen to be zero, so that the flowing in these flow lines is not impeded by the adjacent elastic parts of the plate. Thus, in this case, unimpeded flow at the yield stress for pure compression is possible, so that these flow lines require the smallest force.

It was shown also[7–10] that local plastic deformations of the earth's crust—which find expression in bands of negative gravity anomalies, geosynclines, submarine ridges and troughs, isles series, and chains of mountains—have arisen from flow lines in the earth's crust which are governed by the same laws as those in a steel plate. Later investigations of Vening Meinesz[39] and the author[40] confirmed that the entire system of linear patterns of the earth's crust can be explained by the author's theory of local plastic deformations.

Presented at the Session on Structures—Static Loads, Seventeenth Annual Meeting, I.A.S., New York, January 24–27, 1949.

* The author wishes to express his gratitude to Prof. N. J. Hoff, Polytechnic Institute of Brooklyn, and S. Levy, National Bureau of Standards, for their kind assistance in the preparation of preprints and slides for his lecture during his trip to Europe and to Mr. Levy for his willingness to be prepared to give the lecture in case the author had not returned in time. He is also greatly indebted to Mr. Levy for linguistic corrections in this final paper.

† Professor of Advanced Problems in Applied Mechanics, Delft, Holland; now Associate Professor, College of Engineering, Cornell University.

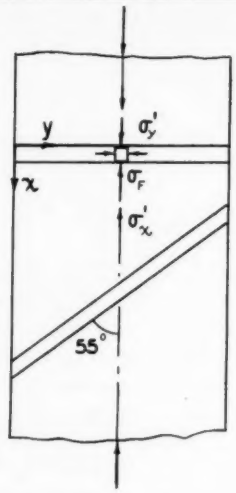

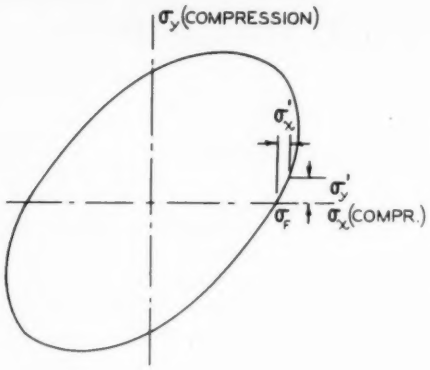

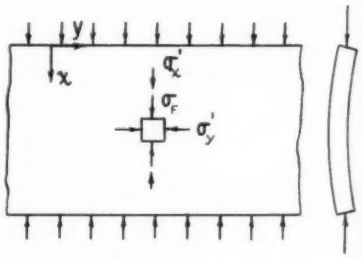

FIG. 1 (*left*). Flow lines in a wide and thin plate. FIG. 2 (*center*). States of stress situated at the yield point. FIG. 3 (*right*). Cylindrical buckling of a wide plate.

BUCKLING OF A WIDE PLATE

In order to make plausible this explanation of flow lines in the earth's crust, it had to be proved that buckling of the earth's crust, as a spherical shell elastically supported by the substratum, does not occur before the yield stress is reached.[7] With the then existing theories on plastic buckling of steel plates in structural engineering (as given by Bleich, Chwalla, and Roš-Eichinger), this was not possible, because according to these theories the buckling modulus of a plate, under a compressive stress equal to the yield stress, is zero. The author can show, however, that this must be wrong. With a wide plate, for example, which is subjected to compression in the x-direction (Fig. 3), the proper buckling will not cause a strain in the y-direction. If, however, with buckling, at the concave side of the plate only a pure compressive stress equal to the yield stress σ_f should occur, the shortening in the x-direction would cause there an expansion of the y-direction. In the same way, as in the case of flow lines perpendicular to the force, however, the condition that this expansion should be zero will cause excess stresses σ_y' and thus also excess stresses σ_x' (Fig. 2). Moreover, it can be shown that in this case the entire plate behaves plastically, by which the excess boundary stresses σ_x' cause inner moments $h^2\sigma_x'/6$ which counteract the buckling of the plate. Consequently, at the yield stress the buckling modulus of a plate is not zero as is that of a bar. Apparently this is caused by the fact that, with buckling of a plate, another state of stress with another ratio of the stress components is superimposed on the initial state of stress, and with changing ratio of the stress components, or rather of the deviator components, the material no longer behaves quasi-isotropically, as in the case for which the ratio of these components is constant.

PLASTIC BEHAVIOR OF A METAL UNDER VARYING STATES OF STRESS

Thus it was necessary to find a more exact theory of the plastic stability of plates and shells. *A sound base for such a theory was the author's theory of local plastic deformations,*[2] *in which it was shown that from the very beginning plastic deformations are governed by the amount of elastic shearing energy at the proper point,* in contradiction with former conceptions (Lode[11]) in which it was thought that in the beginning the yielding in layers in the flow lines depended on the maximum shearing stress.

Plastic deformations occur by sliding in the crystallographic planes of the crystallites. Consequently, hydrostatic pressure, causing no shearing stresses anywhere, will not influence the plastic deformations. The stress tensor

$$\begin{Vmatrix} \sigma_x & \tau_{xy} & \tau_{xz} \\ \tau_{yx} & \sigma_y & \tau_{yz} \\ \tau_{zx} & \tau_{zy} & \sigma_z \end{Vmatrix} \tag{1}$$

may be split into a hydrostatic pressure $\sigma = (\sigma_x + \sigma_y + \sigma_z)/3$ and into the so-called stress deviator

$$\begin{Vmatrix} \bar{\sigma}_x & \tau_{xy} & \tau_{xz} \\ \tau_{yx} & \bar{\sigma}_y & \tau_{yz} \\ \tau_{zx} & \tau_{zy} & \bar{\sigma}_z \end{Vmatrix} \tag{2}$$

in which, consequently, $\bar{\sigma}_x = \sigma_x - \sigma$, $\bar{\sigma}_y = \sigma_y - \sigma$, and $\bar{\sigma}_z = \sigma_z - \sigma$. Thus, only the deviator influences the plastic deformations. Furthermore, it causes elastic strains, being components of the elastic strain deviator.

$$\begin{Vmatrix} \bar{\epsilon}_{xe} & (1/2)\gamma_{xye} & (1/2)\gamma_{xze} \\ (1/2)\gamma_{yxe} & \bar{\epsilon}_{ye} & (1/2)\gamma_{yze} \\ (1/2)\gamma_{zxe} & (1/2)\gamma_{zye} & \bar{\epsilon}_{ze} \end{Vmatrix} \tag{3}$$

in which

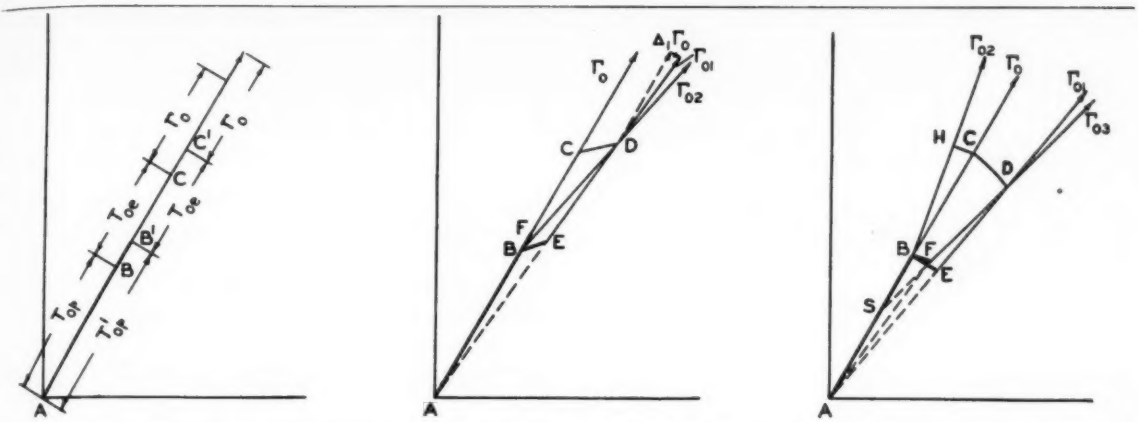

FIG. 4 (*left*). Representative vectors of strain and stress deviators with constant ratios of the deviator components. FIG. 5 (*center*). Representative vectors of strain and stress deviators with changing ratios of the deviator components. FIG. 6 (*right*). Comparison of plastic deformation (Γ_{01}), plastic flow (Γ_{02}), and a new possibility (Γ_{03}).

$$\left.\begin{aligned} \bar{\epsilon}_{xe} = \bar{\sigma}_x/2G, \quad \bar{\epsilon}_{ye} = \bar{\sigma}_y/2G \\ (1/2)\gamma_{xye} = \tau_{xy}/2G, \text{ etc.} \end{aligned}\right\} \tag{4}$$

so that all components are proportional to those of the stress deviator. According to tests of Lode,[11] Roš-Eichinger,[12] and the author,[2] with constant ratio of the deviator components the plastic deformation takes place practically quasi-isotropically, so that the components of the plastic strain deviator are proportional to those of the stress deviator.* The plastic strain deviator is, of course, identical to the plastic strain tensor, since plastic deformations do not cause a change of volume.

The elastic shearing energy V_{se}, which governs the plastic deformations, equals the elastic strain energy due to the stress deviator, so that

$$\begin{aligned} V_{se} = (1/2)(\bar{\sigma}_x\bar{\epsilon}_{xe} + \bar{\sigma}_y\bar{\epsilon}_{ye} + \bar{\sigma}_z\bar{\epsilon}_{ze} + \tau_{xy}\gamma_{xye} + \\ \tau_{yz}\gamma_{yze} + \tau_{zx}\gamma_{zxe}) = (1/4G)[\bar{\sigma}_x^2 + \bar{\sigma}_y^2 + \bar{\sigma}_z^2 + \\ 2(\tau_{xy}^2 + \tau_{yz}^2 + \tau_{zx}^2)] = S_1^2/4G \end{aligned} \tag{5}$$

At the yield stress, where V_s is constant, consequently,

$$S_1 = \sqrt{\bar{\sigma}_x^2 + \bar{\sigma}_y^2 + \bar{\sigma}_z^2 + 2(\tau_{xy}^2 + \tau_{yz}^2 + \tau_{zx}^2)} \tag{6}$$

is constant.

The stress and strain deviators may be indicated by representative vectors Γ_0 and T_0, of which the components are the components of these deviators. Hence, if considering deformations at the yield stress with S_1 in Eq. (6) constant, the length of the stress vector and that of vector T_{0e} of the elastic deformations are also constant, while with constant ratio of the deviator components the direction of all vectors, including that of the plastic strain deviator, will be the same. In that case the vectors of the plastic and elastic deformation [being, for example, $T_{0p} = AB$ (Fig. 4) and $T_{0e} = BC$, respectively] will become, after further deformation, $T_{0p}' = AB'$ and $T_{0e} = B'C' = BC$, respectively, while the vector of the stress deviator, being placed at the end of the total (i.e., elastic plus plastic) deformation course, moves from C to C', its direction and length remaining constant.

If, however, the direction of the total deformation course changes, as is the case with plastic buckling of plates and shells, so that, after having a direction AC (Fig. 5) while AB and BC represent the plastic and elastic deformations, respectively, it proceeds in a direction CD, several possibilities exist for the course of the excess plastic deformation. The excess deformation CD by buckling has to be assumed infinitely small. In the author's theory,[13,14] it was assumed for several reasons that at the representative point D of the total deformation the situation is the same as with a straight deformation course AD, so that as the length of vector ED of the elastic deformations remains constant and equal to BC, the excess plastic deformation is represented by BE, while the stress deviator is given by Γ_{01} at D. So a complete memory was attributed to the material, as in a so-called Hencky body and in accordance with what is called "plastic deformation."

Hohenemser and Prager[15] executed tests at the yield stress with steel tubes that were alternately subjected to pure tension and torsion. They found that preceding free plastic deformations—i.e., deformations during which the ratio of the deviator components does not change—are forgotten. In the present case this means that the free plastic deformation AB is forgotten and that the continuation of the vector of the elastic deformation, $FD = BC$, passes through B, the excess plastic deformation being given by BF and the stress deviator by Γ_{02} in D. As AB is here the total preceding plastic deformation, also a Prandtl-Reuss body, having

* This means that the deformation is the same as with a shearing strain in all planes which is proportional to the shearing stress in these planes. Divergence occurs, however, in the direction of a sliding along the planes of maximum shearing stress. This may be explained by the fact that the crystallites have a certain yield stress themselves, so that no sliding takes place along planes with a too low shearing stress.

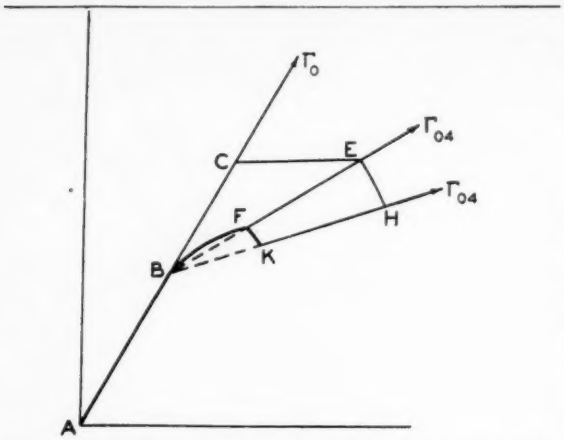

FIG. 7. Deformation according to tests of Hohenemser and Prager.

no memory at all and showing so-called "plastic flow," it will behave in the same way.

The more general assumption of a Hencky body, which includes here the Prandtl-Reuss body as a special case, was used in the theory. This was done for the following reasons. With deformations *below* the yield stress, with which one has to do with buckling, it is not sure that, even with free deformation, the ratio of the deviator components does not change locally in connection with the yielding of the differently orientated crystallites, one after another. Consequently, one is not sure that in the domain of strain hardening the preceding plastic deformation AB will not be remembered. Moreover, by taking it into account, one is sure not to overestimate the buckling stresses of plates, which according to the author's theory were nevertheless much higher than according to the existing theories of Bleich, Chwalla, and Roš-Eichinger. For with a Hencky body (stress vector Γ_{01} in D) the excess stress deviator, which after an excess total deformation course CD is given by $\Delta_1\Gamma_0$, is smaller than with a Prandtl-Reuss body (stress vector Γ_{02} in D), as may be seen directly in Fig. 5.

As, however, a loss of memory amounts only to a neglect of the initial plastic deformation course AB, it may eventually be taken into account in the author's formulas by equating his value e to zero. This was done in his earlier work[14] in order to compare his results with tests by Kollbrunner and Chase. From Kollbrunner's tests with angles[16] he concluded, however, that with aluminum all preceding plastic deformations should be taken into account. This view was confirmed by the good agreement between his theory and the results of Kollbrunner's[30] and Stüssi's[31] later tests with plates.

On the other hand, the author called attention to the fact that a complete behavior as a Hencky body will generally not be possible.[14,17] If, for example, after a deformation course AC, Fig. 6, the total deformation follows the arc CD, the plastic deformation would follow the arc BE. The work done by the stress deviator with a small increment of strain may be written as follows:

$$dV_s = \sigma_x d\tilde{\epsilon}_x + \sigma_y d\tilde{\epsilon}_y + \sigma_z d\tilde{\epsilon}_z + \tau_{xy} d\gamma_{xy} + \tau_{yz} d\gamma_{yz} + \tau_{zx} d\gamma_{zx} \quad (7)$$

being the inner product of the vectors of stress deviator and strain increment. In this case, where the former remains perpendicular to the latter, the stress deviator apparently does no work, although large plastic deformations as given by the curve BE may be involved. The same objection would apply to a deformation according to the tests of Hohenemser and Prager if after a course ACE (Fig. 7) the arc EH should be followed, since here the continuation of the elastic deformation vector passes always through B.

Complete behavior as a Prandtl-Reuss body is also unlikely, since in that case, if after the course AC the arc CH was followed (Fig. 6), the latter course would involve another ratio of the stress deviator components (another direction of Γ_0), while no plastic deformations would occur. As with constant elastic shearing energy, the sum of the squares of the principal shearing stresses is also constant,

$$\tau_1^2 + \tau_2^2 + \tau_3^2 = \text{const.}$$

a rotation of the stress vector Γ_0 will involve an increase of the shearing stresses in one part of the planes and a decrease in the other part. It is plausible to assume that, in the planes where the shearing stress increases, about the same plastic shearing strains will occur as when the final state of stress is applied directly, because much smaller shearing stresses are sufficient for plastic shearing strains in the domain of strain hardening below the yield stress. This leads to the assumption that, for example, with the excess deformation course CD the plastic deformation is about BF, so that the direction of the total plastic deformation vector AF is between that of the original stress vector Γ_0 and that of the resulting stress vector Γ_{03}. This would mean that only part SB of the preceding plastic deformation AB is remembered (Fig. 6). If, at the same time with its rotation, the length of the stress vector—i.e., the shearing energy—increases, as in the case of strain hardening, the shearing stress will increase in most planes, so that a more complete behavior as a Hencky body could be expected. More generally, this will be the case if, even at the yield stress, the plastic shearing strain, belonging to the new total deformation, if reached directly with constant ratio of the deviator components, is larger in most planes than with the original deformation—e.g., if the deformation course deviates only slightly from the direction of the stress deviator vector. This will be possible indeed if one observes that, in the same way that Shanley[18] showed for bars, the load, or here more generally the shortening, increases at the same time that the plate buckles.

A confirmation of this conception is also given by recent tests on tubular specimens of medium steel by Fraenkel.[19] Representing these tests as shown in Fig. 8, where the deformation course is projected on the $\bar{\epsilon}_z - \bar{\epsilon}_t$ plane, it follows from his Fig. 11 that with plastic deformation or plastic flow, respectively, the stress deviator in the points 1–6 of the total deformation course would be represented by the vectors Γ_{01} and Γ_{02}, respectively. From Fraenkel's tests,* however, the present author computed the actual vectors Γ_{0t}. From the vectors in points 3 and 4, of which the continuation passes through S_3 and S_4, respectively, it follows that the material remembers practically free plastic deformations S_3B or S_4B of 3 to 6 times the elastic deformation B-2.

That the results of buckling tests agree with the use of preceding plastic deformations (value e) may be due to some extent to the fact that the sliding in the crystallites, being caused by a migration of Taylor's dislocations, is also going through from one state of equilibrium to another, so that with extremely small deformations some elastic decrease of the plastic sliding in planes with decreasing shearing stress could be possible.

From Fig. 5, where it is consequently assumed that at D vector Γ_{01}, of which the continuation passes through A, applies, it follows furthermore that the more the direction of the excess deformation course CD deviates from that of the initial course AC, the more the direction of Γ_{01} will deviate from that of Γ_0 and the larger the excess stress deviator vector $\Delta_1\Gamma_0$ will be. Hence, the excess stress and thus the resistance to buckling will be the higher the more the proportions of the excess deviator components, by buckling, differ from the proportions of the original deviator components, before buckling.[21,24] This will be demonstrated by comparing plastic buckling stresses for several cases of loading and boundary conditions (Table 1).

Derivation of Stress-Strain Relations

In order to find the buckling stresses in the plastic domain, it is assumed that with pure compression an arbitrary relation exists between the stress σ and the plastic strain ϵ_p (Fig. 9), so that

$$\sigma/\epsilon_p = E_p \qquad \text{and} \qquad d\sigma/d\epsilon_p = \tan\varphi \tag{8}$$

With a complete memory of the material the components of the total plastic strain are proportional to the components of the resulting stress deviator (in Fig. 5 the straight line AE is in the continuation of Γ_{01}), so that by analogy with the elastic domain

$$\left.\begin{aligned} \epsilon_{xp} = \bar{\sigma}_x/2G_p, \quad \epsilon_{yp} = \bar{\sigma}_y/2G_p, \quad \epsilon_{zp} = \bar{\sigma}_z/2G_p \\ (1/2)\gamma_{xyp} = \tau_{xy}/2G_p, \text{ etc.} \end{aligned}\right\} \tag{9}$$

With these relations Eq. (6) yields

* Mr. Fraenkel kindly informed the author which points of his stress and strain curves belong to each other.

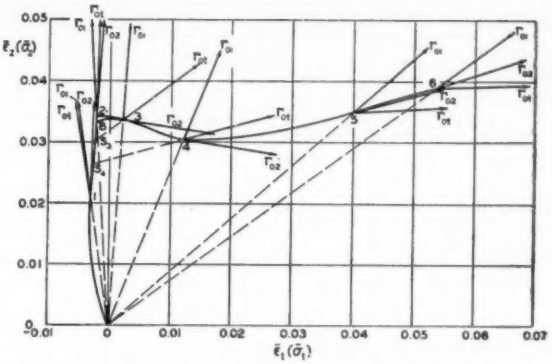

FIG. 8. Determination of representative vectors of the stress deviators for a strain deviator path 0-1-2-3-4-5-6 according to tests by Fraenkel (plastic deformation Γ_{01}, plastic flow Γ_{02}, tests Γ_{0t}).

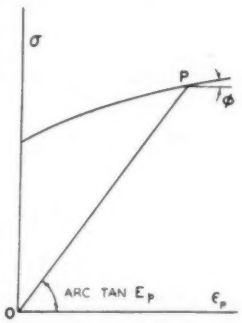

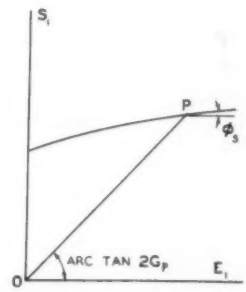

FIG. 9 (*left*). Relation between stress and plastic strain. FIG. 10 (*right*). Relation between S_1 and E_1.

TABLE 1

Cases of Buckling with Decreasing Difference Between the Ratios of the Deviator Components of the Superposed (by Buckling) and the Initial State of Strain (Before Buckling).

Case	Boundary conditions and loading	$\beta = \sigma_2/\sigma_1$	Ratio σ_B/σ_E or τ_B/τ_E with buckling just below the yield stress
1		0	0.878
2		0	0.830
3		0	0.804
4		0	0.778
5		−1	0.775
6		−1	0.747
7		1	0.612
8		1	0.612
9		0	0.530
10		1	0.488
11		½	0.446
12		0	0.417

$$S_1 = 2G_pE_1 \tag{10}$$

in which

$$E_1 = \frac{}{\sqrt{\epsilon_{xp}^2 + \epsilon_{yp}^2 + \epsilon_{zp}^2 + (1/2)(\gamma_{xyp}^2 + \gamma_{yzp}^2 + \gamma_{zxp}^2)}} \tag{11}$$

According to tests of Lode,[11] Roš-Eichinger,[12] and others, with constant ratio of the deviator components a definite relation $S_1 = \Phi(E_1)$ exists between S_1 and E_1 (Fig. 10), practically independent of the state of stress. As with a complete memory of the material the plastic strains are the same as if the deviator components had increased in their resulting ratios, the same relation refers to the present problem. Tests that have been performed since confirm this. With pure compression (Fig. 9), it follows from Eqs. (6) and (11) that $S_1 = \sigma\sqrt{2/3}$ and $E_1 = \epsilon_p\sqrt{3/2}$, so that

$$S_1 = (2/3)E_1\sigma/\epsilon_p = (2/3)E_pE_1$$

which is in accordance with Eq. (10), as with plastic deformation Poisson's ratio $\nu = 1/2$ and $G_p = E_p/3$. Furthermore, it follows from Figs. 9 and 10 that $\tan \varphi_s = (2G_p/E_p) \tan \varphi = 2/3 \tan \varphi$. In order to be able to investigate, besides plates and shells, also three-dimensional cases of plastic stability, the general relations were established between excess strains and excess stresses. Writing the excess strains that occur with buckling as total differentials gives

$$\left.\begin{aligned}
d\epsilon_x &= \frac{\partial\epsilon_x}{\partial\sigma_x}d\sigma_x + \frac{\partial\epsilon_x}{\partial\sigma_y}d\sigma_y + \frac{\partial\epsilon_x}{\partial\sigma_z}d\sigma_z + \frac{\partial\epsilon_x}{\partial\tau_{xy}}d\tau_{xy} + \frac{\partial\epsilon_x}{\partial\tau_{yz}}d\tau_{yz} + \frac{\partial\epsilon_x}{\partial\tau_{zx}}d\tau_{zx}\\
d\epsilon_y &= \frac{\partial\epsilon_y}{\partial\sigma_x}d\sigma_x + \frac{\partial\epsilon_y}{\partial\sigma_y}d\sigma_y + \frac{\partial\epsilon_y}{\partial\sigma_z}d\sigma_z + \frac{\partial\epsilon_y}{\partial\tau_{xy}}d\tau_{xy} + \frac{\partial\epsilon_y}{\partial\tau_{yz}}d\tau_{yz} + \frac{\partial\epsilon_y}{\partial\tau_{zx}}d\tau_{zx}\\
d\epsilon_z &= \frac{\partial\epsilon_z}{\partial\sigma_x}d\sigma_x + \frac{\partial\epsilon_z}{\partial\sigma_y}d\sigma_y + \frac{\partial\epsilon_z}{\partial\sigma_z}d\sigma_z + \frac{\partial\epsilon_z}{\partial\tau_{xy}}d\tau_{xy} + \frac{\partial\epsilon_z}{\partial\tau_{yz}}d\tau_{yz} + \frac{\partial\epsilon_z}{\partial\tau_{zx}}d\tau_{zx}\\
d\gamma_{xy} &= \frac{\partial\gamma_{xy}}{\partial\sigma_x}d\sigma_x + \frac{\partial\gamma_{xy}}{\partial\sigma_y}d\sigma_y + \frac{\partial\gamma_{xy}}{\partial\sigma_z}d\sigma_z + \frac{\partial\gamma_{xy}}{\partial\tau_{xy}}d\tau_{xy} + \frac{\partial\gamma_{xy}}{\partial\tau_{yz}}d\tau_{yz} + \frac{\partial\gamma_{xy}}{\partial\tau_{zx}}d\tau_{zx}\\
d\gamma_{yz} &= \frac{\partial\gamma_{yz}}{\partial\sigma_x}d\sigma_x + \frac{\partial\gamma_{yz}}{\partial\sigma_y}d\sigma_y + \frac{\partial\gamma_{yz}}{\partial\sigma_z}d\sigma_z + \frac{\partial\gamma_{yz}}{\partial\tau_{xy}}d\tau_{xy} + \frac{\partial\gamma_{yz}}{\partial\tau_{yz}}d\tau_{yz} + \frac{\partial\gamma_{yz}}{\partial\tau_{zx}}d\tau_{zx}\\
d\gamma_{zx} &= \frac{\partial\gamma_{zx}}{\partial\sigma_x}d\sigma_x + \frac{\partial\gamma_{zx}}{\partial\sigma_y}d\sigma_y + \frac{\partial\gamma_{zx}}{\partial\sigma_z}d\sigma_z + \frac{\partial\gamma_{zx}}{\partial\tau_{xy}}d\tau_{xy} + \frac{\partial\gamma_{zx}}{\partial\tau_{yz}}d\tau_{yz} + \frac{\partial\gamma_{zx}}{\partial\tau_{zx}}d\tau_{zx}
\end{aligned}\right\} \tag{12}$$

in which the strains may be split in an elastic and plastic part,

$$\left.\begin{aligned}
\epsilon_x &= \epsilon_{xe} + \epsilon_{xp}\\
\partial\epsilon_x/\partial\sigma_x &= (\partial\epsilon_{xe}/\partial\sigma_x) + (\partial\epsilon_{xp}/\partial\sigma_x)
\end{aligned}\right\} \tag{13}$$

It is evident that

$$\frac{\partial\epsilon_{xe}}{\partial\sigma_x} = \frac{1}{E},\quad \frac{\partial\epsilon_{ye}}{\partial\sigma_x} = \frac{\partial\epsilon_{xe}}{\partial\sigma_y} = -\frac{\nu}{E},\quad \frac{\partial\gamma_{xye}}{\partial\tau_{xy}} = \frac{1}{G},\quad \frac{\partial\gamma_{yze}}{\partial\tau_{xy}} = \frac{\partial\gamma_{xye}}{\partial\tau_{yz}} = 0 \tag{14}$$

ν being Poisson's ratio in the elastic domain. In order to compute the partial derivatives of the plastic strains—e.g., $\partial\epsilon_{xp}/\partial\sigma_x = (\partial/\partial\sigma_x)(\bar{\sigma}_x/2G_p)$, it is remarked that both $\bar{\sigma}_x$ and G_p vary. Thus, it is found that

$$\frac{\partial\bar{\sigma}_x}{\partial\sigma_x} = \frac{2}{3},\quad \frac{\partial\bar{\sigma}_y}{\partial\sigma_x} = -\frac{1}{3},\quad \frac{\partial S_1}{\partial\sigma_x} = \frac{\bar{\sigma}_x}{S_1} \tag{15}$$

while, according to Fig. 10,

$$\frac{\partial}{\partial\sigma_x}\frac{1}{G_p} = \frac{\partial}{\partial\sigma_x}\frac{2E_1}{S_1} = 2\frac{d(E_1/S_1)}{dS_1}\frac{\partial S_1}{\partial\sigma_x} = 2\frac{S_1(dE_1/dS_1) - E_1}{S_1^2}\frac{\bar{\sigma}_x}{S_1} =$$

$$2\frac{(S_1/\tan\varphi_s) - E_1}{S_1^2}\frac{\bar{\sigma}_x}{S_1} = \frac{\bar{\sigma}_x}{S_1^2G_p}\left(\frac{2G_p}{\tan\varphi_s} - 1\right) \tag{16}$$

Hence, it follows that

$$\left.\begin{aligned}
\frac{\partial \epsilon_{xp}}{\partial \sigma_x} &= \frac{\partial}{\partial \sigma_x}\frac{\bar{\sigma}_x}{2G_p} = \frac{1}{2G_p}\frac{\partial \bar{\sigma}_x}{\partial \sigma_x} + \frac{\bar{\sigma}_x}{2}\frac{\partial}{\partial \sigma_x}\left(\frac{1}{G_p}\right) = \frac{1}{E_p} + \frac{\bar{\sigma}_x^2}{2S_1^2G_p}\left(\frac{2G_p}{\tan\varphi_s} - 1\right)\\
\frac{\partial \epsilon_{yp}}{\partial \sigma_x} &= \frac{\partial}{\partial \sigma_x}\frac{\bar{\sigma}_y}{2G_p} = \frac{1}{2G_p}\frac{\partial \bar{\sigma}_y}{\partial \sigma_x} + \frac{\bar{\sigma}_y}{2}\frac{\partial}{\partial \sigma_x}\left(\frac{1}{G_p}\right) = -\frac{1}{2E_p} + \frac{\bar{\sigma}_x\bar{\sigma}_y}{2S_1^2G_p}\left(\frac{2G_p}{\tan\varphi_s} - 1\right) = \frac{\partial \epsilon_{xp}}{\partial \sigma_y}\\
\frac{\partial \gamma_{xyp}}{\partial \sigma_x} &= \frac{\partial}{\partial \sigma_x}\frac{\tau_{xy}}{G_p} = \frac{\bar{\sigma}_x\tau_{xy}}{S_1^2G_p}\left(\frac{2G_p}{\tan\varphi_s} - 1\right.
\end{aligned}\right\} \tag{17}$$

In the same way it is found that

$$\left.\begin{aligned}
\frac{\partial}{\partial \tau_{xy}}\frac{1}{G_p} &= \frac{2\tau_{xy}}{S_1^2G_p}\left(\frac{2G_p}{\tan\varphi_s} - 1\right)\\
\frac{\partial \epsilon_{xp}}{\partial \tau_{xy}} &= \frac{\bar{\sigma}_x\tau_{xy}}{S_1^2G_p}\left(\frac{2G_p}{\tan\varphi_s} - 1\right) = \frac{\partial \gamma_{xyp}}{\partial \sigma_x}\\
\frac{\partial \gamma_{xyp}}{\partial \tau_{xy}} &= \frac{1}{G_p} + \frac{2\tau_{xy}^2}{S_1^2G_p}\left(\frac{2G_p}{\tan\varphi_s} - 1\right)\\
\frac{\partial \gamma_{yzp}}{\partial \tau_{xy}} &= \frac{2\tau_{xy}\tau_{yz}}{S_1^2G_p}\left(\frac{2G_p}{\tan\varphi_s} - 1\right) = \frac{\partial \gamma_{xyp}}{\partial \tau_{yz}}
\end{aligned}\right\} \tag{18}$$

For convenience the axes of the excess state of stress are placed in the directions of the principal axes of the original one. By this the original shearing stresses τ_{xy}, τ_{yz}, and τ_{zx} disappear in Eqs. (17) and (18), with the result that all partial derivatives of shearing strains γ or with respect to shearing stresses τ become zero, except for the case in which τ and γ have equal subscripts.

In this way it follows from Eqs. (12), after using Eqs. (13), (14), (17), and (18), with $E_p = E/e$ and denoting differentials such as $d\sigma_x$ by σ_x', that*

$$\left.\begin{aligned}
\epsilon_x' &= \left(\frac{1+e}{E} + \frac{3\bar{\sigma}_x^2}{2S_1^2}\frac{E - e\tan\varphi}{E\tan\varphi}\right)\sigma_x' + \left(-\frac{2\nu+e}{2E} + \frac{3\bar{\sigma}_x\bar{\sigma}_y}{2S_1^2}\frac{E - e\tan\varphi}{E\tan\varphi}\right)\sigma_y' +\\
&\qquad \left(-\frac{2\nu+e}{2E} + \frac{3\bar{\sigma}_x\bar{\sigma}_z}{2S_1^2}\frac{E - e\tan\varphi}{E\tan\varphi}\right)\sigma_z'\\
\epsilon_y' &= \left(-\frac{2\nu+e}{2E} + \frac{3\bar{\sigma}_x\bar{\sigma}_y}{2S_1^2}\frac{E - e\tan\varphi}{E\tan\varphi}\right)\sigma_x' + \left(\frac{1+e}{E} + \frac{3\bar{\sigma}_y^2}{2S_1^2}\frac{E - e\tan\varphi}{E\tan\varphi}\right)\sigma_y' +\\
&\qquad \left(-\frac{2\nu+e}{2E} + \frac{3\bar{\sigma}_y\bar{\sigma}_z}{2S_1^2}\frac{E - e\tan\varphi}{E\tan\varphi}\right)\sigma_z'\\
\epsilon_z' &= \left(-\frac{2\nu+e}{2E} + \frac{3\bar{\sigma}_x\bar{\sigma}_z}{2S_1^2}\frac{E - e\tan\varphi}{E\tan\varphi}\right)\sigma_x' + \left(-\frac{2\nu+e}{2E} + \frac{3\bar{\sigma}_y\bar{\sigma}_z}{2S_1^2}\frac{E - e\tan\varphi}{E\tan\varphi}\right)\sigma_y' +\\
&\qquad \left(\frac{1+e}{E} + \frac{3\bar{\sigma}_z^2}{2S_1^2}\frac{E - e\tan\varphi}{E\tan\varphi}\right)\sigma_z'\\
\gamma_{xy}' &= \frac{2+2\nu+3e}{E}\tau_{xy}', \quad \gamma_{yz}' = \frac{2+2\nu+3e}{E}\tau_{yz}', \quad \gamma_{zx}' = \frac{2+2\nu+3e}{E}\tau_{zx}'
\end{aligned}\right\} \tag{19}$$

Inversely expressing the differentials of the stresses in terms of the strains, expressions of the following form were obtained:

$$\left.\begin{aligned}
\sigma_x' &= C_{11}\epsilon_x' + C_{12}\epsilon_y' + C_{13}\epsilon_z'\\
\sigma_y' &= C_{12}\epsilon_x' + C_{22}\epsilon_y' + C_{23}\epsilon_z'\\
\sigma_z' &= C_{13}\epsilon_x' + C_{23}\epsilon_y' + C_{33}\epsilon_z'\\
\tau_{xy}' &= C_{44}\gamma_{xy}'\\
\tau_{yz}' &= C_{55}\gamma_{yz}'\\
\tau_{zx}' &= C_{66}\gamma_{zx}'
\end{aligned}\right\} \tag{20}$$

in which the constants C are rather extensive and will not be written down here. However,

* Consequently, value $e = E/E_p = (\sigma/\epsilon_e)/(\sigma/\epsilon_p) = \epsilon_p/\epsilon_e$, in which ϵ_p and ϵ_e are the plastic and elastic strains, respectively, for the equivalent pure compressive stress $\sigma = \sqrt{\sigma_x^2 - \sigma_x\sigma_y + \sigma_y^2}$ at which the plate buckles.

$$C_{44} = C_{55} = C_{66} = E/(2 + 2\nu + 3e)$$

Thus, apparently the deformation is governed by seven different constants. This anistropic behavior is between the elastic behavior of a crystal of the rhombic and one of the regular system. In the regular system the number of constants is diminished from nine to three with respect to the rhombic system, because of the equivalence of the three axes. In the present case, however, this equivalence exists only for the shearing stresses, so that only $C_{44} = C_{55} = C_{66}$, by which $9 - 2 = 7$ constants remain.

In order to study three-dimensional cases of plastic stability, relations (20) may be inserted in the differential equations of the general theory of elastic stability of Biezeno and Hencky.[20–22]

With plane states of stress, as occur in plates and shells, in Eq. (19) σ_z' is zero, while ϵ_z' does not interest us. Expressing $\bar{\sigma}_x$, $\bar{\sigma}_y$ and S_1^2 in terms of the principal stresses $\sigma_x = \rho_1$ and $\sigma_y = \rho_2$, while σ_z is zero, it is seen that

$$\bar{\sigma}_x = \frac{1}{3}(2\rho_1 - \rho_2), \quad \bar{\sigma}_y = \frac{1}{3}(2\rho_2 - \rho_1), \quad S_1^2 = \frac{2}{3}(\rho_1^2 - \rho_1\rho_2 + \rho_2^2)$$

Expressing again the excess stresses in terms of the excess strains, it follows now from Eqs. (19) that

$$\left.\begin{aligned}
&\sigma_x' = E(A\epsilon_x' + B\epsilon_y'), \quad \sigma_y' = E(B\epsilon_x' + D\epsilon_y') \\
&\text{in which } A = \varphi_1/\varphi_4, \quad B = \varphi_2/\varphi_4, \quad D = \varphi_3/\varphi_4 \\
&\text{and} \quad \varphi_1 = (1 - 2\beta)^2E + (4\eta^2 + 3e)\tan\varphi \\
&\qquad \varphi_2 = (2 - \beta)(1 - 2\beta)E + (4\nu\eta^2 + 3e\beta)\tan\varphi \\
&\qquad \varphi_3 = (2 - \beta)^2E + (4\eta^2 + 3e\beta^2)\tan\varphi \\
&\qquad \varphi_4 = [(5 - 4\nu)(1 + \beta^2) + 2(5\nu - 4)\beta + 3e\eta^2]E + \\
&\qquad\qquad \{4(1 - \nu^2)\eta^2 + 3e[\eta^2 + (1 - 2\nu)\beta]\}\tan\varphi \\
&\qquad \beta = \rho_2/\rho_1 \text{ and } \eta^2 = \beta^2 - \beta + 1 \\
&\text{while} \quad \tau_{xy}' = [E/(2 + 2\nu + 3e)]\gamma_{xy}' = EF\gamma_{xy}'
\end{aligned}\right\} \quad (21)$$

In reference 13 the author derived these same equations in another way—namely, by subtracting the initial stresses and strains before buckling from the total stresses and strains after buckling.

In Eqs. (21) values A, B, and D may also be expressed in terms of the tangent modulus $E_t = d\sigma/d\epsilon$ instead of in terms of

$$\tan\varphi = d\sigma/d\epsilon_p = d\sigma/(d\epsilon - d\epsilon_e) = 1/[(1/E_t) - (1/E)] = EE_t/(E - E_t)$$

Introducing this expression for $\tan\varphi$ in Eqs. (21) it follows that

$$\left.\begin{aligned}
&A = \psi_1/\psi_4, \quad B = \psi_2/\psi_4, \quad D = \psi_3/\psi_4 \\
&\text{in which } \psi_1 = (1 - 2\beta)^2E + 3(1 + e)E_t \\
&\psi_2 = (2 - \beta)(1 - 2\beta)E - [(2 - \beta)(1 - 2\beta) - 4\nu\eta^2 - 3e\beta]E_t \\
&\psi_3 = (2 - \beta)^2E + 3(1 + e)\beta^2E_t \\
&\psi_4 = [(5 - 4\nu)(1 + \beta^2) + 2(5\nu - 4)\beta + 3e\eta^2]E - \\
&\qquad (1 - 2\nu)[(1 - 2\nu)\eta^2 - 3(1 + e)\beta]E_t
\end{aligned}\right\} \quad (21a)$$

while $e = (E/E_s) - 1$, in which E_s is the secant modulus.

Derivation of the Differential Equation for Plastic Buckling of Plates

In order to derive the differential equation for plate buckling, the stress distribution in the buckling plate has to be examined. As was shown by the author,[13] when buckling occurs at the yield stress, the entire plate deforms plastically. Furthermore, Chwalla showed that with rectangular bars a strain reversal in the plastic domain according to the Engesser-Kármán theory will only occur if the eccentricity is less than 1/50 of the thickness. In practical cases one has to take into account larger eccentricities, so that from the beginning the author contended that it was logical to base the allowable buckling stresses for bars as well as for plates on a completely plastic behavior.[14, 23, 25] The partially elastic behavior has only academic value and does not influence at all the real buckling stresses with the existing eccentricities. It is, therefore, logical to take for the critical stress of columns $\sigma_c = \pi^2E_t/\lambda^2$, in which $E_t = d\sigma/d\epsilon$ is the tangent modulus. This is in agreement with general practice in aeronautical engineering. Shanley[18] has shown that even a centrically loaded column cannot remain straight above this critical stress, while according to tests the maximum stress does practically not surpass σ_c. Consequently, there is still more reason to assume that for plates and shells the buckling stress is equal to that which would occur if the entire plate deformed plastically. With the infinitesimal deflections assumed for buckling this leads to a linear stress distribution, so that the bending

and twisting moments can be expressed in terms of the excess stresses. If, for example, σ_x' is the stress at the boundary, the bending moment is $M_x' = (h^2/6)\sigma_x'$. After using Eqs. (21) and expressing the strains in terms of the deflections w, so that ϵ_x' at the boundary is, for example, $-(1/2)h\partial^2 w/\partial x^2$, this leads to the bending and twisting moments

$$\left.\begin{aligned} M_x' &= -EI\left(A\frac{\partial^2 w}{\partial x^2} + B\frac{\partial^2 w}{\partial y^2}\right) \\ M_y' &= -EI\left(B\frac{\partial^2 w}{\partial x^2} + D\frac{\partial^2 w}{\partial y^2}\right) \\ M_{xy}' &= -M_{yx}' = 2EIF\frac{\partial^2 w}{\partial x \partial y} \end{aligned}\right\} \quad (22)$$

in which I is the moment of inertia $h^3/12$ of the plate.

After insertion of these values in the well-known condition of equilibrium with reference to a translation in the z-direction,

$$\frac{\partial^2 M_x'}{\partial x^2} - 2\frac{\partial^2 M_{xy}'}{\partial x \partial y} + \frac{\partial^2 M_y'}{\partial y^2} = h\rho_1\frac{\partial^2 w}{\partial x^2} + h\rho_2\frac{\partial^2 w}{\partial y^2}$$

the following governing differential equation for the plastic buckling of plates is obtained:[13]

$$EI\left[A\frac{\partial^4 w}{\partial x^4} + 2(B+2F)\frac{\partial^4 w}{\partial x^2 \partial y^2} + D\frac{\partial^4 w}{\partial y^4}\right] + h\rho_1\frac{\partial^2 w}{\partial x^2} + h\rho_2\frac{\partial^2 w}{\partial y^2} = 0 \quad (23)$$

In a similar way the differential equations for the buckling of shells may be derived.[24,25]

Buckling Stresses of Plates and Shells with Various Loading and Boundary Conditions

With these differential equations the buckling stresses for various loading and boundary conditions have been determined.[14,23,24] In order to show that indeed the plastic buckling stress σ_B is higher as compared to that in the elastic domain, σ_E, the more the ratio of the deviator components, as superposed by buckling, differs from that of the original deviator components. In Table 1 the ratio σ_B/σ_E is given for twelve cases for mild steel buckling just below the yield stress.[21,22,24]

With Case 1 for example, an infinitely long plate subjected to compression in axial direction, of which one unloaded side is simply supported while the other one is free, with buckling pure shearing stresses are superimposed on the original pure compressive stresses, yielding a high ratio σ_B/σ_E. With Case 2, besides the shearing stresses of the twisting moments, bending stresses σ_x' and σ_y' are superposed on the original compressive stresses σ_x, so that σ_B/σ_E is somewhat less. For Cases 3 and 4, again, the twisting moments are less pronounced. With Cases 5 and 6, bending stresses σ_x' and σ_y' are superposed on the original shearing stresses, but with Case 6 the shearing stresses due to the twisting moments are more pronounced. Therefore, for Case 6, the ratio τ_B/τ_E is smaller than for Case 5, because in both of these cases the resistance to shearing stresses is the smaller one. With Case 10, for example, with buckling biaxial bending stresses are superposed on the original ones, yielding a small ratio σ_B/σ_E. With buckling of a bar, Case 12, exactly the same state of stress is superposed on the original one, so that the ratio σ_B/σ_E is as small as possible.*

The theory proved to be in splendid accordance with the beautiful and systematic tests on plates of avional, an aluminum alloy, as published by Kollbrunner in Zürich 8 years later.[30] The number of half waves in which the plates buckled proves that the plates behaved anisotropically to the same extent as predicted by the author's theory.

In Tables 2, 3, and 4 the data for the Cases 2, 3, and 4, as given in Table 1, with lengths a and widths b, have been compiled. According to the theory the number of half waves is p_B, while $a_L - a_L$ represents the limiting lengths between which this number of half waves will occur. The number of half waves as found by Kollbrunner from his tests is given by p_T, followed

* When the author wanted to apply his theory to the buckling of the webs of built-up sections of compression members, he came to the conclusion that the existing theories of Bleich[26] and Chwalla[27] on this matter were incorrect in the *elastic* domain, since they did not take into account in the right way the restraining action of vertical and horizontal plates upon each other. Therefore he developed an exact theory of the buckling of those sections by writing down the general solution of the differential equation for the deflection surfaces of vertical, as well as horizontal, plates after which the conditions for the connection of all plates yield the buckling condition.[23,26,29] This theory also takes account of the fact that, in general, with buckling of the webs the intersection lines of the middle surfaces of the plates do not remain straight. For soft steel design, formulas were derived for the ratios b/h of the webs as a function of the slenderness ratios l/r of the members, which were chosen in such a way that the buckling stress of the webs is equal to that of the members as a whole.[23,29]

Table 2

a	$3.2\,b$	$4.85\,b$	$6.45\,b$	$8.1\,b$
$a_L - a_L$	$2.49\,b - 3.40\,b$	$4.31\,b - 5.21\,b$	$6.10\,b - 6.98\,b$	$7.87\,b - 8.75\,b$
p_B	3	5	7	9
p_T	3 (3)	5 (3)	7 (3)	9 (3)

Table 3

a	$3.8\,b$	$5.65\,b$	$7.55\,b$	$9.45\,b$
$a_L - a_L$	$3.36\,b - 4.05\,b$	$5.44\,b - 6.12\,b$	$7.50\,b - 8.20\,b$	$8.88\,b - 9.56\,b$
p_B	5	8	11	13
p_T	5 (1), 6 (3)	8 (3)	10 (1), 11 (2)	13 (1), 14 (2)

Table 4

a	$4.55\,b$	$6.80\,b$	$9.10\,b$	$11.35\,b$
$a_L - a_L$	$4.11\,b - 4.58\,b$	$6.43\,b - 6.88\,b$	$8.73\,b - 9.19\,b$	$11.04\,b - 11.50\,b$
p_B	9	14	19	24
p_T	9 (3)	13 (2), 14 (1)	18 (2), 19 (1)	24 (3)

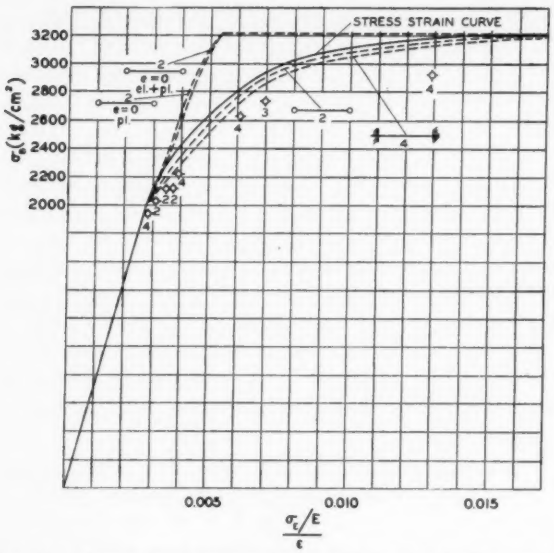

FIG. 11. Comparison between theory and tests by Kollbrunner and Stüssi.

by the number of tests in brackets. The conformity between theory and tests is better than could be demanded.

The stress-strain curve of the avional used is given by the full curve in Fig. 11. In the same figure the buckling stress σ_B is plotted as a function of σ_E/E, as is customary in this country. The tangent modulus curve gives the buckling stress for bars (Case 12, Fig. 13), while the stress strain curve would apply for plates if the ratio σ_B/σ_E were equal to the ratio E_s/E, in which E_s is the secant modulus, as proposed by Gerard.[38]

For Case 2 (Table 1) the plastic buckling stress is[14,23]

$$\sigma_B = (2\pi^2 EI/hb^2)\ (\sqrt{AD} + B + 2F)$$

while in the elastic domain, with $\nu = 0.3$, the coefficient of the last term is equal to 2.2, so that the ratio σ_B/σ_E given in Table 5 is obtained.

The exact buckling stress for Case 4 follows from a transcendental equation[14,23,29] but may be written sufficiently accurately, as given in Table 5.[31]

In Fig. 11 the plate compressive curves (buckling stresses) according to these formulas are given for Cases 2 and 4. The curve for Case 3, not shown, falls between the curves for Cases 2 and 4. The average values of Kollbrunner's tests are given by the open circles, denoted by the case in question. Tables 2, 3, and 4 refer to the tests indicated by the highest circle 2 and circles 3 and 4, respectively. The discrepancies in the bucking stresses are apparently due to unavoidable eccentricities. The exact conformity between the theoretical and experimental half waves may be explained by the fact that these eccentricities affect the rigidity of the plates in both directions to practically the same extent.

New tests, executed in Zürich with an improved apparatus, are given in Fig. 11 by the three full circles, and these give still better agreement.[31]

If the material had no memory at all for preceding plastic deformations (plastic flow), value e would have to be equated to zero in Eq. (21).[14] Assuming the entire plate to be plastic, this would lead, for Case 2, to the curve denoted by 2, $e = 0$, pl. According to the tests this curve would apparently overestimate the buckling stress considerably. Still higher buckling stresses would result if at the same time elastic regions according to the Engesser-Kármán theory were assumed (curve 2, $e = 0$, el. + pl.).

A still better agreement with the author's theory is shown by the results of tests with Z- and H- sections and channels in extruded aluminum alloys, as published

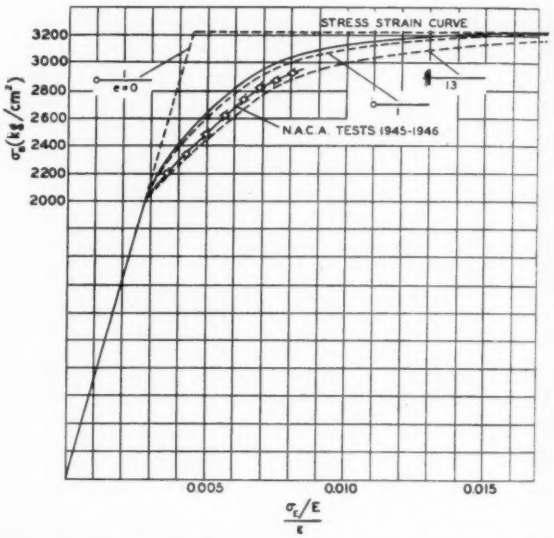

FIG. 12. Comparison between theory and tests by N.A.C.A.

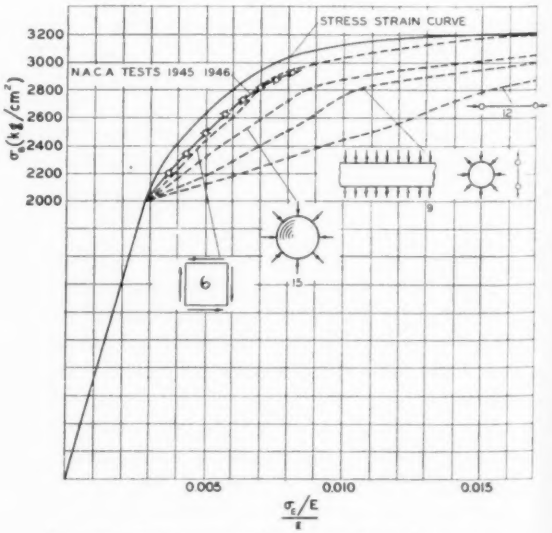

FIG. 13. Plate compressive curves for various cases.

by the N.A.C.A.[41–46] Using the method given by Schuette and McDonald,[32] the plate compressive curve that would follow from these tests for avional (with a stress strain curve according to the full curves in Figs. 11, 12, and 13) is given in Figs. 12 and 13 by the full curve connecting the eight circles. If the width to thickness ratio of the flanges is more than about one-third of that of the web, the flanges will be elastically built in by the web, so that the circles should be situated between the theoretical curves for Cases 1 and 13, Table 5, with one unloaded side free and the other simply supported and clamped, respectively.

For Case 1 and sufficiently long buckling length, the buckling stress is [24,33]

$$\sigma_B = EFh^2/b^2$$

while in the elastic domain $F = 1/2(1 + \nu) = 1/2.6$, so that the ratio σ_B/σ_E is as given in Table 5. The corresponding plate compressive curve in Fig. 12 is denoted by 1. If Poisson's ratio for elastic deformations were equated to 0.5, according to Eq. (21) value F would be equal to $1/3(1 + e)$, while in the elastic domain, with $e = 0$, it would be $1/3$, which would yield a ratio

$$\sigma_B/\sigma_E = 1/(1 + e) = E_s/E$$

since in the author's notation the secant modulus E_s is equal to $E/(1 + e)$. In this case the plate compressive curve for Case 1 would coincide with the stress-strain diagram.

For Case 13 (Table 5) the buckling stress may be calculated approximately according to the energy method in order to find it in explicit form. As only the ratio between plastic and elastic buckling stress is needed, the accuracy of this ratio will still be sufficient. It follows that the ratio will be that given in Table 5. It may be stated that here, in contradiction to other cases of plate buckling, a higher value of B, representing the lateral contraction, involves a lower value of σ_B. This is a consequence of the fact that in this case the plate buckles according to an anticlastic surface, so that the higher the ratio of lateral contraction, the more the curvatures in longitudinal and lateral directions will promote each other. The plate compressive curve for this case is denoted in Fig. 12 by Case 13.

The experimental N.A.C.A. curve is between the theoretical curves for Cases 1 and 13, indicating agreement between theory and tests.

Assuming plastic flow ($e = 0$), the theoretical curve for Case 1 would be a straight line (line 1, $e = 0$ in Fig. 12), predicting apparently much too high buckling stresses.

In case the width to thickness ratio of the flanges is less than one-third of that of the web, the latter will be less buckling proof and will behave as elastically built in by the flanges. The theoretical curve would be situated between the curves for Cases 2 and 4 in Fig. 11, so that here also good agreement between theory and tests exists.

TABLE 5

CASE	BOUNDARY CONDITIONS AND LOADING	$\beta = \rho_2/\rho_1$	RATIO σ_B/σ_E OR τ_B/τ_E
1	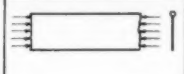	0	2.6F
2	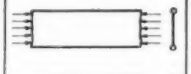	0	$0.455(\sqrt{AD}+B+2F)$
4	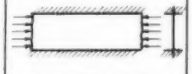	0	$0.598\sqrt{AD}+0.312(B+2F)$
13	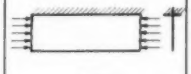	0	$0.473(\sqrt{AD}+2.97F-0.405B)$
6		-1	$6.71(A+B+2F)\sqrt{\frac{41A+9(B+2F)}{8249A+2601(B+2F)}}$
9	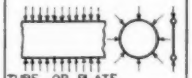 TUBE OR PLATE	0	0.91A
12	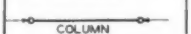 COLUMN	0	E_t/E
14	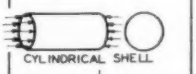 CYLINDRICAL SHELL	0	$\sqrt{0.91(AD-B^2)}$
15	SPHERICAL SHELL	1	$\sqrt{0.91(A^2-B^2)}$

It follows, however, from Table 1 that for other cases the ratios σ_B/σ_E or τ_B/τ_E may be much lower. The general formulas for these ratios are given in Table 5 for the Cases 6, 9, and 12 of Table 1,[14,24] for a cylindrical shell under uniform axial compression[24,25] (Case 14), and for a uniformly compressed spherical shell (Case 15), both for buckling symmetrically with respect to the axis or a diameter, respectively. The corresponding curves for Cases 6, 9, 12, and 15 are given in Fig. 13, the lowest curve, that for a bar (Case 12), being determined by the tangent modulus.*

It may be observed that, in order to compute the ratios for Cases 14 and 15 as given in Table 5, the buckling stress was assumed to be a continuous function of the wave length, while in the latter case smaller terms were neglected, both as usual in the elastic domain. Therefore, these two ratios do not apply exactly for the extreme case of buckling at the yield stress, where $\tan \varphi$ is zero, for which both ratios appear to become zero just as for a bar. This may be understood, since, for example, for a cylinder the corresponding most unfavorable buckling length (half wave length) is infinite, so that the strips parallel to the axis would

* For Cases 6 and 15 in Fig. 13, values of σ_B and σ_E refer to the equivalent pure compressive stresses $\sigma = \sqrt{\sigma_x^2 - \sigma_x\sigma_y + \sigma_y^2 + 3\tau_{xy}^2}$ under which the plate buckles.

have no proper buckling strength. If, furthermore, the shell buckles symmetrically with respect to the axis, the necessary strain in the circumferential direction may be effected by a shortening in the axial direction, which requires no excess stresses at the yield stress, so that with this mode of buckling no excess inner stresses are involved, as with buckling of a bar. In reality, the half wave length l/p cannot be more than the length of the shell, denoted by l, so that the buckling force per unit breadth is[24,25]

$$N_x = h\sigma_B = (EIA\pi^2/l^2) + [D - (B^2/A)](Eh/a^2)l^2/\pi^2$$

At the yield stress $D - (B^2/A) = 0$, so that

$$N_x = h\sigma_B = \pi^2 EIA/l^2$$

in which $I = h^3/12$, h is the thickness, and $2a$ is the diameter of the shell. At the yield stress the buckling stress is the same as that for a wide plate (Case 9 in Tables 1 and 5) with the same buckling length l.

Case 9 also applies for a tube under external pressure, so that the theory also solves, for example, the plastic collapse of deep well casing under external pressure, which was dealt with before by using the same ratio σ_B/σ_E as applies for bars.[31]

Later Papers on the Same Subject

In his first papers the author, in 1938, found that (assuming the plate to remain straight up to the buckling stress, as in the theory of Engesser-Kármán for bars), even for a wide plate that buckles cylindrically (Case 9), the boundary surface between plastic and elastic region is curved.[14,23] This results in a varying flexural rigidity so that the plate will not buckle according to a sine wave. As this makes an exact solution practically impossible and as the author was of the opinion that the elastic regions do not influence the actual buckling stresses in practical cases, he did not go further in this matter and reckoned with entirely plastic plates.[23] Ilyushin (1944)[35] refers to the present author's efforts on the determination of this boundary surface and intended to give an exact solution for it. In deriving the differential equation of the plate, however, he assumes that the resulting normal and shearing forces in buckling do not vary, yielding a boundary surface parallel to the middle plane. It follows, however, from the present author's earlier papers, that both of these conclusions are incorrect.[14,23] Ilyushin's differential stress-strain relations for the plastic region are the same as the author's Eqs. (21) or (21a) if Poisson's ratio ν for the elastic region is equated to 0.5. Using this assumption gives, in general, too high buckling stresses.

Handelman and Prager[36] also conclude that the above-mentioned boundary surface is parallel to the middle plane of the plate. Furthermore, they consider only buckling under pure compression and plastic flow, by which their stress strain relations follow from Eqs. (21) or (21a) by equating $\beta = \rho_2/\rho_1$ and e to zero. This assumption is dealt with here (curve 2, $e = 0$, el. + pl. in Fig. 11 and line 1, $e = 0$ in Fig. 12) and proves to give too high buckling stresses.

The stress strain relations of Stowell (1948)[37] are the same as those of Ilyushin, and, where he also considers buckling under pure compression, they follow directly from Eqs. (21) or (21a) by equating $\beta = \rho_2/\rho_1$ to zero and ν to 0.5. He considers the entire plate plastic in his buckling analysis and thereby obtains results in agreement with tests.

REFERENCES

[1] Bierett, G., *Ein Beitrag zur Frage der Spannungsstörungen in Bolzenverbindungen*, Mitteilungen d. deutsche Materialprüfanst., Sonderheft XV, pp. 3–39, 1931; also other papers.

[2] Bijlaard, P. P., *Theory of local plastic deformations*, Publ. Internat. Assoc. f. Bridge and Struct. Engineering, Zürich, Vol. 6, pp. 27–44, 1940–1941, being a summary of the author's preceding papers in De Ingenieur, 1931, 1933, and in De Ingenieur in Ned. Indie, 1935, 1936, 1939.

[3] Bijlaard, P. P., *Verklaring van de schijnbare verhooging van de vloeigrens bij spanningsspitsen in staalconstructies*, De Ingenieur in Ned. Indie, Vol. 6, No. 8, pp. I166–I172, August, 1939.

[4] Bijlaard, P. P., *Theory of Local Plastic Deformations in Structural Steel*, De Ingenieur in Ned. Indie, Vol. 7, No. 8, pp. I130–I142, August, 1940.

[5] Bijlaard, P. P., *Verklaring van de richting der vloeilijnen en van de optredende breukhoek in stalen platen*, De Ingenieur in Ned. Indie, Vol. 2, No. 6, pp. I59–I66, June, 1935.

[6] Bijlaard, P. P., *Theorie der plaatselijke plastische vervormingen in dikke stalen staven*, De Ingenieur in Ned. Indie, Vol. 3, No. 8, pp. I106–I112, August, 1936.

[7] Bijlaard, P. P., *Beschouwingen over de knikzekerheid en de plastische vervormingen van de aardkorst in verband met de geologie van den Oost Indischen archipel*, De Ingenieur in Ned. Indie, Vol. 2, No. 11, pp. I135–I156, November, 1935.

[8] Bijlaard, P. P., *Théorie des déformations plastiques et locales par rapport aux anomalies négatives de la gravitation, aux fosses océaniques, aux géosynclinaux, au volcanisme, à l'orogénie et à la géologie de l'océan pacifique occidental*, Assoc. de Géodesie, Rapport au Congrès d'Edinbourg, 1936.

[9] Bijlaard, P. P., *Plasticiteit in staalconstructie en geologie*, Natuurkundig Tijdschrift v. Ned. Indie, Vol. 99, No. 2, pp. 43–64, March, 1939.

[10] Bijlaard, P. P., *Over plasticiteit en stabiliteit van stalen platen en van de aardkorst*, Inaugural lecture, Delft, May, 1947.

[11] Lode, W., *Der Einfluss der mittleren Hauptspannung auf das Fliessen der Metalle*, Forschungsarbeiten V.D.I., Heft 303, 1928.

[12] Roš, M., and Eichinger, A., *Versuche zur Klärung der Bruchgefahr*, Diskussionsbericht E.M.P.A. Zürich, No. 34, 1929.

[13] Bijlaard, P. P., *A theory of plastic buckling with its application to geophysics*, Proc. Kon. Akad. v. Wetensch., Amsterdam, Vol. 41, No. 5, pp. 468–480, May, 1938.

[14] Bijlaard, P. P., *A theory of plastic stability and its application to thin plates of structural steel*, Proc. Kon. Akad. v. Wetensch., Amsterdam, Vol. 41, No. 7, pp. 731–743, September, 1938.

[15] Hohenemser, K., and Prager, W., *Beitrag zur Mechanik des bildsamen Verhaltens von Flusstahl*, Zeitschr. f. angew. Math. u. Mech., Vol. 12, pp. 1–14, 1932.

[16] Kollbrunner, C. F., *Das Ausbeulen des auf Druck beanspruchtem freistehenden Winkels*, Mitt. a. d. Institut f. Baustatik a. d. E.T.H. Zürich, No. 4, 1935.

[17] Bijlaard, P. P., *On the restricted applicability of the principle of least work in the plastic domain*, Proc. Kon. Akad. v. Wetensch., Amsterdam, Vol. 50, No. 4, pp. 397–405, April, 1947.

[18] Shanley, F. R., *Inelastic Column Theory*, Journal of the Aeronautical Sciences, Vol. 14, No. 5, pp. 261–268, May, 1947.

[19] Fraenkel, S. J., *Experimental Studies of Biaxially Stressed Mild Steel in the Plastic Range*, Journal of Appl. Mech., Vol. 15, No. 3, pp. 193–200, September, 1948.

[20] Biezeno, C. B., and Hencky, H., *On the general theory of elastic stability*, Proc. Kon. Akad. v. Wetensch., Amsterdam, Vol. 31, No. 6, p. 569, 1928; Vol. 32, No. 4, p. 444, 1929.

[21] Bijlaard, P. P., *Stress-Strain Relations of an Elastoplastic Body, Subjected to an Infinitely Small Excess Stress Tensor*, 6th International Congress Appl. Mech., Paris, September, 1946.

[22] Bijlaard, P. P., *Grundlegende Betrachtungen zum Ausbeulen der Platten und Schalen im plastischen Bereich*, Mitt. a. d. Institut f. Baustatik a.d. E.T.H., Zürich, No. 21, 1947.

[23] Bijlaard, P. P., *Theory of the plastic stability of thin plates*, Publ. Internat. Assoc. f. Bridge and Struct. Engineering, Zürich, Vol. 6, pp. 45–69, 1940–1941 (see also footnote 10 of that paper).

[24] Bijlaard, P. P., *Some contributions to the theory of elastic and plastic stability*, Publ. Internat. Assoc. f. Bridge and Struct. Engineering, Zürich, Vol. 8, pp. 17–80, 1947.

[25] Bijlaard, P. P., *On the plastic stability of thin plates and shells*, Proc. Kon. Akad. v. Wetensch., Amsterdam, Vol. 50, No. 7, pp. 765–775, September, 1947.

[26] Bleich, F., *Theorie und Berechnung der eisernen Brücken;* Springer, Berlin, 1924.

[27] Chwalla, E., *Das allgemeine Stabilitätsproblem der gedruckten, durch Randwinkel verstärkten Platte*, Ingenieur Archiv, Vol. 5, p. 54, 1934.

[28] Bijlaard, P. P., *Exacte berekening voor het plooien van de wanden der in de bruggenbouw gebruikelijke staafprofielen*, De Ingenieur in Ned. Indie, Vol. 6, No. 2, pp. I17–I23, February, 1939.

[29] Bijlaard, P. P., *Afleiding van eenvoudige gebruiksformules en grafieken ter bepaling van het plooigevaar van de wanden van vloeistalen staafprofielen*, De Ingenieur in Ned. Indie, Vol. 6, No. 10, pp. I239–I256, October, 1939.

[30] Kollbrunner, C. F., *Das Ausbeulen der auf einseitigen, gleichmässig verteilten Druck beanspruchten Platten im elastischen und plastischen Bereich*, Mitt. a. d. Institut f. Baustatik a.d. E.T.H. Zürich, No. 17, 1946.

[31] Bijlaard, P. P., Kollbrunner, C. F., and Stüssi, F., *Theorie und Versuche über das plastische Ausbeulen von Rechteckplatten unter gleichmässig verteilten Langsdruck*, Internat. Assoc. f. Bridge and Struct. Engineering, 3rd Congress, Liège, September, 1948, Preliminary Publication, pp. 119–128, 1948.

[32] Schuette, E. H., and McDonald, J. C., *Prediction and Reduction to Minimum Properties of Plate Compressive Curves*, Journal of the Aeronautical Sciences, Vol. 15, No. 1, pp. 23–27, January, 1948.

[33] Bijlaard, P. P., *Nauwkeurige berekening van de plooispanning van hoekstalen, zoowel voor het elastische als voor het plastische gebied*, De Ingenieur in Ned. Indie, Vol. 6, No. 3, pp. I35–I45, March, 1939.

[34] Holmquist, J. H., and Nadai, A., *A Theoretical and Experimental Approach to the Problem of Collapse of Deep-Well Casing*, 1939, Annual Meeting Am. Petroleum Inst., Chicago, pp. 392–407.

[35] Ilyushin, A. A., *Stability of Plates and Shells Beyond the Proportional Limit*, N.A.C.A. T.M. No. 1116, October, 1947 (Transl. from Prikl. Mat. Mekh., Vol. 8, p. 337, 1944).

[36] Handelman, G. H., and Prager, W., *Plastic Buckling of a Rectangular Plate Under Edge Thrusts*, N.A.C.A. T.N. No. 1530, August, 1948.

[37] Stowell, E. Z., *A Unified Theory of Plastic Buckling of Columns and Plates*, N.A.C.A. T.N. No. 1556, April, 1948.

[38] Gerard, G., *Secant Modulus Method for Determining Plate Instability Above the Proportional Limit*, Journal of the Aeronautical Sciences, Vol. 13, No. 1, p. 38, January, 1946.

[39] Vening Meinesz, F. A., *Shear Patterns of the Earth's Crust*, Transactions American Geophysical Union, Vol. 28, No. 1–61, February, 1947.

[40] Bijlaard, P. P., *On the linear patterns of the earth's crust*, Proc. Kon. Akad. v. Wetensch., Amsterdam, Vol. 51, No. 4, pp. 450–456, April, 1948.

[41] Lundquist, E. E., Schuette, E. H., Heimerl, G. J., and Roy, J. A., *Column and Plate Compressive Strengths of Aircraft Structural Materials—24S-T Aluminum-Alloy Sheet*, N.A.C.A. A.R.R. No. L5F01, June, 1945 (Wartime Report).

[42] Heimerl, G. J., and Roy, J. A., *Column and Plate Compressive Strengths of Aircraft Structural Materials—17S-T Aluminum-Alloy Sheet*, N.A.C.A. A.R.R. No. L5F08, June, 1945 (Wartime Report).

[43] Heimerl, G. J., and Roy, J. A., *Column and Plate Compressive Strengths of Aircraft Structural Materials—Extruded 75S-T Aluminum Alloy*, N.A.C.A. A.R.R. No. L5FO8a, July, 1945 (Wartime Report).

[44] Heimerl, G. J., and Roy, J. A., *Column and Plate Compressive Strengths of Aircraft Structural Materials—Extruded 24S-T Aluminum Alloy*, N.A.C.A. A.R.R., No. L5FO8b, July, 1945 (Wartime Report).

[45] Heimerl, G. J., and Fay, D. P., *Column and Plate Compressive Strengths of Aircraft Materials—Extruded R303-T Aluminum Alloy*, N.A.C.A. A.R.R. No. L5HO4, October, 1945 (Wartime Report).

[46] Heimerl, G. J., and Niles, D. E., *Column and Plate Compressive Strengths of Aircraft Structural Materials—Extruded 14S-T Aluminum Alloy*, N.A.C.A. A.R.R. No. L6C19, May, 1946 (Wartime Report).

Interference Between Wing and Body at Supersonic Speeds—Note on Wind-Tunnel Results and Addendum to Calculations*

CARLO FERRARI†

Cornell Aeronautical Laboratory, Inc.

ABSTRACT

A correction is made to the numerical example worked out in a previous paper for the pressure distribution on a rectangular wing operating in the upwash from a pointed inclined body of revolution in a supersonic stream. Wind-tunnel results confirm the amended calculated pressures and bring to light the drastic falling off of lift in the wing-body juncture.

INTRODUCTION

THIS NOTE IS PROMPTED through realization that part of the numerical example used to illustrate the theoretical results of a previous paper on wing-body interference by the author[1] contains an error in one of the boundary conditions. In order to assure a safe basis for proper application of the boundary conditions, it is necessary to review this facet of the calculations in some detail. The boundary condition, which is applied incorrectly in reference 1, is depicted in Fig. 10 of that paper. This oversight resulted from an attempt to bring together several steps in an iteration process, but it appears that a more carefully worked-out sequence should be followed. The basis of this iteration process lies in the following considerations.

REVIEW OF THEORETICAL STEPS

General Observations

The solution of the wing-body interference problem, by the method of small perturbations that is carried out in the theoretical part of reference 1, consists essentially of finding a potential (or the velocity field derived from such a potential) for the wing-body system as a result of adding to the potential for the undisturbed impinging stream, $\vec{V}_\infty$, the sum of the potentials related to the appropriate distributions of supersonic doublets which exist on the surface of the wing and on the body. These distributions are uniquely determined by the boundary conditions, which will be examined more critically below.

In conformity with the usual procedure followed in the linear theory, the distribution of supersonic doublets is obtained along the body axis and not at the surface, but this is entirely legitimate. Likewise, the distribution for the wing actually occurs on the x,y-plane in the region bounded by the wing surface, including the part extending inside the body, when the wing is considered as flattened down upon the x,y-plane. Here again the procedure conforms with the usual one used in linearized theory.

Within the framework of the linearized theory, an exact solution of the wing plus body problem may thus be found by a process that depends upon the following precise formulations:

Stepwise Detailed Procedure

Let Σ_1 be the distribution of supersonic doublets in the region of the whole wing, including the extension within the body, and let Σ_2 be the distribution along the body axis. Now represent by V_{n1}, V_{n2}, $V_{n\infty}$ the components of velocity normal to the wing (flattened), which are due to the distributions Σ_1, Σ_2, and free stream, $\vec{V}_\infty$, respectively. In addition, let V_{n1}', V_{n2}', $V_{n\infty}'$ denote the velocity components that are normal to the body surface, where these components also arise from the distributions Σ_1, Σ_2, and $\vec{V}_\infty$, respectively.

Consequently, the supersonic doublet distributions will be determined through satisfaction of the equations

$$\underset{\text{(on the wing)}}{V_{n1} + V_{n2} + V_{n\infty} = 0} \quad \text{and} \quad \underset{\text{(on the body)}}{V_{n1}' + V_{n2}' + V_{n\infty}' = 0} \qquad (1)$$

When these expressions are written out in explicit form, they constitute a system of integral equations of the Volterra type, and they may be solved by the method of iteration, as follows:

Step 1.—Calculate Σ_1 by means of the boundary condition $V_{n1} + V_{n\infty} = 0$, where V_{n2} has been set $= 0$ (this is the zero approximation, equivalent to neglecting all interference effect).

Step 2.—Calculate Σ_2 by means of $V_{n2}' + V_{n\infty}' = 0$, where V_{n1}' has been set $= 0$ (this is the zero approximation for the body distribution).

Step 3.—Recalculate Σ_1 using the first relation of Eq. (1), wherein the value of V_{n2} is that obtained from the Σ_2 calculated in Step 2 (this is now the first-stage approximation for the wing).

Received March 25, 1949.

* This work, both experimental and theoretical, was carried out under Navy BuOrd sponsorship.

† Member of C.A.L. consulting staff. Professor, Laboratorio di Aeronautica, Politecnico di Torino.

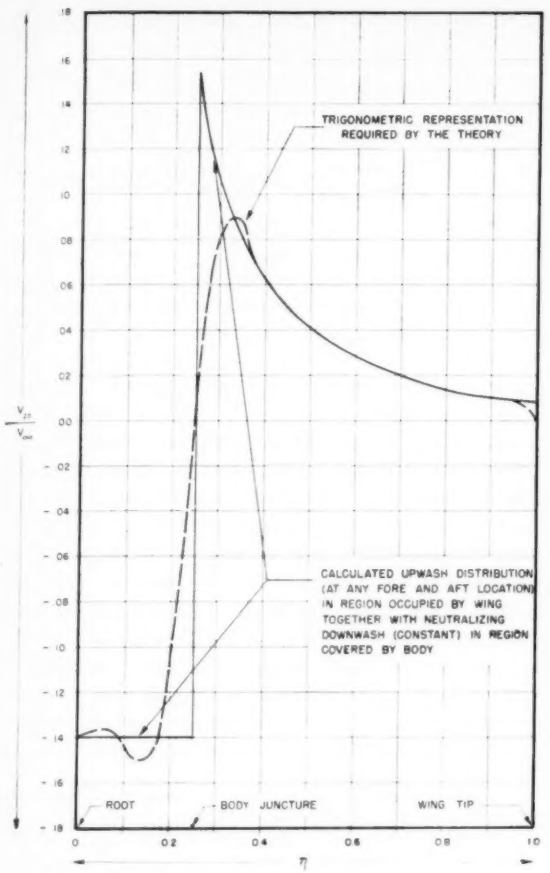
TRIGONOMETRIC REPRESENTATION REQUIRED BY THE THEORY
CALCULATED UPWASH DISTRIBUTION (AT ANY FORE AND AFT LOCATION) IN REGION OCCUPIED BY WING TOGETHER WITH NEUTRALIZING DOWNWASH (CONSTANT) IN REGION COVERED BY BODY
ROOT
BODY JUNCTURE
WING TIP
η

FIG. 1. Upwash distribution out along wing span.

Step 4.—Recalculate Σ_2 using the second relation of Eq. (1), wherein the value of V_{n1}' is that obtained from the Σ_1 calculated in Step 1 (this is now the first-stage approximation for the body).

Step 5.—This process is continued by employing, in the second-stage approximation, the distributions Σ_1 and Σ_2, which were obtained in Steps 3 and 4.

Because the integral equations are of the Volterra type, it is assured that this iteration process will converge to give the same solution as would be obtained if both sets of boundary conditions were satisfied simultaneously.

Recasting of Step 3 as an Incremental Distribution

In applying this procedure to the problem at hand, it is essential to note that Step 1 is the two-dimensional solution for a flat plate inclined at an angle β_2—i.e., there is a uniform down-wash of magnitude $V_\infty\beta_2$ in the region confined between the two Mach planes emanating from the leading and trailing edges of the wing. Step 2 is the Tsien or Ferrari (see references given in original paper) derivation for the flow around an isolated body at an angle of attack, β_1, to the free-stream flow. For the purposes of Step 3, it is found more convenient to solve for the increment in the distribution of doublets on the wing (flattened) rather than for the first-stage approximation to Σ_1 directly. Consequently, the upwash *increments* on the wing due to the flow around the inclined body are just as calculated previously, but in the region of the wing, which is covered by the body, the *increment* upwash distribution will, of necessity, be equal in magnitude but of opposite sign to the basic distribution for the wing, determined as Step 1—i.e., the total solution for this Step 3 requires that there be no flow through the body, where the boundary condition is again being applied in the x,y-plane.

Numerical Calculations of Upwash Increments

The correct boundary condition for finding this first-stage approximation to the increment of lift on the wing due to interference is thus the one depicted here by means of a solid line (two pieces) in Fig. 1. This spanwise distribution of upwash is taken to apply independently of the fore-and-aft location on the wing with good approximation, because it is the average of two distributions, one calculated at a section near the leading edge and the other near the trailing edge. That these two calculated spanwise distributions at opposite edges of the wing are almost identical, to the degree of accuracy expected from this linearized theory, is borne

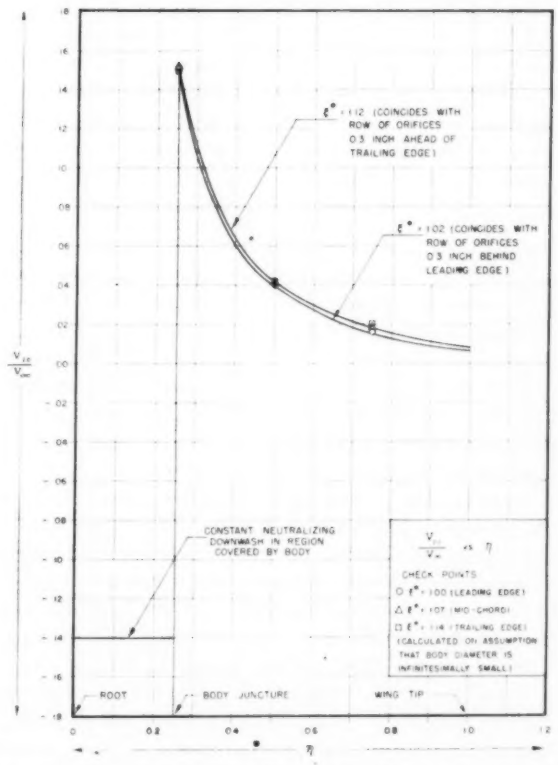
ξ* = 1.12 (COINCIDES WITH ROW OF ORIFICES 0.5 INCH AHEAD OF TRAILING EDGE)
ξ* = 1.02 (COINCIDES WITH ROW OF ORIFICES 0.3 INCH BEHIND LEADING EDGE)
CONSTANT NEUTRALIZING DOWNWASH IN REGION COVERED BY BODY
CHECK POINTS
ROOT
BODY JUNCTURE
WING TIP
η

FIG. 2. Spanwise upwash distributions in region occupied by wing, showing small variations due to fore-and-aft location.

out by the curves plotted in Fig. 2. The values of the upwash at the three spanwise stations, $\eta = 0.25$, 0.5, and 0.75, which were obtained previously (see Fig. 10 of reference 1) through assumption that the body diameter was infinitesimally small, are also reproduced on Fig. 2 in order to re-emphasize that the upwash varies but a slight amount from front to rear locations in the region in which the wing is situated. In addition, these check points also agree so well with the more detailed stepwise calculations represented by the two smooth curves that they give good assurance that the former procedure of assuming the body diameter to be infinitesimally small [see Eq. (44) of reference 1] was justified for all practical purposes.

For orientation it should be remembered that the configuration selected for computation is one having the general features as represented in Fig. 3, and the specific case of Mach Number = 2.0 and angle of attack = $+8°$ is the one chosen for numerical illustration. Of course, under these conditions, the new correct boundary condition applicable to the *incremental* upwash in the region of the wing that is covered by the body necessitates a neutralizing value of upwash equal to -0.1396 ($-8°$), so that these *additional* normal velocity components actually constitute down-wash increments here.

Trigonometric Representation of Upwash Distribution

By means of a curve-fitting procedure that is entirely analogous to that already illustrated in reference 1, it will be found that a trigonometric series of cosine terms of odd multiples of the argument will represent the now amended boundary condition in a manner shown by means of the dashed line in Fig. 1. This trigonometric representation is required in order to carry out subsequent steps in the theory.

The formula of Clairaut-de la Vallée Poussin used in reference 1 gives a trigonometric series representation that passes exactly through a discrete number of selected points. The same series may also be obtained by using a tabular scheme such as devised by Runge and illustrated by J. P. Den Hartog in reference 2. The dashed curve of Fig. 1 is obtained by use of Runge's 48-Point Tabular Schedule, wherein the calculated upwash values for $\eta = 0$ to 1.0 are extended antisymetrically from $\eta = 1.0$ to 2.0, and the resulting distribution is then extended again to give an even function in the interval $\eta = -2$ to $\eta = +2$. This process thus defines an upwash distribution whose trigonometric representation is composed solely of cosine terms with odd multiples of the argument and the period of which is 4. The subsequent determinations of pressure distributions out along the wing span will also be expressed in terms of such periodic functions, but the detailed behavior of these distributions is only of interest in the quarter interval from $\eta = 0$ to 1, which corresponds to the actual wing semispan—that is, the pressure distributions are of the form

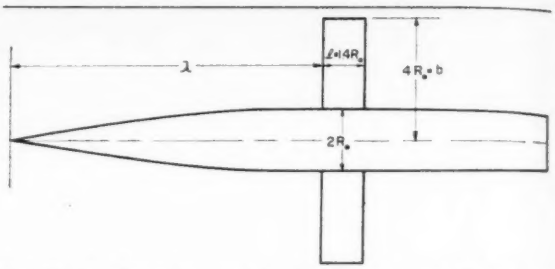

FIG. 3. Configuration used in the numerical application and upon which the wind-tunnel tests were performed.

$$C_p = 2\pi \sum_m H_m^{(r)} \cos\left[(1/2)\pi m\eta\right]$$

where the superscript (r) denotes that this particular spanwise distribution applies over the small chordwise strip, wherein $H_m^{(r)} = dh_m(\xi)/d\xi$ is assumed constant. For purposes of the numerical application made here, the chord has been divided into only three sections of equal length, and the resulting distributions have been designated simply as applying to locations at one-sixth chord aft of the leading edge, at the wing axis (50 per cent chord points), and at one-sixth chord forward of the trailing edge. The notation follows exactly that employed previously, and in particular $\eta = 0$ corresponds to the root chord (plane of symmetry), while $\eta = 1.0$ represents the wing tip.

Fourier Representation and Occurrence of the Gibbs Phenomenon

Close scrutiny of Fig. 1 discloses that there are rather large discrepancies between the original upwash distribution and the trigonometric representation in the region of the discontinuity at the body juncture, even though the 48-Point Schedule allowed a determination of twelve terms ($m = 23$). It may be more satisfactory to use a Fourier representation and to take a great number of harmonics in order to match closely the calculated upwash distribution, but such refinements are not needed to show the acceptable correspondence between theory and experiment, which is presented in Fig. 5.

It may be noted that the behavior of such a Fourier representation in the neighborhood of the discontinuity is characterized by the Gibbs phenomenon, which predicts that large discrepancies will be maintained between the given curve and the representing Fourier development regardless of the number of terms employed. This difficulty can be obviated by an appeal to the smoothing effect of the boundary layer on the mathematical sharpness of the discontinuity—i.e., it is obvious physically that the discontinuity at the wing-body juncture is not actually as precise as depicted by the solid line in Fig. 1. Consequently, the discontinuity can be replaced legitimately by a continuous smooth curve that will deviate so slightly from the one having a discrete jump that for all practical purposes the smooth curve can be employed without fear of any essential

discrepancy arising; in fact, a closer approximation to physical truth is likely to follow. Of course, such a continuous curve can then be represented at *every* point to any desired degree of accuracy by a Fourier series consisting of a sufficient number of terms.

Computational Results for the Pressures on the Wing

Once the trigonometric representation of the upwash has been obtained to the desired degree of accuracy, the subsequent calculations required to determine the increments in pressure distributions on a wing placed in this field of upwash may be carried out through following a procedure already illustrated in reference 1. The results of such a calculation in the present case turn out to be the three distributions plotted in Fig. 4, which apply to the three fore-and-aft sections into which the wing was arbitrarily divided. It is significant that a wider and wider region near the wing-body juncture shows a falling off of the interference-induced pressures as the trailing edge is approached, in distinction to what occurs at the leading edge; of course, the foremost tip of the leading edge supports the two-dimensional distribution, but no two-dimensional theory would account for the interesting phenomenon occurring farther aft in the wing-body juncture. (See Fig. 4.)

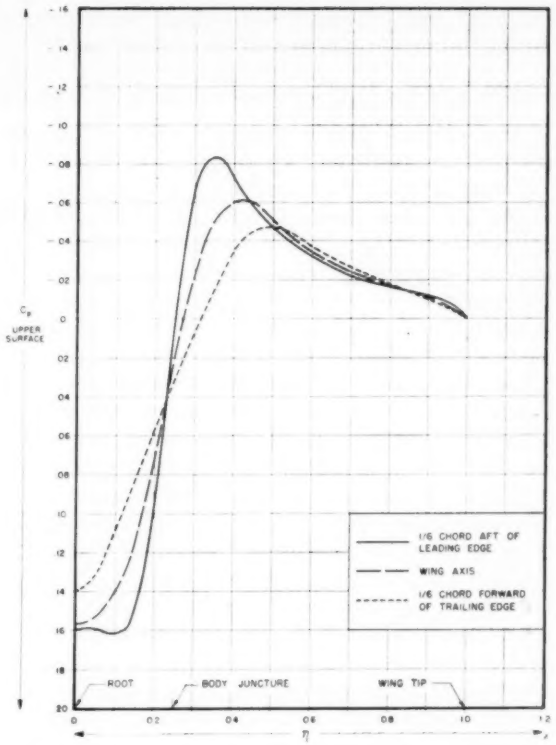

FIG. 4. Spanwise distribution of increment in pressure due to interference from body. (Case of Mach Number = 2, and angle of attack = +8°.)

EXPERIMENTAL RESULTS

Description of Model and Stream Conditions

Wind-tunnel tests have been made on a configuration possessing the same geometric characteristics as used in computing the above-mentioned numerical results. The wing was a 10 per cent thick double wedge with a flat upper surface that was aligned with the centerline of the body. The orifices were located on the flat surface, and thus a complete run of both positive and negative ranges of angle of attack gave the equivalent of the flat-plate condition analyzed numerically. The experiments were carried out at the Naval Ordnance Aerophysics Laboratory at Daingerfield, Tex. The test section width is 19 in., while the height is 27.5 in.; thus, the 3.0-in. diameter (maximum along cylindrical section) model is accommodated with sufficient clearance to ensure the absence of shock reflection between the model and the tunnel walls at all angles of attack tested. The flow was close to $M = 2.0$, and calibration surveys reveal that this working section is remarkably free of anomalies. The Reynolds Number of the free stream, based on the 2.1-in. wing chord, was approximately 1,270,000 (wing span from tip to tip = 12.0 in. and overall body length = 26.25 in.). The moisture content was controlled to ensure a dew point in the range +19° to −4°F.

Comparison with Theory

The experimentally determined pressure coefficients along a spanwise row of ordinates located on the wing axis (50 per cent chord point) are plotted in Fig. 5 for

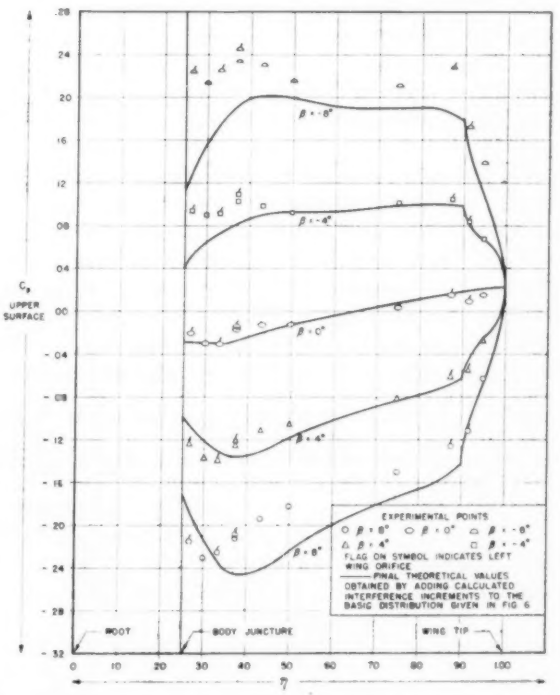
C_p UPPER SURFACE
EXPERIMENTAL POINTS
FLAG ON SYMBOL INDICATES LEFT WING ORIFICE
FINAL THEORETICAL VALUES OBTAINED BY ADDING CALCULATED INTERFERENCE INCREMENTS TO THE BASIC DISTRIBUTION GIVEN IN FIG 6
ROOT
BODY JUNCTURE
WING TIP
η

FIG. 5. Pressure coefficients along the wing axis: comparison of experimental and theoretical results.

±8°, ±4°, and 0° angles of attack, and the theoretical first approximation is presented for confirmation.*

Build-Up of Pressure Coefficient from Basic Components

The theoretical curve is obtained by use of the *increment* pressure coefficient for the wing axis given in Fig. 4, to which is added the basic coefficients represented in Fig. 6. The basic distribution for any angle of attack is obtained by computing the two-dimensional pressures for the corresponding angle of attack (which change sign as the angle of attack changes sign) and adding the constant "contour" effect shown in dotted line on Fig. 6. The "contour" effect is merely the radial distribution of pressure at the particular longitudinal station along the missile axis at which the wing axis happens to fall; this radial distribution of pressure for zero angle of attack results from the longitudinal component of the impinging stream and accounts for the distortion to this stream which occurs as the flow makes accommodation for the bulk of the body. The distortion is appreciable in the present example because the nose, with its rapidly changing contour, is so near the wing. The theoretical variations in the pressures encountered at the wing tip are also included in the basic distributions. This use of theoretical basic pressures will not introduce any error in the final comparison of theoretical and experimental pressure coefficients, which include interference effects, because exact correspondence was found to exist (within the degree of accuracy of the experimental results) between wing-alone tests (not presented here) and the theoretical basic values just mentioned, which pertain to the wing before interference increments are added. Examination of Fig. 5 also discloses that the magnitude of the "contour" effect from the body, for zero degree angle of attack, is also adequately confirmed by the experimental data.

The correspondence between experimental points and the theoretical result obtained by summing the angle of attack and "contour" effects of the basic distribution with the increment due to interference occurring along the wing axis, as shown in Fig. 4, is extremely close, even for this first approximation step. The adequacy of the small perturbation theory to deal with this phase of the wing-body interference problem is manifest, particularly because the experimental data of Fig. 5 confirm the falling off of pressure in the wing-body juncture.

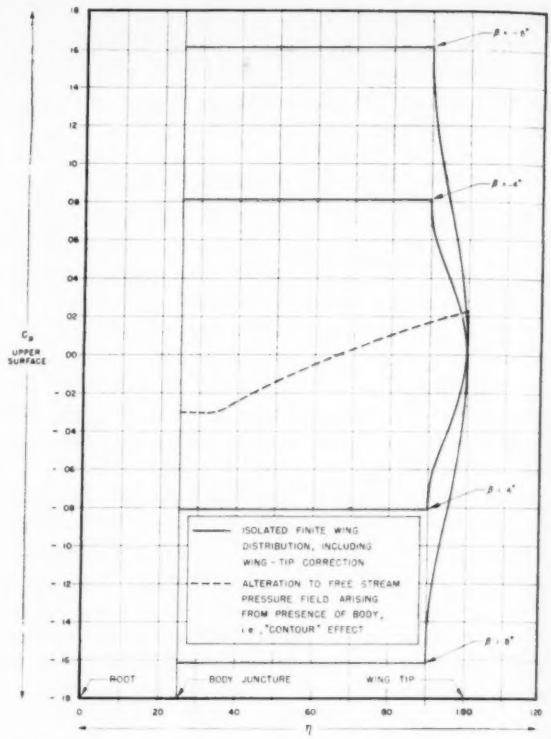

FIG. 6. "Basic" distribution components for build-up of spanwise pressure variations.

Influence of Wing upon the Body

The calculations previously given for determining the influence of the wing upon the body need no revision, but it should be recognized that the numerical data adduced are for the first approximation step only.

More detailed comparisons of wing-body interference for the configuration tested are expected to be made available for publication at a later date in a separate paper to be devoted entirely to presentation of such experimental results.

* The author wishes to express his indebtedness to R. H. Cramer, of the Cornell Aeronautical Laboratory, for planning and performing the experimentation, as well as the analysis which provides this comparison of theory with test data.

REFERENCES

[1] Ferrari, C., *Interference Between Wing and Body at Supersonic Speeds—Theory and Numerical Application*, Journal of the Aeronautical Sciences, Vol. 15, No. 6, pp. 317–336, June, 1948.

[2] Den Hartog, J. P., *Mechanical Vibrations*, 2nd Ed., pp. 25–30; McGraw-Hill Book Company, Inc., New York, 1940.

Temperature and Velocity Profiles in the Compressible Laminar Boundary Layer with Arbitrary Distribution of Surface Temperature

DEAN R. CHAPMAN* AND MORRIS W. RUBESIN†

Ames Aeronautical Laboratory, N.A.C.A.

SUMMARY

An analysis is presented which enables the temperature profiles, velocity profiles, heat transfer, and skin friction to be calculated for laminar flow over a two-dimensional or axially symmetric surface without pressure gradient but with an arbitrary analytic distribution of surface temperature. The general theory is applicable to a gas of any Prandtl Number, although the numerical results given herein have been computed for air ($Pr = 0.72$). The predictions of the theory for the special case of constant surface temperature are compared with the calculations of Crocco. On the basis of this comparison, it is inferred that the present theory enables heat-transfer and skin-friction calculations accurate to within about 5 per cent to be made for flight conditions up to Mach Numbers near 5 and to within about 1 or 2 per cent for supersonic wind-tunnel conditions up to considerably higher Mach Numbers.

A particular effort has been made to present the results, which are simple considering their generality, in a form that can be used readily in practical applications. From the mathematical point of view, the theory is applicable to an arbitrary analytic distribution of surface temperature, but in any given practical case it is necessary that the surface-temperature distribution be approximated by a polynomial. The only unknowns in the final equations developed are the coefficients of this polynomial, so that the work involved in applying the theory in any given case depends entirely on the work involved in approximating a given surface-temperature distribution by a polynomial.

An example is worked out in detail which illustrates some of the principal effects of variable surface temperature. It is shown that both positively infinite and negatively infinite heat-transfer coefficients can occur. The anomaly of infinite and negative heat-transfer coefficients is discussed and attributed to the customary definition of the heat-transfer coefficient, which is shown to be fundamentally inappropriate for flows with variable surface temperature. In the particular example considered, a conventional method for calculating the net heat transferred yields completely incorrect results. A brief qualitative discussion of the possible effects of the heat transfer on flow separation is given. In order to facilitate the use of the results, all of the principal equations developed are collected and summarized in the section entitled "Practical Use of Results."

INTRODUCTION

RECENT THEORETICAL INVESTIGATIONS of the stability of laminar boundary-layer flow have shown that it is possible for extensive regions of laminar flow to be maintained at supersonic velocities even though the Reynolds Number is extremely large. The calculations of Lees[1, 2] indicate, for example, that in the absence of adverse pressure gradients the cooling due to radiation alone at a Mach Number of 3 and at 50,000 ft. altitude can be sufficient to stabilize the laminar boundary layer regardless of Reynolds Number. Although these predictions of the stability theory have not as yet been quantitatively verified by experiments, there is little doubt as to their qualitative correctness. Consequently, the characteristics of the laminar boundary layer have recently assumed a much greater degree of importance to the engineer than was generally the case in the past. The maintenance of extensive laminar flow is, of course, highly desirable in order to minimize the friction drag as well as the cooling requirements resulting from aerodynamic heating.

The practical applications wherein the laminar boundary layer appears to be of most importance are those flows that simultaneously involve both heat transfer and high Mach Numbers. This complicates a theoretical analysis in two ways. First, the well-known boundary-layer equations for an incompressible fluid are inapplicable, and the more complicated equations for a compressible fluid are necessarily involved. Second, the heat-transfer and stability characteristics of the boundary layer are intimately connected with each other—that is, with both the velocity and temperature profiles in the boundary layer. This means that temperature and velocity profiles cannot be considered separately and that imprudent assumptions about either of these profiles cannot justifiably be made. Thus, velocity and temperature profiles have to be solved simultaneously (at least indirectly) in each particular problem wherein both heat transfer and high Mach Numbers are involved.

Several studies of the characteristics of laminar boundary layers in the presence of heat transfer have been made, but all are subject to rather severe limitations. For the particular case of constant surface temperature, a complete set of calculations for both velocity and temperature profiles was made by Crocco[3, 4] and to some extent also by Hantzsche and Wendt.[5, 6] In many practical applications, however, the surface tem-

Presented at the Fluid Mechanics Session, Seventeenth Annual Meeting, I.A.S., New York, January 24–27, 1949.

* High Speed Research Division.

† Full Scale and Flight Research Division.

perature is not constant, and appreciable errors are introduced by basing heat-transfer calculations on values obtained under the assumption of constant surface temperature. In an attempt to evaluate these errors, several investigations have been made of certain types of surface-temperature distribution.[7–9] These analyses, however, are too restricted to be of use quantitatively in the problems that at present appear to be of considerable importance in aerodynamics. One severe limitation of these analyses is that they are applicable only to low-speed gas flows. Moreover, in each of these investigations certain assumptions have been made which are admittedly only rough approximations. As a result the existing analyses are not entirely satisfactory even for low-speed flows.

As far as high-speed flows are concerned, probably the least accurate assumption that has been made in the previous investigations is that the velocity profile does not change with different rates of heat transfer through the boundary layer. This, of course, cannot be the case, since cooling and heating have markedly different effects on the velocity profiles, particularly at high Mach Numbers. Analyses that assume an invariant velocity profile are, therefore, restricted to low rates of head transfer as well as to low velocities. In references 7, 8, and 9, different types of invariant velocity profiles and different surface-temperature distributions were used, and, hence, it is not surprising that some of the quantitative results of these investigations are not in complete agreement. Nevertheless, these investigations are qualitatively consistent with each other and with the present investigation in indicating a pronounced effect of a variable surface temperature on the heat-transfer characteristics.

The purpose of the present investigation is twofold: first, to avoid the restriction to low-speed flows and low rates of heat transfer which is inherent in existing theoretical analyses; and, second, to obtain a solution applicable to an arbitrary surface-temperature distribution. It is emphasized that the present investigation makes no assumptions about the velocity profile. Likewise, no restrictive assumptions regarding the distribution of surface temperature are made aside from those that are necessary in order for the usual boundary-layer theory to be applicable. The solution given herein, therefore, enables the velocity profiles, temperature profiles, and, hence, heat-transfer characteristics to be calculated for a compressible laminar boundary-layer flow without pressure gradient but with an arbitrary analytic distribution of surface temperature.

Although the analysis is formally worked out for two-dimensional flow, the end results can also be applied to bodies of revolution by using the general relationship between axially symmetric and two-dimensional boundary-layer flows given by Mangler in reference 10. It is to be noted that the results of Mangler are valid for boundary-layer flows with variable surface temperature.

The absence of assumptions (in the present investigation) about the velocity profile and distribution of surface temperature would at first appear to hopelessly complicate the solution. It turns out, however, that the analysis yields surprisingly simple end results, which can be readily used. Since the mathematical development leading to these results is somewhat lengthy, it will be advantageous to outline briefly in the remainder of this introduction the more salient features of the analysis by means of which the simple yet general results are obtained.

The first salient feature consists of the use of the stream function ψ, instead of the normal space coordinate y, as one of the independent variables, thereby transforming the boundary-layer equations to a much simpler form. This transformation was first used for incompressible flow by von Mises[11] and for compressible flow by von Kármán and Tsien.[12] It has since been used in obtaining solutions to other compressible flow problems.[2, 13]

A second and less essential feature of the analysis consists of the use of a parameter C in the assumed linear relationship between viscosity ratio and temperature ratio ($\mu/\mu_\infty = CT/T_\infty$). This parameter was employed in the analysis of laminar mixing given in reference 13, wherein its use was shown to yield accurate laminar-mixing velocity profiles at Mach Numbers up to 5. The merit of using such a parameter stems from the fact that it does not complicate the analysis, yet for any free-stream temperature it allows the approximating equation for the viscosity to be more accurate in the region of boundary-layer flow near the surface rather than in the less important region near the free stream. As is discussed later on, the additional flexibility provided by the parameter C allows calculations of velocity and temperature distributions, accurate to within a few per cent, to be made at high Mach Numbers over an unusually wide range of free-stream temperatures. This should prove useful in comparing the laminar boundary-layer characteristics obtained in high-Mach-Number supersonic wind tunnels with those to be expected in flight.

Symbols and Notation

b_n = coefficients defined by Eq. (56)

C = factor of proportionality in the equation $\mu/\mu_\infty = C(T/T_\infty)$

C_w = the factor $\sqrt{T_w/T_\infty}(T_\infty + S)/(T_w + S)$ (a function of x)

c_{df} = section skin-friction drag coefficient of a plate of length $L[\int_0^L \tau\, dx/(1/2)\rho_\infty U_\infty{}^2 L]$

c_p = specific heat at constant pressure

h = local heat-transfer coefficient $[q/(T_w - T_e)]$

$\bar{h}$ = local heat-transfer coefficient for the special case of constant surface temperature

k = thermal conductivity

L = characteristic length of body

M = Mach Number

Nu = local Nusselt Number (hx/k_∞)

$\overline{Nu}$ = local Nusselt Number for the special case of constant surface temperature ($\overline{hx}/k_\infty$)
p = pressure
Pr = Prandtl Number of the gas ($c_p\mu/k$), 0.72 for air
q = local rate of heat transfer from the surface, per unit area
Q = total rate of heat transfer from a surface of length L, per unit width
Re_x = Reynolds Number based on the length $x(U_\infty x/\nu_\infty)$
Re = Reynolds Number based on the length $L(U_\infty L/\nu_\infty)$
S = Sutherland's constant
T = absolute temperature
$\overline{T}_w$ = average wall temperature ($\int_0^L T_w dx/L$)
U_∞ = velocity outside the boundary layer
u, v = velocity components in x and y directions, respectively
x, y = coordinates parallel and perpendicular to surface, respectively
ρ = mass density
μ = coefficient of viscosity
γ = ratio of specific heats
ν = coefficient of kinematic viscosity (μ/ρ)
δ = thickness of boundary-layer velocity profile
δ_t = thickness of boundary-layer temperature profile
ω = exponent in the equation $\mu/\mu_\infty = (T/T_\infty)^\omega$
τ = shear stress [$\mu(\partial u/\partial y)$]
ψ = stream function
η = dimensionless independent variable occurring in the Blasius function $f(\eta)$ [this variable is related to y by Eq. (42)]
$f(\eta)$ = the solution to Eq. (17) (the Blasius equation)
$Y_n(\eta)$, $\overline{Y}_n(\eta)$ = characteristic functions of the problem, defined as the solution to Eqs. (33) and (44), respectively, for a given value of n
$N(\eta)$ = function defined by Eq. (28)
$r(\eta)$, $\bar{r}(\eta)$ = functions defined by Eqs. (25) and (43), respectively
$\sim$ = order of magnitude

Subscripts

∞ = conditions outside of the boundary layer
w = conditions at the wall or surface of the body
e = equilibrium conditions of an insulated surface

Superscripts

$*$ = dimensionless quantities as defined in Eq. (11)
$'$ = ordinary differentiation

Basic Equations and Assumptions

Basic Equations

In the classical boundary-layer theory, temperature gradients, as well as velocity gradients, in the direction of flow are neglected in comparison to those perpendicular to the direction of flow. (See Fig. 1.) It is the purpose of the present investigation, however, to account for large temperature gradients in the direction of flow. Consequently, the first step in the analysis is to examine the basic differential equations of laminar motion of a viscous compressible fluid in order to see what restriction on the magnitude of the temperature gradient along the wall is necessary in order to be consistent with the approximations of the usual boundary-layer theory. Since these considerations are somewhat lengthy, the details are presented in Appendix A. It will suffice here to state that the analysis given therein shows that the usual boundary-layer equations,*

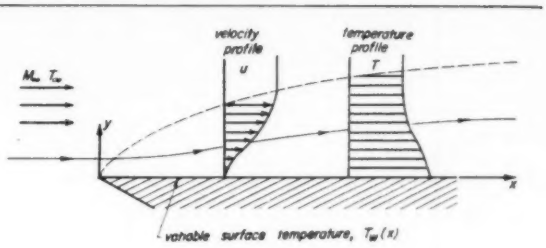

Figure 1.—Schematic drawing of the flow.

$$\left.\begin{aligned} \rho u\frac{\partial u}{\partial x} + \rho v\frac{\partial u}{\partial y} &= \frac{\partial}{\partial y}\left(\mu\frac{\partial u}{\partial y}\right) && \text{momentum equation}\\ \frac{\partial}{\partial x}(\rho u) + \frac{\partial}{\partial y}(\rho v) &= 0 && \text{continuity equation}\\ \rho u\frac{\partial (c_p T)}{\partial x} + \rho v\frac{\partial (c_p T)}{\partial y} &= \\ \frac{\partial}{\partial y}\left(k\frac{\partial T}{\partial y}\right) &+ \mu\left(\frac{\partial u}{\partial y}\right)^2 && \text{energy equation}\end{aligned}\right\} \quad (1)$$

are applicable to flows with large temperature gradients in the x direction provided

$$(\partial T/\partial x)_w \sim (T_w - T_\infty)/\delta \text{ or less} \quad (2)$$

At supersonic Mach Numbers the surface temperature T_w is normally of the same order of magnitude as the equilibrium temperature $T_e = T_\infty(1 + 0.169M_\infty^2)$, and the boundary-layer thickness is approximately $6L/\sqrt{Re}$. Under these circumstances condition (2) becomes

$$\left[\frac{\partial(T/T_\infty)}{\partial(x/L)}\right]_w \sim 0.03M_\infty^2\sqrt{Re} \text{ or less} \quad (2a)$$

This means, for example, that at a Mach Number of 1 and a Reynolds Number of 10^6 the maximum surface-temperature gradient consistent with the usual boundary-layer approximation is equivalent to a linear gradient that would produce a thirty-fold increase in T/T_∞ over the length of the surface. Thus, for high-speed flows, condition (2) does not impose any restrictions of practical importance on the present theory for reasonably smooth and continuous surface-temperature distributions. For low subsonic Mach and Reynolds Numbers, however, condition (2) may in some cases restrict the applicability of the theory.

* Throughout this report all equations are written in absolute units; hence, the acceleration of gravity and Joule's constant do not appear in the analysis.

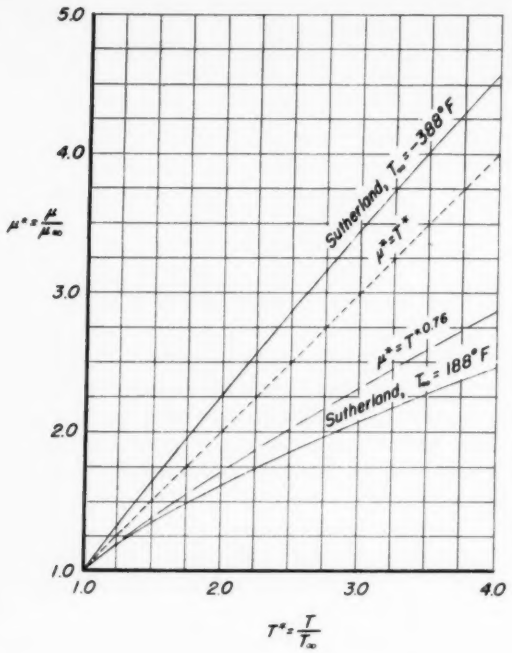

Figure 2.—Variation of viscosity with temperature.

Assumptions

If no additional assumptions are made other than those implied in condition (2), the problem under consideration then involves the solution of the three simultaneous partial differential equations [Eqs. (1)] for the three dependent variables u, v, T. It is apparent that some additional assumptions are needed in order to make Eqs. (1) amenable to solution. The important assumptions, including those already made, which are used in obtaining a solution to the basic equations of conservation of momentum, mass, and energy are:

(i) $\delta/L << 1$ (usual boundary-layer approximation).
(ii) $(\partial T/\partial x)_w \sim (T_w - T_\infty)/\delta$ or less.
(iii) $Pr = c_p\mu/k$ = constant (0.72 for air).
(iv) c_p = constant.
(v) $\mu/\mu_\infty = CT/T_\infty$, where C can depend on T_w, T_∞, and M_∞.

Assumptions (i) and (ii) are discussed in Appendix A. For normal aerodynamic applications these two assumptions do not restrict the usefulness of results based upon them. Likewise, assumptions (iii) and (iv) do not unduly restrict the applicability of the theory, since c_p and Pr for air are constant to within a few per cent over a wide range of temperature. These first four assumptions are usually made. Assumption (v), however, is not made so often and requires some discussion.

It is known that an accurate equation for the variation of viscosity with temperature is given by Sutherland's formula

$$\mu/\mu_\infty = (T/T_\infty)^{3/2}[(T_\infty + S)/(T + S)] \quad (3)$$

where S is Sutherland's constant and is approximately 216°F. absolute for air. Curves representing this formula are shown by solid lines in Fig. 2 for two free-stream temperatures that are considered to be representative of the two extremes encountered in aerodynamic applications. One free-stream temperature is 188°F., which is typical of the high temperatures encountered in the atmosphere near 160,000-ft. elevation. The other free-stream temperature is −388°F., which corresponds approximately to the free-stream temperature of a supersonic wind tunnel operating in the Mach Number range near and beyond 5. Also shown in Fig. 2 are the approximating formulas $\mu/\mu_\infty = (T/T_\infty)^{0.76}$ and $\mu/\mu_\infty = (T/T_\infty)$. It is apparent from a glance at Fig. 2 that no single value of ω in the functional relationship $\mu/\mu_\infty = (T/T_\infty)^\omega$ can adequately represent the viscosity over the wide range of free-stream temperatures encountered on passing from supersonic wind-tunnel to flight conditions. Of course, by using a different value of ω for each free-stream temperature and Mach Number, a sufficiently accurate description of the actual boundary-layer characteristics could be obtained. Since the structure of the boundary-layer equations is such that this latter procedure would require a prohibitive amount of work for flows where the surface temperature varies, it is necessary to use some other approximate equation.

It has been shown in references 2, 3, and 5 that the assumption $\omega = 1$ greatly simplifies the boundary-layer equations yet provides a sufficiently accurate solution in many cases. This fact has also been used to advantage in the analyses given in references 4 and 14. The linear approximation used in these references is $\mu/\mu_\infty = T/T_\infty$,* which always gives the correct value for the viscosity in a region near the outside of the boundary layer but unfortunately gives grossly inaccurate values in the much more important region near the surface. (See Fig. 2.) As a result, the assumption $\mu/\mu_\infty = T/T_\infty$ does not predict satisfactorily all of the important boundary-layer characteristics at high Mach Numbers and high free-stream temperatures. This shortcoming of the usual linear equation for viscosity can be largely overcome by the simple artifice of adding to the linear approximation a factor C[13] that can depend explicitly on the free-stream temperature as well as the average surface temperature. Thus, regardless of Mach Number, free-stream temperature, or average surface temperature, the approximation

$$\mu/\mu_\infty = C(T/T_\infty) \quad (4)$$

can be made to yield nearly correct values for the viscosity in the important region near the surface. If,

* Hantzsche and Wendt use $\mu/\mu_w = T/T_w$ in reference 5 and apply this approximation at all steps in their analysis. Near the free stream this becomes $\mu_\infty/\mu_w = T_\infty/T_w$, so that division of these two equations yields $\mu/\mu_\infty = T/T_\infty$.

for example, the approximate Eq. (4) is matched with Sutherland's Eq. (3) at a temperature equal to the average surface temperature $\bar{T}_w$, then C is given by

$$C = \sqrt{T_w/T_\infty}\,[(T_\infty + S)/(T_w + S)] \tag{5}$$

This constant is not to be confused with the variable $C_w \equiv (\mu_w/\mu_\infty)(T_\infty/T_w)$, which is introduced later.

It is shown in the discussion of results that, even at Mach Numbers near 5, the use of Eq. (4) [assumption (v)] in simplifying the differential equations does not limit the accuracy of the final results by more than about 5 or 6 per cent over the entire range of free-stream temperatures encountered both in extreme supersonic wind-tunnel and flight conditions. This is not surprising in view of the fact that the very approximate assumption $\mu/\mu_\infty = T/T_\infty$ (Fig. 2) predicts the skin-friction and heat-transfer characteristics to within about 15 per cent at $M_\infty = 5$ and to within a smaller percentage at lower Mach Numbers.

Solution of Equations

Method of Solution

Using the assumptions that c_p and Pr are constant, the basic Eqs. (1) can be written as

$$\left.\begin{aligned} &\rho u\frac{\partial u}{\partial x} + \rho v\frac{\partial u}{\partial y} = \frac{\partial}{\partial y}\left(\mu\frac{\partial u}{\partial y}\right) && \text{momentum}\\ &\frac{\partial}{\partial x}(\rho u) + \frac{\partial}{\partial y}(\rho v) = 0 && \text{continuity}\\ &\rho u\frac{\partial T}{\partial x} + \rho v\frac{\partial T}{\partial y} = \frac{1}{Pr}\frac{\partial}{\partial y}\left(\mu\frac{\partial T}{\partial y}\right) + \mu\left(\frac{\partial u}{\partial y}\right)^2 && \text{energy}\end{aligned}\right\} \tag{6}$$

This set of partial differential equations can be greatly simplified by transforming them to a new coordinate system. As is indicated in the introduction, the transformation that is used employs the stream function ψ, instead of y, as one of the independent variables. By using ψ as one of the independent variables, the continuity equation is automatically satisfied, and the velocity components are given by

$$u = \frac{\rho_\infty}{\rho}\frac{\partial \psi}{\partial y}, \qquad v = -\frac{\rho_\infty}{\rho}\frac{\partial \psi}{\partial x} \tag{7}$$

The formulas for making the transformation from the independent variables (x, y) to an arbitrary and completely new set (s, ψ) are

$$\left.\begin{aligned} \frac{\partial}{\partial y} &= \frac{\partial s}{\partial y}\frac{\partial}{\partial s} + \frac{\partial \psi}{\partial y}\frac{\partial}{\partial \psi}\\ \frac{\partial}{\partial x} &= \frac{\partial s}{\partial x}\frac{\partial}{\partial s} + \frac{\partial \psi}{\partial x}\frac{\partial}{\partial \psi}\end{aligned}\right\} \tag{8}$$

Using Eqs. (7) and letting $s \equiv x$ gives†

$$\partial/\partial y = (\rho u/\rho_\infty)(\partial/\partial\psi)$$
$$(\partial/\partial x)_y = (\partial/\partial x)_\psi - (\rho v/\rho_\infty)(\partial/\partial\psi)$$

Hence,

$$\rho u(\partial/\partial x)_y + \rho v(\partial/\partial y)_x = \rho u(\partial/\partial x)_\psi$$

and by using the relation

$$\rho\mu = C\rho_\infty\mu_\infty \tag{9}$$

which is a consequence of the assumption that μ is proportional to the temperature, then the basic Eqs. (6) become

$$\left.\begin{aligned} \frac{\partial u}{\partial x} &= \frac{\mu_\infty}{\rho_\infty}\frac{\partial}{\partial\psi}\left(Cu\frac{\partial u}{\partial\psi}\right) && \text{momentum}\\ \frac{\partial T}{\partial x} &= \frac{\mu_\infty}{Pr\rho_\infty}\frac{\partial}{\partial\psi}\left(Cu\frac{\partial T}{\partial\psi}\right) + \frac{\mu_\infty C u}{c_p\rho_\infty}\left(\frac{\partial u}{\partial\psi}\right)^2 && \text{energy}\end{aligned}\right\} \tag{10}$$

The above system of equations can be further simplified by introducing the dimensionless variables

$$\begin{aligned} u^* &= u/U_\infty, & x^* &= x/L\\ T^* &= T/T_\infty, & \rho^* &= \rho/\rho_\infty\\ \mu^* &= \mu/\mu_\infty, & \psi^* &= \psi/\sqrt{\nu_\infty U_\infty LC}\end{aligned} \tag{11}$$

Using these dimensionless variables, Eqs. (10) become

$$\frac{\partial u^*}{\partial x^*} = \frac{\partial}{\partial\psi^*}\left(u^*\frac{\partial u^*}{\partial\psi^*}\right) \quad \text{momentum} \tag{12a}$$

$$\frac{\partial T^*}{\partial x^*} = \frac{1}{Pr}\frac{\partial}{\partial\psi^*}\left(u^*\frac{\partial T^*}{\partial\psi^*}\right) + (\gamma - 1)M_\infty^2 u^*\left(\frac{\partial u^*}{\partial\psi^*}\right) \quad \text{energy} \tag{12b}$$

for which the boundary conditions are

$$\begin{aligned} &u^* = 0 \text{ at } \psi^* = 0 (y = 0)\\ &u^* = 1 \text{ at } \psi^* = \infty\ (y = \infty)\\ &T^* = T_w^* \text{ at } \psi^* = 0\\ &T^* = 1 \text{ at } \psi^* = \infty\end{aligned}$$

The dimensionless surface temperature T_w^* is, of course, a function only of x.

It is important to note that the momentum Eq. (12a) and the boundary conditions on u^* are completely independent of the energy Eq. (12b) and the boundary conditions on T^*. This is, in fact, the fundamental point of the entire theoretical analysis, since it is only through the independence of the momentum equation from the energy equation in the coordinate system employed that a simple solution to the problem is possible. It also may be noted that, if the viscosity were not taken as proportional to the first power of the tempera-

† The variables held constant in a differentiation process are explicitly indicated in those cases where ambiguity could result if the subscript notation were not used.

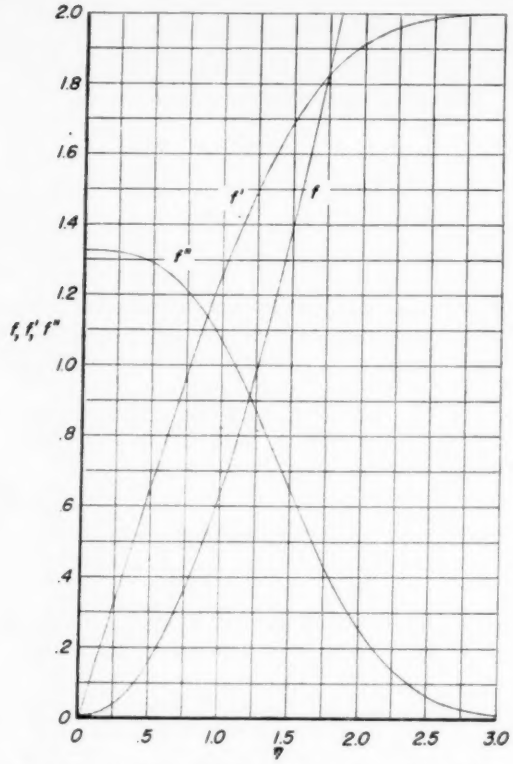

Figure 3 —Variation of Blasius functions f, f' and f'' with boundary-layer characteristic variable η.

ture, the density ρ^* (and hence T^*) would appear in Eq. (12a). This, of course, would excessively complicate matters even in the (x, ψ) coordinate system, since the equation representing conservation of momentum would not be independent of the energy equation, and, hence, the energy equation would not be a linear differential equation.

The fact that the density ρ^* does not appear in the momentum equation means that the function that solves Eq. (12a) must be the well-known Blasius function for incompressible flow. Hence,

$$u^* = (1/2)f'(\eta) \tag{13}$$

where η is defined by

$$f(\eta) = \psi^*/\sqrt{x^*} \tag{14}$$

The fact that Eq. (13) solves Eq. (12a) can easily be verified by direct substitution. Thus, differentiating Eq. (14),

$$f' \frac{\partial \eta}{\partial x^*} = -\frac{\psi^*}{2x^{*3/2}} = -\frac{f}{2x^*} \tag{15}$$

$$f'(\partial \eta / \partial \psi^*) = 1/\sqrt{x^*} \tag{16}$$

and substituting into Eq. (12a) gives

$$\frac{1}{2} f'' \frac{-f}{2x^* f'} = \frac{\partial}{\partial \psi^*} \left(\frac{1}{2} f' \frac{f''}{2\sqrt{x^* f'}} \right) = \frac{f'''}{4x^* f'}$$

or

$$ff'' + f''' = 0 \tag{17}$$

which is the familiar equation of Blasius satisfying the boundary conditions

$$f'(\infty) = 2$$
$$f'(0) = f(0) = 0$$

These boundary conditions are, of course, consistent with those imposed on Eq. (12a). Since complete tables of the functions f, f', and f'' can be found in many places (e.g., reference 16), the numerical solution to Eq. (12a) is known. Curves of these functions are shown in Fig. 3.

The continuity and momentum equations are solved by Eqs. (7) and (13), respectively. Consequently, the only equation now remaining to be solved is the energy Eq. (12b). Substituting Eq. (13) into Eq. (12b),

$$\frac{\partial T^*}{\partial x^*} = \frac{1}{2Pr} \frac{\partial}{\partial \psi^*} \left(f' \frac{\partial T^*}{\partial \psi^*} \right) + \frac{\gamma - 1}{8} \frac{M_\infty^2}{x^*} \frac{(f'')^2}{f'} \tag{18}$$

Because f' and f'' are functions of η alone, the independent variables (x^*, ψ^*) are changed to (x^*, η). This is done by the transformation formulas

$$\left.\begin{aligned} \left(\frac{\partial}{\partial x^*}\right)_\psi &= \left(\frac{\partial}{\partial x^*}\right)_\eta + \frac{\partial \eta}{\partial x^*} \frac{\partial}{\partial \eta} = \left(\frac{\partial}{\partial x^*}\right)_\eta - \frac{f}{2x^* f'} \frac{\partial}{\partial \eta} \\ \left(\frac{\partial}{\partial \psi^*}\right)_z &= \frac{\partial \eta}{\partial \psi^*} \frac{\partial}{\partial \eta} = \frac{1}{\sqrt{x^* f'}} \frac{\partial}{\partial \eta} \end{aligned}\right\} \tag{19}$$

Substituting Eq. (19) into Eq. (18) gives the following final form for the energy equation

$$\frac{\partial^2 T^*}{\partial \eta^2} + Prf \frac{\partial T^*}{\partial \eta} - 2Prf' x^* \frac{\partial T^*}{\partial x^*} = -\frac{Pr}{4} \times (\gamma - 1) M_\infty^2 (f'')^2 \tag{20}$$

with boundary conditions on the function $T^*(x^*, \eta)$ which can be written as

$$T^*(x^*, 0) = T_e^* + t(x^*)$$
$$T^*(x^*, \infty) = 1$$

where T_e^* is the dimensionless equilibrium temperature that would exist if the surface were insulated and $t(x^*)$ is an arbitrary function that specifies the surface-temperature distribution. Eq. (20) is a linear, second order, inhomogeneous partial differential equation (of parabolic type) with inhomogeneous boundary conditions. The standard mathematical methods of separating variables are thus applicable for its solution.

It may be noted that the transformation from (x, y) to (x, ψ) is not the only transformation that produces the same end result [Eq. (20)]. The transformation introduced by Crocco[3] and also used by Hantzsche and Wendt[5] will lead precisely to Eq. (20). Likewise, the transformation used recently by Howarth[14] will also make the momentum equation independent of the

energy equation and thus eventually lead to Eq. (20) when applied to the present problem.

Solution for Temperature Profile

Particular Solution of Inhomogeneous Equation.—Since Eq. (20) is linear, a particular solution of the form

$$T^*(x^*, \eta) = X(x^*) + N(\eta) \tag{21}$$

can easily be found. Substituting Eq. (21) into Eq. (20) gives

$$\frac{1}{2Prf'}\left[N'' + Prf N' + \frac{Pr}{4}(\gamma - 1)M_\infty{}^2(f'')^2\right] = x^* X' \tag{22}$$

Hence, both sides of Eq. (22) must be equal to a constant K. This yields as a solution for x

$$X = K \log x^*$$

which will give a logarithmic singularity at the origin unless $K = 0$. Setting $K = 0$ the function $N(\eta)$ is determined from

$$N'' + PrfN' = -(Pr/4)(\gamma - 1)M_\infty{}^2(f'')^2 \tag{23}$$

This ordinary differential equation is the same equation, apart from the constant factor $(\gamma - 1)M_\infty{}^2$, which has already appeared in the investigation of Pohlhausen.[15] The solution to Eq. (23) is obtained by the usual methods of solving first-order ordinary differential equations. It is

$$N(\eta) = 1 + [(\gamma - 1)/2]M_\infty{}^2 r(\eta) - (\gamma - 1)C_1 g(\eta) \tag{24}$$

where

$$r(\eta) = \frac{Pr}{2}\int_\eta^\infty [f''(\xi)]^{Pr}\int_0^\xi [f''(\theta)]^{2-Pr} d\theta d\xi \tag{25}$$

and

$$g(\eta) = \int_\eta^\infty [f''(\xi)]^{Pr} d\xi \tag{26}$$

The function $r(\eta)$ is plotted in Fig. 4 for $Pr = 0.72$ (air). Since Eq. (24) is a particular solution to Eq. (20), the arbitrary constant C_1 can, for convenience, be taken as zero. It is easily verified that $C_1 = 0$ corresponds to an insulated surface, since Eqs. (24) and (25) show that $(\partial N/\partial \eta)_w$ is zero. Hence, $N(0)$ is the dimensionless equilibrium surface temperature T_e^*,

$$N(0) = T_e^* \equiv \frac{T_e}{T_\infty} = 1 + r(0)\frac{\gamma - 1}{2}M_\infty{}^2 \tag{27}$$

This, of course, is the well-known expression for the surface equilibrium temperature in a compressible fluid. The "recovery factor" $r(0)$ is independent of Mach Number and equal to 0.845 for $Pr = 0.72$. (See Fig. 4.) It may be noted that Eq. (25) immediately gives $r(0) = 1$ for any gas wherein $Pr = 1$.

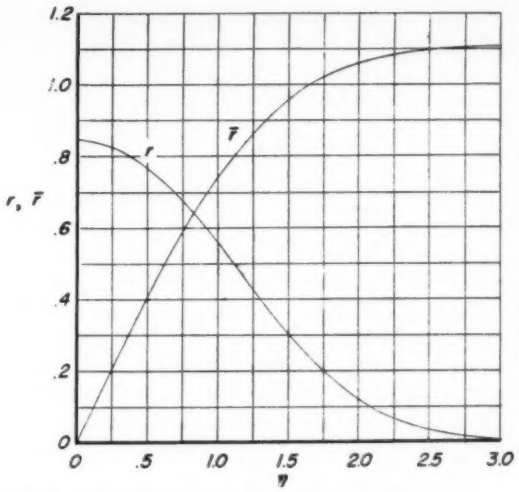

Figure 4.— Variation of r and r̄ with boundary-layer characteristic variable η, for P_r = 0.72.

Summarizing, a particular solution to the inhomogeneous Eq. (20) is

$$N(\eta) = 1 + [(\gamma - 1)/2]M_\infty{}^2 r(\eta) \tag{28}$$

which satisfies the boundary conditions

$$\begin{aligned} T^*(x^*, 0) &= T_e^* \qquad [(\partial N/\partial \eta)_w = 0] \\ T^*(x^*, \infty) &= 1 \end{aligned} \tag{29}$$

Solution to Homogeneous Equation.—The homogeneous part of Eq. (20) is

$$\frac{\partial^2 T^*}{\partial \eta^2} + Prf\frac{\partial T^*}{\partial \eta} - 2Prf'x^*\frac{\partial T^*}{\partial x^*} = 0 \tag{30}$$

Solutions to this equation can be obtained by separation of variables in the form

$$T^* = X(x^*)T(\eta)$$

which, when substituted into Eq. (30), gives,

$$(1/f'Y)(Y'' + PrfY') = 2Prx^* X'/X \tag{31}$$

Hence, both sides of Eq. (31) must be equal to a constant, say $2Prn$. Then

$$X_n(x^*) = x^{*n} \tag{32}$$

and $Y_n(\eta)$ is determined from the equation

$$Y_n'' + PrfY_n' - 2Prf'nY_n = 0 \tag{33}$$

The boundary conditions most convenient to impose on the functions $Y_n(\eta)$ are

$$\left.\begin{aligned} Y_n(0) &= 1 \\ Y_n(\infty) &= 0 \end{aligned}\right\} \tag{34}$$

Since the homogeneous equation is linear, solutions of the form $a_n x^{*n} Y_n(\eta)$, where a_n is an arbitrary constant can be superimposed to give as a general solution

$$\sum_{n=0}^{\infty} a_n x^{*n} Y_n(\eta) \tag{35}$$

which satisfies the following boundary conditions on $T^*(x^*, \eta)$:

$$T^*(x^*, 0) = \sum_0^\infty a_n x^{*n}$$

$$T^*(x^*, \infty) = 0$$

These functions $Y_n(\eta)$ that solve the homogeneous part of the energy equation have been calculated numerically for values of $n = 0, 1, 2, 3, 4, 5$, and 10. The method of numerical computation used is described in Appendix B, and curves of the functions $Y_n(\eta)$ are shown in Fig. 5.

Complete Solution.—Since Eq. (20) is linear, the complete solution is obtained by adding the particular solution (24) of the inhomogeneous equation to the general solution (35) of the homogeneous equation,

$$T^*(x^*, \eta) = N(\eta) + \sum_0^\infty a_n x^{*n} Y_n(\eta) \qquad (36)$$

The complete solution satisfies boundary conditions equal to the sum of the boundary conditions imposed on Eqs. (23) and (35)—namely,

$$T_w^* \equiv T^*(x^*, 0) = T_e^* + \sum_0^\infty a_n x^{*n} \qquad (37)$$

$$T^*(x^*, \infty) = 1$$

Comparing this with the boundary condition for an arbitrary surface-temperature distribution, which, for convenience, was written in the form

$$T_w^* = T_e^* + t(x^*) \qquad (38)$$

it is obvious that the coefficients a_n are determined by the arbitrary function $t(x^*)$ through the relation

$$t(x^*) = \sum_0^\infty a_n x^{*n} \qquad (38a)$$

Thus the coefficients a_n are simply the coefficients in the Taylor series for $t(x^*)$, so that if $t(x^*)$ is known analytically,

$$a_n = t^{(n)}(0)/n! \qquad (39)$$

In practical applications, however, Eq. (38) would be replaced by a finite sum—that is, $t(x^*)$ would be approximated by a polynomial—the coefficients a_n of which are the coefficients appearing in the final Eq. (36) for the temperature distribution.

Although the temperature distribution is given in terms of η, the corresponding value of y can be found in a simple manner. Thus, Eq. (7) can be written as

$$y = \int (\rho_\infty/\rho u) d\psi \qquad (40)$$

where the integration is carried out with x held constant. Substituting Eqs. (13) and (14) into Eq. (40) gives

$$(y/2)\sqrt{U_\infty/\nu_\infty x C} = \int_0^\eta T^* d\eta \qquad (41)$$

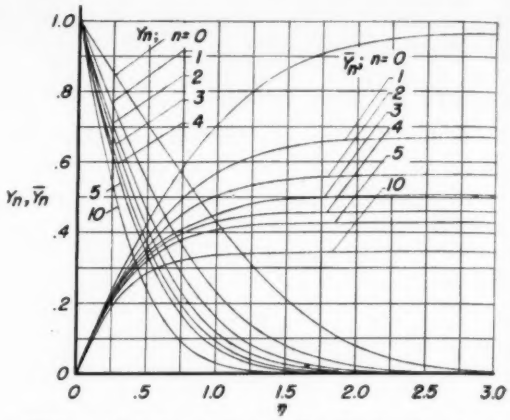

Figure 5.—Variation of Y_n and $\bar{Y}_n$ with boundary-layer characteristic variable η, for $P_r = 0.72$.

This can be integrated in closed form simply by substituting Eqs. (36) and (28) into the integrand of Eq. (41) and then integrating term by term

$$\frac{y}{2}\sqrt{\frac{U_\infty}{\nu_\infty x C}} = \eta + \frac{\gamma - 1}{2} M_\infty^2 \bar{r}(\eta) + \sum_0^\infty a_n x^{*n} \bar{Y}_n(\eta) \qquad (42)$$

The fixed functions $\bar{r}$ and $\bar{Y}_n$ are the integrals of r and Y_n, respectively,

$$\bar{r}(\eta) = \int_0^\eta r(\eta) d\eta \qquad (43)$$

$$\bar{Y}_n(\eta) = \int_0^\eta Y_n(\eta) d\eta \qquad (44)$$

Curves of these functions are given in Figs. 4 and 5 so that the value of y corresponding to a given value of η can be found readily from these curves and Eq. (42).

Heat Transfer

The convective heat q transferred from a unit area of surface per unit time at a given point is

$$q \equiv -k_w (\partial T/\partial y)_w \qquad (45)$$

Although this equation does not include a term accounting for the heat radiated from the surface, it is an easy matter to do so by the conventional method. The equations that follow, therefore, represent the heat transferred through the boundary layer by convection and conduction.

Differentiating Eq. (36), substituting into Eq. (45), and noting that $(\partial r/\partial \eta)_w = 0$,

$$q = -k_w T_\infty \left(\frac{\partial \eta}{\partial y}\right)_w \sum_0^\infty a_n x^{*n} Y_n'(0) \qquad (46)$$

By using Eqs. (7), (13), and (16), $\partial\eta/\partial y$ can be evaluated to give

$$\frac{\partial \eta}{\partial y} = \frac{\partial \eta}{\partial \psi^*} \frac{\partial \psi}{\partial y} \frac{1}{\sqrt{\nu_\infty U_\infty L C}} = \sqrt{\frac{U_\infty}{\nu_\infty x C}} \frac{1}{2T^*} \qquad (47)$$

hence,

$$\left(\frac{\partial \eta}{\partial y}\right)_w = \sqrt{\frac{U_\infty}{\nu_\infty x C}} \frac{1}{2T_w^*} \tag{48}$$

The ratio k_w/T_w^* can be written as

$$\frac{k_w}{T_w^*} = \frac{\mu_w}{\mu_\infty}\frac{k_\infty}{T_w^*} = \frac{\mu_w^*}{T_w^*} k_\infty \equiv C_w k_\infty \tag{49}$$

where, according to Eq. (3),

$$C_w \equiv \mu_w^*/T_w^* = \sqrt{T_w/T_\infty}[(T_\infty + S)/(T_w + S)] \tag{49a}$$

The variable C_w is a function of x since T_w depends upon x, and is not to be confused with the constant C defined by Eq. (5). For the special case of constant surface temperature C_w is equal to C. The rate of heat transfer is

$$q = -\frac{k_\infty T_\infty}{2} C_w \sqrt{\frac{U_\infty}{\nu_\infty x C}} \sum_0^\infty a_n x^{*n} Y_n'(0) \tag{50}$$

Usually q is expressed as the product of a heat-transfer coefficient and the difference between the surface temperature and the equilibrium temperature. The usual expression, however, involves a constant surface temperature, so that a slightly different expression will have to be used for the case of a variable surface temperature. Actually, there are many possible definitions that will reduce to the customary one in the special case of constant surface temperature. The most logical equation to choose for defining the heat-transfer coefficient h is

$$q = h[T(x, 0) - T_e] = h(T_w - T_e) \tag{51}$$

where $T(x, 0)$ is the local surface temperature T_w. Eq. (51), of course, is identical to the customary equation if the surface temperature T_w is constant. Comparing Eqs. (50) and (51) and noting that the leading-edge surface temperature is $T^*(0, 0) = T_e^* + a_0$, it follows that

$$h = \bar{h}\frac{[T^*(0, 0) - T_e^*]C_w}{(T_w^* - T_e^*)C} - \frac{k_\infty C_w}{2} \times \frac{\sqrt{U_\infty/(\nu_\infty x C)}}{T_w^* - T_e^*} \sum_{n=1}^\infty a_n x^{*n} Y_n'(0) \tag{52}$$

where $\bar{h}$ is the heat-transfer coefficient for the case of constant surface temperature and is given by

$$\bar{h} \equiv -(k_\infty/2)\sqrt{U_\infty C/\nu_\infty x}\, Y_0'(0) \tag{53}$$

Thus, Eq. (52) simply gives the additional corrective terms necessary to account for the effects of variable surface temperature on the local heat-transfer coefficient. The use of the temperature T_e in the defining Eq. (51) for the heat-transfer coefficient does not enable the final expression (52) to be completely independent of Mach Number, as is the case for flows with constant surface temperature. Nevertheless, Eq. (52) is substantially independent of the Mach Number, since the only effect of Mach Number would be its indirect effect on T_w, which indirectly would have a small effect on C and C_w.

The relation between the local Nusselt Number and Reynolds Number is

$$Nu \equiv \frac{hx}{k_\infty} = \overline{Nu}\frac{[T^*(0, 0) - T_e^*]C_w}{(T_w^* - T_e^*)C} - \frac{1}{2}\frac{C_w}{\sqrt{C}}\frac{\sqrt{Re_x}}{(T_w^* - T_e^*)} \sum_{n=1}^\infty a_n x^{*n} Y_n'(0) \tag{54}$$

where $\overline{Nu} = \bar{h}x/k_\infty = -(\sqrt{C}/2)\sqrt{Re_x}\, Y_0'(0)$ is the local Nusselt Number for constant surface temperature and Re_x is the Reynolds Number based on free-stream conditions and the length x. The total rate of heat transfer Q per unit width of a two-dimensional surface is obtained by integrating Eq. (50) from $x = 0$ to $x = L$,

$$Q = -\frac{k_\infty T_\infty}{2}\sqrt{\frac{U_\infty L}{C\nu_\infty}} \sum_{n=0}^\infty a_n b_n Y_n'(0) \tag{55}$$

where the coefficients

$$b_n = \int_0^1 C_w x^{*n - 1/2} dx^* \tag{56}$$

can be evaluated for any given distribution of surface temperature (given C_w).

The quantities $Y_n'(0)$ that appear in all the foregoing equations for heat transfer are given in Table 1 for $n = 0, 1, 2, 3, 4, 5$, and 10.

TABLE 1
Numerical Values for $Y_n'(0)$

n	$Y_n'(0)$
0	−0.5915
1	−0.9775
2	−1.1949
3	−1.3680
4	−1.4886
5	−1.5975
10	−2.0121

Solution for Velocity Profile

The dimensionless velocity is related to the independent variable η by the Blasius function

$$u^* = (1/2)f'(\eta) \tag{13}$$

so that the velocity is immediately known for any given value of η. Moreover, the value of y corresponding to a given value of η is obtained from the relation

$$\frac{y}{2}\sqrt{\frac{U_\infty}{\nu_\infty x C}} = \eta + \frac{\gamma - 1}{2} M_\infty^2 \bar{r}(\eta) + \sum_0^\infty a_n x^{*n} \bar{Y}_n(\eta) \tag{42}$$

which was previously derived. Since the functions $\bar{r}(\eta)$ and $\bar{Y}_n(\eta)$ are fixed functions for all problems (they are given in Figs. 4 and 5) and since the coefficients a_n are determined once the surface-temperature dis-

tribution is specified, it is therefore a relatively simple matter to calculate velocity, as well as temperature, profiles for an arbitrary distribution of surface temperature.

Skin Friction

By differentiating Eq. (13), the shear stress can be evaluated at any point in the boundary layer

$$\tau \equiv \mu \frac{\partial u}{\partial y} = \frac{\mu}{2} f''(\eta) \frac{\partial \eta}{\partial y} U_\infty$$

Using Eq. (47), the shear at a given value of η becomes

$$\tau = f''(\eta) \sqrt{U_\infty / \nu_\infty x C} (\mu U_\infty / 4T^*) \qquad (57)$$

which reduces to

$$\tau_w = (f''(0)/4) U_\infty C_w \sqrt{\rho_\infty U_\infty \mu_\infty / Cx} \qquad (57a)$$

for the shear stress at the surface. Integration from $x = 0$ to $x = L$ gives the section skin-friction drag coefficient

$$c_{df} = [f''(0)/\sqrt{ReC}](1/2) \int_0^1 C_w dx^*/\sqrt{x^*} \qquad (58)$$

which reduces to

$$c_{df} = [f''(0)/\sqrt{Re}] \sqrt{C} = (1.328/\sqrt{Re})\sqrt{C} \qquad (58a)$$

for flows with constant surface temperature. In a later part of this paper, this formula is compared with the results of other analyses. (See discussion of results.)

Relation Between Skin Friction and Heat Transfer

Although the equation relating heat transfer and skin friction for the general variable surface-temperature flows is too complicated to be of much practical use, it is derived here not only for the sake of completeness but also for the purpose of illustrating that the familiar heat-transfer and skin-friction analogy is not applicable to flows where the surface temperature varies. This conclusion could be deduced directly from the dissimilar boundary conditions imposed on the energy and the momentum equations—that is, $u \equiv 0$ at surface while T_w varies—however, the following gives a quantitative indication at the relationships.

The ratio between local rate of heat transfer and local skin friction (shear) is obtained by dividing Eqs. (50) and (57a).

$$\frac{q}{\tau} = \frac{2k_\infty T_\infty}{f''(0) U_\infty \mu_\infty} \sum_{n=0}^{\infty} a_n x^{*n} [-Y_n'(0)]$$

This can be put in a more illustrative form by evaluating $Y_0'(0)$. Thus, it is easily verified by direct substitution into Eq. (33) that

$$Y_0(\eta) = \int_\eta^\infty [f''(\eta)]^{Pr} d\eta \Big/ \int_0^\infty [f''(\eta)]^{Pr} d\eta$$

hence,

$$Y_0'(0) = -[f''(0)]^{Pr} \Big/ \int_0^\infty [f''(\eta)]^{Pr} d\eta$$

The numerical calculations of Pohlhausen show, however, that for $0.6 < Pr < 1.0$ an approximation valid to within less than 1 per cent is

$$\int_0^\infty [f''(\eta)]^{Pr} d\eta = 2[f''(0)]^{Pr-1}/Pr^{1/3}$$

so that to within 1 per cent,

$$Y_0'(0) = -[f''(0)/2] Pr^{1/3} \qquad (59)$$

Using this equation, the ratio q/τ becomes

$$\frac{q}{\tau} = \frac{c_p T_\infty}{U_\infty Pr^{2/3}} \sum_{n=0}^{\infty} a_n x^{*n} \frac{Y_n'(0)}{Y_0'(0)} \qquad (60)$$

This equation shows that there is no simple relation between heat transfer and skin friction valid for flows with variable surface temperature. For the special case of constant surface temperature, however, Eq. (60) reduces to

$$q/\tau = c_p (T_w - T_e)/U_\infty Pr^{2/3} \qquad (61)$$

which is the same relation as that given by Hantzsche and Wendt.[5]

The ratio between total rate of heat transfer and the integrated skin friction also reduces to a simple expression for the particular case of constant surface temperature. Thus, dividing Eq. (55) by Eq. (58a) and remembering that for constant surface temperature $a_0 = T_w^* - T_e^*$,

$$\frac{Q}{k_\infty (T_w - T_e)\sqrt{Re}} = \frac{c_{df}\sqrt{Re}}{f''(0)} [-Y_0'(0)] \qquad (62)$$

Substituting Eq. (59) into Eq. (62) gives, finally,

$$Q/k_\infty (T_w - T_e)\sqrt{Re} = (c_{df}\sqrt{Re}/2) Pr^{1/3} \qquad (63)$$

This expression also is applicable only to flows with constant surface temperature.

Practical Use of Results

Statement of Complete Solution to Problem

The foregoing solution to the laminar boundary-layer equations has been obtained for an arbitrary surface-temperature distribution, which for convenience is expressed in the dimensionless form

$$T_w^* \equiv T_w/T_\infty = T_e^* + t(x^*) \qquad (38)$$

where

$$T_e^* \equiv \frac{T_e}{T_\infty} = 1 + r(0) \frac{\gamma - 1}{2} M_\infty^2$$

$$= 1 + 0.169\, M_\infty^2 \text{ (for air with } Pr = 0.72)$$

is the dimensionless equilibrium temperature and $t(x^*)$

is an arbitrary analytic function of $x^* \equiv x/L$. Since any regular function such as $t(x^*)$ can be expressed in a power series (or approximated by a polynomial for practical applications), the coefficients a_n in the Taylor series

$$t(x^*) \equiv \sum_{n=0}^{\infty} a_n x^{*n} \tag{38a}$$

may be considered as known for any given surface temperature distribution. It is important to note that the final results of the analysis, which are summarized below, involve as unknowns only these coefficients a_n. The work involved in applying the theory, therefore, depends only on the work involved in approximating a given surface temperature distribution $T_w^*(x)$ by a polynomial. If $t(x^*)$ is given in analytic form, then

$$a_n = t^{(n)}(0)/n! \tag{39}$$

Many of the equations summarized below are expressed in terms of the characteristic boundary-layer variable η, which is related to the physical coordinates through the relation

$$\frac{y}{2}\sqrt{\frac{U_\infty}{\nu_\infty x C}} = \eta + \frac{\gamma - 1}{2} M_\infty^2 \bar{r}(\eta) + \sum_{n=0}^{\infty} a_n x^{*n} \bar{Y}_n(\eta) \tag{42}$$

This relation allows those equations that are expressed in terms of η to be converted to physical coordinates, since $\bar{r}(\eta)$ and $\bar{Y}_n(\eta)$ are known functions (Figs. 4 and 5). The principal equations developed in the course of the analysis are:

$$T^*(x^*, \eta) \equiv \frac{T}{T_\infty} = 1 + \frac{\gamma - 1}{2} M_\infty^2 r(\eta) + \sum_{n=0}^{\infty} a_n x^{*n} Y_n(\eta) \tag{36}$$

$$u^*(x^*, \eta) \equiv \frac{u}{U_\infty} = \frac{1}{2} f'(\eta) \tag{13}$$

$$q \equiv -k_w \left(\frac{\partial T}{\partial y}\right)_w = -\frac{k_\infty T_\infty C_w}{2}\sqrt{\frac{U_\infty}{C\nu_\infty x}} \times \sum_{n=0}^{\infty} a_n x^{*n} Y_n'(0) \tag{50}$$

$$h \equiv \frac{q}{T_w - T_e} = \bar{h}\,\frac{[T_w^*(0, 0) - T_e^*]C_w}{(T_w^* - T_e^*)C} - \frac{k_\infty C_w}{2}\sqrt{\frac{U_\infty}{C\nu_\infty x}}\,\frac{\sum_{n=1}^{\infty} a_n x^{*n} Y_n'(0)}{T_w^* - T_e^*} \tag{52}$$

$$\bar{h} = -(k_\infty/2)\sqrt{U_\infty C/\nu_\infty x}\, Y_0'(0) \tag{53}$$

$$Nu \equiv \frac{hx}{k_\infty} = \overline{Nu}\,\frac{C_w}{C}\,\frac{[T_w^*(0, 0) - T_e^*]}{(T_w^* - T_e^*)} - \frac{C_w}{2}\sqrt{\frac{U_\infty x}{\nu_\infty C}}\,\frac{\sum_{n=1}^{\infty} a_n x^{*n} Y_n'(0)}{(T_w^* - T_e^*)} \tag{54}$$

$$\overline{Nu} \equiv \bar{h}x/k_\infty = -[Y_0'(0)/2]\sqrt{Re_x C}$$

$$c_{d_f} = [f''(0)/\sqrt{ReC}](1/2)\int_0^1 (C_w dx^*/\sqrt{x^*}) \tag{58}$$

$$\left.\begin{aligned} c_{d_f} &= [f''(0)/\sqrt{Re}]\sqrt{C} \\ &= (1.328/\sqrt{Re})\sqrt{C} \end{aligned}\right\} \begin{array}{l}\text{(for flows with constant surface temperature)}\end{array} \tag{58a}$$

It is to be remembered that these equations are for two-dimensional flow but may be applied to axially symmetric flows without pressure gradient by making the modifications indicated in reference 10.

Numerical values of $Y_n'(0)$ applicable for all flows with variable surface temperature are given in Table 1. Curves of the fixed functions $f'(\eta)$, $f''(\eta)$, $r(\eta)$, $\bar{r}(\eta)$, $Y_n(\eta)$, and $\bar{Y}_n(\eta)$ appearing in the above equations are shown in Figs. 3, 4, and 5. The expression $T_w^*(0, 0)$ is, of course, the leading-edge surface temperature. The variable C_w appearing in these equations is defined by the relation

$$C_w \equiv \mu_w^*/T_w^* \tag{49}$$

Using Sutherland's formula [Eq. (3)], C_w is given by

$$C_w = \sqrt{T_w/T_\infty}\,[(T_\infty + S)/(T_w + S)]$$

The constant

$$C = \sqrt{\bar{T}_w/T_\infty}\,[(T_\infty + S)/(\bar{T}_w + S)] \tag{5}$$

matches the viscosity as given by the approximate Eq. (4) with Sutherland's formula at the particular temperature $\bar{T}_w$. For general engineering use, Eq. (5) should be sufficiently accurate to account for the temperature level of a particular boundary layer.

Once the surface temperature has been approximated by a polynomial, the procedure for calculating a given quantity involves only the substitution of the coefficients (a_n) of the polynomial into the appropriate equations and the use of the appropriate curves in Figs. 3, 4, and 5.

In practical applications, the local Nusselt Number $\overline{Nu}$ for constant surface temperature,

$$\overline{Nu} = -\frac{Y_0'(0)}{2}\sqrt{Re_x C} = 0.296\sqrt{Re_x C}$$

could, if desired, be replaced by some other expression that explicitly includes the effect of Mach Number. (The above expression only implicitly includes the effect of Mach Number through the constant C.) Although such a procedure would possibly improve the accuracy slightly, a rigorous justification of it has not been attempted. The most complete set of calculations available to date for $\overline{Nu}$ has been made by Crocco.[3, 4]

The foregoing equations are applicable if the distribution of the rate of heat transfer is prescribed rather than the distribution of surface temperature. For such cases, Eq. (50) determines the coefficients a_n,

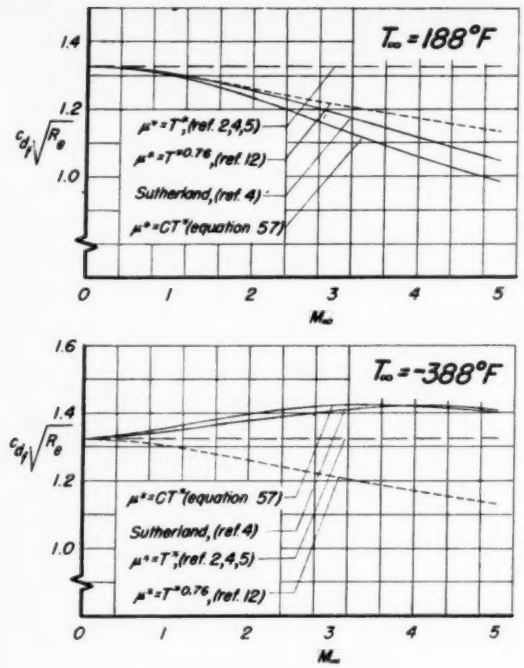

Figure 6.—Skin friction drag of an insulated plate using different variations of viscosity with temperature.

which, once determined, can be substituted into the remaining equations to calculate the temperature distribution, velocity distribution, and other quantities of interest.

Discussion

Reduction of Present Theory to the Solutions of Blasius and Pohlhausen for Incompressible Flow over an Insulated or Heated Plate

For flow over an insulated plate, the surface temperature is equal to the equilibrium temperature T_e, and all coefficients a_n are zero [Eqs. (38) and (38a)]. Moreover, for low-speed subsonic flows, the absolute temperature within the boundary layer never departs appreciably from the free-stream temperature, so that $C \to 1$ as $M_\infty \to 0$. Therefore, the velocity distribution is

$$u = (1/2)f'(\eta)$$

where the relation between η and y [Eq. (42)] reduces to

$$(y/2)\sqrt{U_\infty/\nu_\infty x} = \eta$$

This is the well-known solution of Blasius for incompressible flow.

Writing the free-stream Mach Number as $U_\infty/\sqrt{\gamma RT_\infty}$, Eq. (36) for the temperature distribution becomes

$$T/T_\infty = 1 + [(\gamma - 1)/2](U_\infty^2/\gamma RT_\infty)r(\eta)$$

or

$$(T - T_\infty)/T_\infty = r(\eta)(U_\infty^2/2c_pT_\infty)$$

which is a solution of Pohlhausen.[15] The present theory, therefore, contains as special cases the familiar solutions of Blasius and Pohlhausen for low-speed flow over an insulated plate.

Another low-speed solution for heat transfer from a constant temperature plate to an incompressible boundary layer is also a particular solution of the present analysis. Thus, as $M_\infty \to 0$, $C \to 1$, and Eq. (53) becomes

$$Nu = 0.296\sqrt{Re}$$

which is identical with the expression obtained by Pohlhausen for $Pr = 0.72$.

Comparison with Other Results for Compressible Flow Surface of Constant Temperature

Before discussing some of the effects of a variable surface temperature, it will be well to compare the results of the theory given herein with those of other investigations of compressible laminar boundary-layer flow Such comparisons must, of course, be restricted to cases of constant surface temperature, but nevertheless will serve to illustrate the degree to which the present theory [based on the approximation $\mu/\mu_\infty = C(T/T_\infty)$] agrees with other more precise and much more complicated calculations of boundary-layer flow at high Mach Numbers.

Skin Friction.—Fig. 6 shows a comparison of the skin friction coefficient of an insulated surface as determined from Eq. (58a) and also as determined from other calculations. In this figure the various methods of calculation are compared for two free-stream temperatures: 188° and −388°F., which are considered to be representative of extreme conditions in the stratosphere and in high Mach Number supersonic wind tunnels, respectively. For each free-stream temperature three different methods have been chosen for comparison with the present theory. One method is based on the assumption $\mu/\mu_\infty = (T/T_\infty)^{0.76}$, often considered to be adequate for general aerodynamic applications. A second method is based on the simple assumption $\mu/\mu_\infty = T/T_\infty$ used by Crocco and Lees. The third method chosen for comparison is labeled "Sutherland" on the figures, and is taken from the calculations of Crocco.[4] This latter method of calculation is considered to be the most reliable method available since it uses Sutherland's Eq. (3) for the variation of viscosity with temperature.

It is apparent from Fig. 6 that the assumption $\mu^* = T^*$ is a first approximation. The assumption $\mu^* = T^{*0.76}$ is seen to be good at flight temperatures (for which it was proposed) but unsatisfactory at the low temperatures of supersonic wind tunnels. On the other hand, the assumption $\mu^* = CT^*$ yields good results for both free-stream temperatures at Mach Numbers up to 5. From these curves in Fig. 6, it can be

seen that for an insulated surface the skin friction is predicted by the present theory to within about 1 per cent for free-stream temperatures encountered in high Mach Number supersonic wind tunnels and to within about 5 per cent for extreme free-flight conditions up to Mach Numbers near 5. For noninsulated surfaces heated or cooled within reasonable practical limitations, the order of accuracy of the present theory is about the same as that illustrated by Fig. 6.

Heat Transfer.—For the special case of constant surface temperature, the relationship between heat transfer and skin friction is

$$Q/k_\infty(T_w - T_e)\sqrt{Re} = (c_{df}\sqrt{Re}/2)Pr^{1/3} \quad (63)$$

as was previously derived. The calculations of Crocco show that, even if Sutherland's equation is used, Eq. (63) is still valid to within about 0.5 per cent for any free-stream temperature. Therefore, the order of accuracy with which the present theory predicts the skin friction, as illustrated by Fig. 6, is also the order of accuracy with which it predicts the rate of heat transfer.

General Effects of Variable Surface Temperature

Heat-Transfer Coefficient.—Probably the most important single effect of variable surface temperature appears in the heat-transfer coefficient and, hence, Nusselt Number. Thus, the conventional definition of heat-transfer coefficient by means of the Newtonian cooling law

$$q = h(T_w - T_e)$$

yields

$$h = \bar{h}\frac{[T_w^*(0, 0) - T_e^*]C_w}{(T_w^* - T_e^*)C} - \frac{k_\infty C_w}{2} \times \sqrt{\frac{U_\infty}{C\nu_\infty x}}\frac{\sum_1^\infty a_n x^{*n} Y_n'(0)}{T_w^* - T_e^*} \quad (52)$$

as was previously derived. Unfortunately, at each point where the surface temperature T_w^* is equal to the equilibrium temperature T_e^*, this expression will become both positively infinite and negatively infinite in all but a few exceptional cases. (The physical explanation for this is given later.) The exceptional flows where an infinity does not appear are those with constant surface temperature, wherein Eq. (52) reduces to $h = \bar{h}$, and those wherein the surface-temperature distribution possesses the extraordinary property that the limit

$$\lim_{T_w^* \to T_e^*} \sum_0^\infty a_n x^{*n} \; Y_n'(0) \Big/ (T_w^* - T_e^*)$$

is finite at every point where $T_w = T_e$. Of course, this latter condition generally is not possible. Since the equations for all boundary-layer characteristics other than $h(T, u, q, \text{and } Q)$ do not become infinite under any physically possible conditions, it is clear that the customary definition of heat-transfer coefficient is fundamentally inappropriate for flows with variable surface temperature. For variable surface temperatures it appears more convenient to deal directly with the dimensionless group $qx/k_\infty T_e$, rather than hx/k_∞.

Total Heat Transferred.—As far as the total rate of heat transfer is concerned, an illustrative comparison can be made between the present theory that accounts for the effects of a variable surface temperature and a customary calculation that assumes that the heat-transfer coefficient is that determined for a constant surface temperature ($\bar{h}$). In order to simplify this comparison, C and C_w temporarily will be taken as unity, since their actual values are unimportant for the purpose at hand. The customary method gives $\bar{q} = \bar{h}(T_w - T_e)$, and

$$\bar{Q} = \int_0^L \bar{h}(T_w - T_e)dx = -\frac{T_\infty k_\infty Y_0'(0)}{2} \times \sqrt{\frac{U_\infty L}{\nu_\infty}} \sum_0^\infty \int_0^1 a_n x^{*n - (1/2)}\, dx^* = -\frac{T_\infty k_\infty Y_0'(0)}{2}\sqrt{\frac{U_\infty L}{\nu_\infty}} \sum_0^\infty \frac{a_n}{n + (1/2)}$$

The present theory gives, from Eq. (55), when $C = C_w = 1$,

$$Q = -\frac{k_\infty T_\infty}{2}\sqrt{\frac{U_\infty L}{\nu_\infty}} \sum_0^\infty \frac{a_n}{n + (1/2)} \; Y_n'(0)$$

Thus, the ratio of the total heat transferred as given by the two methods is approximately

$$\frac{Q}{\bar{Q}} = \sum_0^\infty \frac{a_n}{n + (1/2)} \; Y_n'(0) \Big/ Y_0'(0) \sum_0^\infty \frac{a_n}{n + (1/2)} \quad (64)$$

This ratio obviously is not unity except in special cases. In fact, for different surface-temperature distributions, this ratio can be either positive, negative, zero, or infinite. The particular example discussed later on yields a negative value for this ratio.

Flow Separation.—The calculations for the velocity profile allow some useful qualitative information to be obtained with regard to the effect of a heated surface on flow separation. Eq. (57), when evaluated at the surface, yields

$$\left(\frac{\partial u}{\partial y}\right)_w = \left(\frac{\tau}{\mu}\right)_w = f''(0)\sqrt{\frac{U_\infty}{\nu_\infty x C}}\frac{U_\infty}{4T_w^*}$$

In theoretical calculations the separation point of a flow is taken as that point where $(\partial u/\partial y)_w = 0$. Hence, the above equation shows that, for a heated plate in the absence of a pressure gradient, the slope of the velocity profile at the surface will vary approximately as the reciprocal of the absolute temperature. Consequently, it would theoretically take an infinite surface temperature under these conditions to cause flow separation.

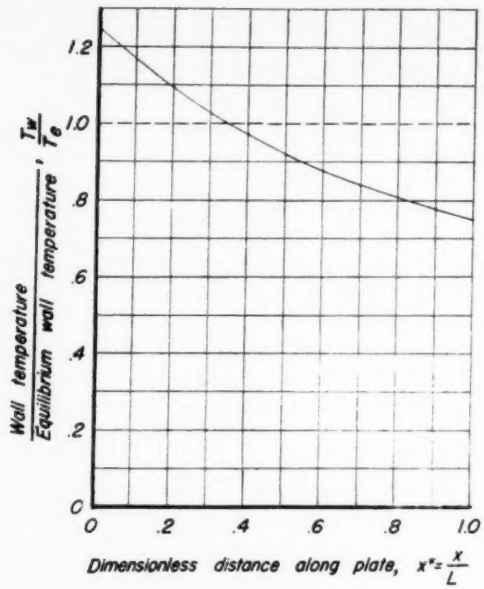

Figure 7. —Surface temperature distribution for example problem.

If, on the other hand, the upstream part of a surface is heated and the downstream part is subjected to an increasing pressure (adverse pressure gradient), then a smaller increase in pressure will cause separation than would be necessary if no heat were added to the upstream part. Likewise, if an adverse pressure gradient simultaneously exists over a heated region of a surface, flow separation will occur more readily than if that same surface were not heated. In general, it can be concluded that the addition of heat can contribute to but cannot by itself cause flow separation.

Discussion of an Example

The particular example to be considered in detail is designed to illustrate conveniently some of the more important results of the theory. Thus, for simplicity, two-dimensional flow is considered with C_w and C set equal to unity. This means that the small indirect effect of Mach Number on C_w and C and, consequently, on the heat transfer is neglected. The other boundary-layer characteristics (u and T) are calculated for two Mach Numbers, $M_\infty = 0.5$ and $M_\infty = 3.0$, which are considered to be representative of subsonic and supersonic flows, respectively.

The distribution of surface temperature selected for the example is given by the quadratic

$$t(x^*) \equiv T_w^* - T_e^* = T_e^*(0.25 - 0.83x^* + 0.33x^{*2})$$

so that

$$a_0 = 0.25T_e^*$$
$$a_1 = -0.83T_e^*$$
$$a_2 = 0.33T_e^*$$
$$a_n = 0,\ n > 2$$

This distribution is plotted in Fig. 7 with the ratio of surface temperature to equilibrium temperature as the ordinate. This distribution is considered to exist at both $M_\infty = 0.5$ and $M_\infty = 3.0$, and, therefore, the actual level of surface temperature becomes a function of M_∞ through the explicit dependence of T_e on Mach Number. The purpose of this figure is to indicate the relative change of surface temperature with respect to the overall effective temperature difference $(T_w - T_e)$ between the surface and the free stream. It will be noted that a rather severe case has been analyzed, since the overall temperature variation in the plate is one-half the equilibrium temperature—or looking at it in another light, it is twice the maximum difference between T_w and T_e.

Heat-Transfer Coefficient

By substituting the coefficients a_0, a_1, and a_2 into Eqs. (52) and (53) and using the values of $Y_n'(0)$ given in Table 1, the heat-transfer coefficient is obtained as a quadratic function of x^*. The resulting effect of the surface-temperature distribution (Fig. 7) on the local heat-transfer coefficient is illustrated in Fig. 8a, where the Nusselt Number divided by the square root of local Reynolds Number is plotted (solid line) as a function of the dimensionless distance along the plate. It may be noted from Eq. (52) that the effect of Mach Number is eliminated when $C = 1$ and the ratio T_w/T_e is independent of M_∞. Fig. 8a, therefore, applies for both $M_\infty = 0.5$ and $M_\infty = 3.0$ in the example under consideration. The dotted line in Fig. 8a represents the local heat-transfer coefficient determined by the conventional method wherein the effect of the variable surface temperature is not included. The dotted line is represented by

$$\frac{\overline{Nu}}{\sqrt{Re_x}} = \frac{\bar{h}x}{k_\infty\sqrt{Re_x}} = -\frac{Y_0'(0)}{2} = 0.296$$

Several interesting effects may be observed from this figure. In the region of decreasing temperature potential ($0 < x^* < 0.35$), the local heat-transfer coefficient is less than that for a constant surface temperature plate. The heat-transfer coefficient is reduced so markedly that it becomes zero ($x^* = 0.2$) and then even becomes negative ($0.22 < x^* < 0.35$), which means that heat flows into the plate although the overall temperature potential is in the direction that would normally cause heat to flow from the plate to the free stream. Since the heat flows in a direction opposite to the local overall temperature potential, the heat-transfer coefficient h in Newton's law of cooling

$$h \equiv q_w/(T_w - T_e)$$

is necessarily negative over part of the surface. This anomalous behavior continues downstream to $x^* =$

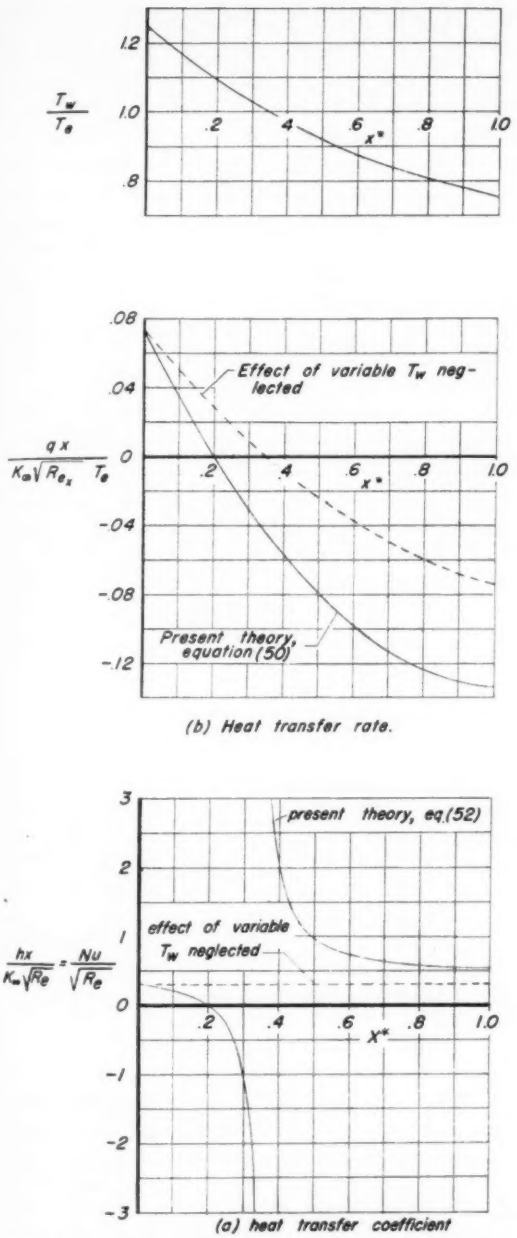

Figure 8—Effect of variable surface temperature on the heat transfer characteristics of the example problem.

0.35, where h becomes first negatively infinite and then suddenly becomes positively infinite. As was stated earlier, this behavior is due to the inappropriateness of the conventional heat-transfer coefficient when applied to flows with variable surface temperature. From the physical point of view, this inappropriateness exists because the definition of h at a given point involves only conditions at that particular point (*i.e.*, the local value of $T_w - T_e$); whereas the boundary-layer properties at a given point do not depend only on the local temperature potential but, instead, depend in a complicated manner on the entire distribution of surface temperature upstream of the point in question. (The distribution of surface temperature downstream of a given point has only an extremely small effect on the boundary-layer flow upstream.) Thus, if the surface temperature at a fixed point were maintained at the equilibrium temperature T_e and if the distribution of surface temperature upstream of that point were varied widely, then the changes in the velocity and temperature profiles that would take place upstream would propagate downstream, thereby causing the temperature profile, and, hence, q at the point concerned also to vary widely. The local temperature potential $(T_w - T_e)$, however, is always zero in such a process, so that h is necessarily both positively infinite and negatively infinite at isolated points where $T_w = T_e$.

In the region of increasing temperature potential $(0.35 < x^* \leq 1)$, the heat-transfer coefficient (Fig. 8a) is higher than that for a plate of constant surface temperature. This is attributed primarily to the infinity at $x^* = 0.35$. Actually, all of the wide variations illustrated by Fig. 8a are a consequence of the fundamental inappropriateness of h when applied to variable surface temperature flows.

Heat-Transfer Rate

The local rate of heat transfer (q) for the example under consideration is obtained by substituting the coefficients a_0, a_1, and a_2 into Eq. (50) and using the values of $Y_n'(0)$ given in Table 1. The result is plotted as a solid line in Fig. 8b where the dimensionless group $qx/k_\infty T_e\sqrt{Re_x}$ is used as the ordinate. Also shown in Fig. 8b is the relation

$$\frac{\bar{q}x}{k_\infty T_e\sqrt{Re_x}} = -\frac{1}{2}\,Y_0'(0)\sum_0^\infty \frac{a_n}{T_e^*}\,x^{*n} = \frac{Y_0'(0)}{2T_e^*}\,(T_w^* - T_e^*)$$

which is obtained by neglecting the effects of variable surface temperature on the heat-transfer coefficient. The difference in the two methods of calculation is less pronounced in terms of the local heat-transfer rates than in the local heat-transfer coefficients. This is due to the fact that in the example considered the overall temperature differences are a minimum where the coefficients differ by a maximum.

By substituting the coefficients a_0, a_1, and a_2 into Eq. (64), it is found that the ratio between the total heat transferred as given by the two methods is $Q/\bar{Q} = -1.9$. This means that not only is there a difference in the absolute value of the total heat transferred from the plate but that the actual direction of net heat transfer is different. Thus, for the example under consideration, the conventional method gives a completely incorrect picture of the total rate of heat transfer by the plate.

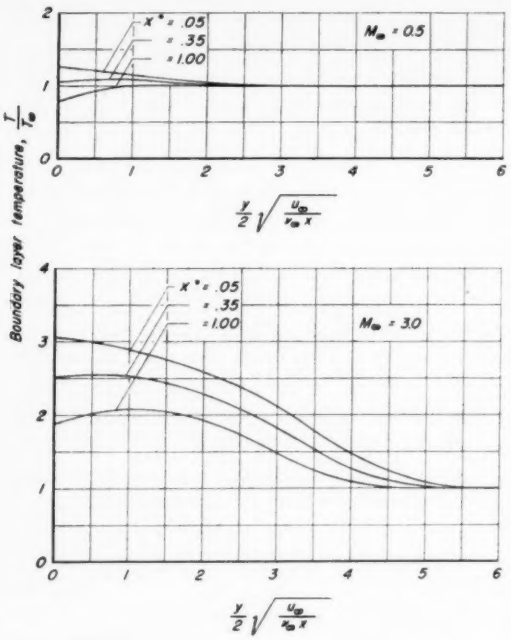

Figure 9.- Temperature distribution in boundary layer of example problem.

Temperature and Velocity Distributions

The temperature distribution as a function of η is obtained by substituting the coefficients a_0, a_1, and a_2 into Eq. (36), using the curves for $r(\eta)$ and $Y_n(\eta)$ given in Figs. 4 and 5. The value of y corresponding to each value of η is calculated from Eq. (42), using the curves for $\bar{r}(\eta)$ and $\bar{Y}_n(\eta)$ given in Figs. 4 and 5. The resulting temperature profiles are shown in Fig. 9. Although the thermal boundary layer is considerably thicker at the higher Mach Number, there is more heat transferred than in the low Mach Number case. Because the local rate of heat transfer can be expressed as

$$q = -k_w \left(\frac{\partial T}{\partial y}\right)_w = -k_w T_e \left[\frac{\partial (T^*/T_e^*)}{\partial y}\right]_w$$

it is apparent that this phenomenon is caused by the larger thermal conductivity at the high temperatures of the supersonic flow and also by the higher equilibrium temperature.

The boundary-layer velocity distributions for the example under consideration are indicated in Fig. 10 at three positions along the plate, $x^* = 0.05$, 0.35, and 1.0. These profiles are obtained in a simple manner [Eq. (13)] by first using the curve of $f'(\eta)$ in Fig. 3 and then using the same relation between η and y as was used for the temperature profiles. Although the velocity profiles at $M_\infty = 0.5$ very nearly correspond to the Blasius profile for isothermal incompressible flow, it is seen that the thicker profiles at $M_\infty = 3.0$ depart considerably from each other and also from the Blasius profile. The smaller velocity gradients and, hence, larger boundary-layer thickness at $M_\infty = 3.0$ are attributable to the lower densities (higher temperatures). The decrease in density causes the streamlines to spread more for the supersonic flow than for the subsonic flow. Fig. 10 also shows that the cool portion at the rear of the plate tends to make the velocity distributions more convex, possibly indicating increased stability. The high temperatures at the leading edge produce an inflection point in the velocity profile at $x^* = 0.05$ (barely noticeable in the figures) and probably indicate decreased stability.

It is stressed that the above statements on stability are of a qualitative nature and are included primarily to make the reader aware of the application of this solution in the consideration of boundary-layer stability. It is known from reference 2 that the boundary-layer-density distribution is also important in stability considerations. The density distribution (see temperature distributions) is more markedly affected by the surface-temperature variations than the velocity distribution. The maintenance of stable boundary layers by adjust-

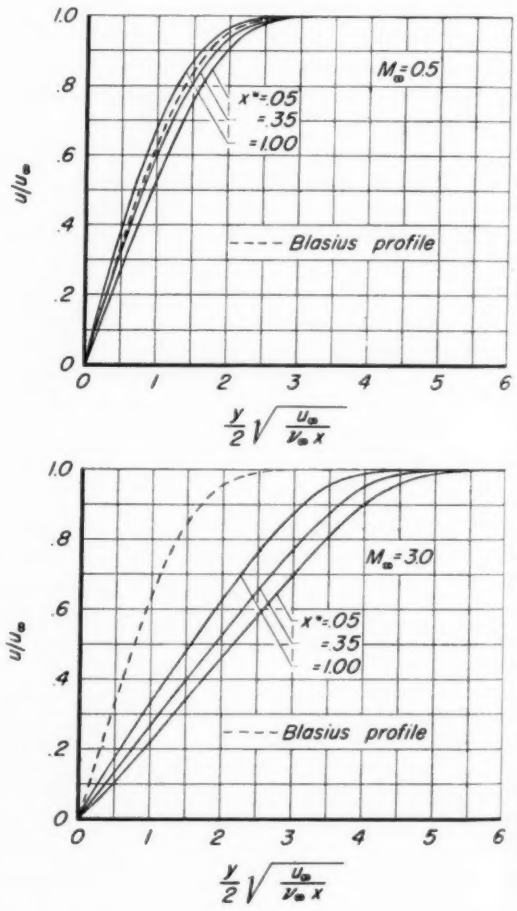

Figure 10.- Velocity distribution in boundary layer of example problem.

ing surface-temperature distributions, therefore, may have practical possibilities. This solution provides a basis for such studies but they are omitted here because they are beyond the intended scope of the present paper.

Appendix A

Maximum Surface-Temperature Gradient Consistent with Boundary-Layer Theory

Since the effects of relatively large temperature gradients along the direction parallel to the wall are to be included in the analysis, it is necessary to re-examine the boundary-layer momentum and energy relationships in order to see what restrictions or what additional terms, if any, are needed in the usual boundary-layer equations. The Navier-Stokes equations expressing conservation of momentum for the steady flow of a viscous compressible fluid are (using the summation convention for conciseness, wherein a repeated index in a term designates summation):

$$\rho u_j \frac{\partial u_i}{\partial x_j} = -\frac{\partial p}{\partial x_i} + \frac{\partial}{\partial x_j}\left[\mu\left(\frac{\partial u_i}{\partial x_j} + \frac{\partial u_j}{\partial x_i}\right)\right] - \frac{2}{3}\frac{\partial}{\partial x_i}\left(\mu \frac{\partial u_j}{\partial x_j}\right) \quad \text{(A1)}$$

The left side of this equation represents the mass times acceleration of a unit volume of fluid, and the right side represents the unbalanced pressure and viscous force per unit volume. Thus, for the case of two-dimensional flow $i = 1$ ($x_1 \equiv x$, $x_2 \equiv y$, $u_1 \equiv u$, $u_2 \equiv v$), the above equation reduces to

$$\rho u \frac{\partial u}{\partial x} + \rho v \frac{\partial u}{\partial y} = -\frac{\partial p}{\partial x} + \frac{\partial}{\partial x}\left(2\mu \frac{\partial u}{\partial x}\right) + \frac{\partial}{\partial y}\left[\mu\left(\frac{\partial u}{\partial y} + \frac{\partial v}{\partial x}\right)\right] - \frac{2}{3}\frac{\partial}{\partial x}\left[\mu\left(\frac{\partial u}{\partial x} + \frac{\partial v}{\partial y}\right)\right] \quad \text{(A2)}$$

Throughout the following analysis the pressure will be taken as constant along the x direction, which is parallel to the surface (Fig. 1). By tracing along a streamline such as shown in Fig. 1, and repeating the method given by Prandtl for estimating the order of magnitude of the various terms in Eq. (A2), it is seen that

$$\partial u/\partial x \sim U_\infty/L, \quad \partial u/\partial y \sim U_\infty/\delta$$

Moreover, the continuity equation

$$(\partial/\partial x)(\rho u) + (\partial/\partial y)(\rho v) = 0 \quad \text{(A3)}$$

allows the remaining terms in Eq. (A2) to be estimated as follows:

$$\partial v/\partial y \sim \partial u/\partial x \sim U_\infty/L$$

$$v \sim \int_0^\delta (\partial u/\partial x)dy \sim (U_\infty/L)\delta$$

$$\partial v/\partial x \sim v/L \sim (U_\infty/L)(\delta/L)$$

Terms in Eq. (A2) such as $\partial u/\partial x$ can be neglected compared to $\partial u/\partial y$, since the foregoing estimations show that this amounts to neglecting terms of order δ/L compared to unity. This, of course, is valid for Reynolds Numbers of the order encountered in aerodynamics since

$$\delta/L \cong 6/\sqrt{Re}$$

Neglecting the terms in Eq. (1), which are of the order δ/L compared to unity, gives the familiar momentum equations for laminar boundary-layer flow

$$\left.\begin{aligned} &i = 1; \quad \rho u \frac{\partial u}{\partial x} + \rho v \frac{\partial u}{\partial y} = \frac{\partial}{\partial y}\left(\mu \frac{\partial u}{\partial y}\right) \\ &i = 2; \quad \partial p/\partial y = 0 \end{aligned}\right\} \quad \text{(A4)}$$

It is now necessary to repeat the above analysis using the energy equation, since it is this latter equation that explicitly involves temperature gradients in the x direction. The differential equation giving the balance of energy for steady flow of a viscous compressible fluid is

$$\rho u_j \frac{\partial (c_p T)}{\partial x_j} = u_j \frac{\partial p}{\partial x_j} + \frac{\partial}{\partial x_j}\left(k \frac{\partial T}{\partial x_j}\right) + \mu\left[\frac{\partial u_i}{\partial x_j}\left(\frac{\partial u_i}{\partial x_j} + \frac{\partial u_j}{\partial x_i}\right) - \frac{2}{3}\left(\frac{\partial u_j}{\partial x_j}\right)^2\right] \quad \text{(A5)}$$

It is to be noted that this is a single equation, since energy is a scalar quantity, whereas the momentum Eqs. (1) actually represents three separate equations, one for each component of the momentum. The left side of Eq. (A5) represents the rate of increase in enthalpy per unit volume of fluid, and the three terms on the right side represent the rate of work done by pressure forces, the rate of heat transfer by conduction, and the rate that heat is dissipated by viscosity, respectively. Eq. (A5) written out in full for two space dimensions becomes

$$\rho u \frac{\partial (c_p T)}{\partial x} + \rho v \frac{\partial (c_p T)}{\partial y} = u \frac{\partial p}{\partial x} + v \frac{\partial p}{\partial y} + \frac{\partial}{\partial x}\left(k \frac{\partial T}{\partial x}\right) + \frac{\partial}{\partial y}\left(k \frac{\partial T}{\partial y}\right) + \mu\left[2\left(\frac{\partial u}{\partial x}\right)^2 + \frac{\partial u}{\partial y}\left(\frac{\partial u}{\partial y} - \frac{\partial v}{\partial x}\right) + \frac{\partial v}{\partial x}\left(\frac{\partial v}{\partial x} + \frac{\partial u}{\partial y}\right)\right] + \mu\left[2\left(\frac{\partial v}{\partial y}\right)^2 - \frac{2}{3}\left(\frac{\partial u}{\partial x} + \frac{\partial v}{\partial y}\right)^2\right] \quad \text{(A6)}$$

With constant pressure and with those velocity terms neglected which have already been shown to be of order δ/L compared to unity, Eq. (A6) reduces to

$$\rho u \frac{\partial (c_p T)}{\partial x} + \rho v \frac{\partial (c_p T)}{\partial y} = \frac{\partial}{\partial x}\left(k \frac{\partial T}{\partial x}\right) + \frac{\partial}{\partial y}\left(k \frac{\partial T}{\partial y}\right) + \mu\left(\frac{\partial u}{\partial y}\right)^2 \quad \text{(A7)}$$

This differs from the usual energy equation for boundary-layer flow only by the presence of the first term on

the right-hand side. Considering order of magnitudes again,

$$(\partial/\partial x)[k(\partial T/\partial x)] \sim k(\partial T/\partial x)/L$$

$$\frac{\partial}{\partial y}\left(k\frac{\partial T}{\partial y}\right) \sim \frac{k(\partial T/\partial y)}{\delta_t} \sim k\frac{T_w - T_\infty}{(\delta_t)^2}$$

For gases such as air, where the Prandtl Number is nearly unity, the thickness (δ_t) of the thermal boundary layer is of the same order of magnitude as the thickness δ of the velocity boundary layer. Hence,

$$\frac{(\partial/\partial x)[k(\partial T/\partial x)]}{(\partial/\partial y)[k(\partial T/\partial y)]} \sim \frac{\delta}{L}\left[\frac{(\partial T/\partial x)_w}{(T_w - T_\infty)/\delta}\right] \quad \text{(A8)}$$

For applications wherein the temperature gradient $(\partial T/\partial x)_w$ along the surface is of the same order or less than the gradient $(T_w - T_\infty)/\delta$ normal to the surface—that is, for applications wherein

$$(\partial T/\partial x)_w \sim (T_w - T_\infty)/\delta \text{ or less} \quad \text{(A9)}$$

Eq. (A8) becomes

$$\frac{(\partial/\partial x)[k(\partial T/\partial x)]}{(\partial/\partial y)[k(\partial T/\partial y)]} \sim \frac{\delta}{L}$$

Terms of order δ/L compared to unity, however, have already been consistently neglected. Hence, within the order of accuracy of the momentum Eqs. (A4), the first term on the right-hand side of Eq. (A7) may be neglected, provided, of course, that Eq. (A9) is satisfied.

The results of the foregoing considerations on order of magnitudes may be summarized by stating that the usual boundary-layer equations

$$\left.\begin{aligned} \rho u\frac{\partial u}{\partial x} + \rho v\frac{\partial u}{\partial y} &= \frac{\partial}{\partial y}\left(\mu\frac{\partial u}{\partial y}\right) && \text{momentum}\\ \frac{\partial}{\partial x}(\rho u) + \frac{\partial}{\partial y}(\rho v) &= 0 && \text{continuity}\\ \rho u\frac{\partial(c_pT)}{\partial x} + \rho v\frac{\partial(c_pT)}{\partial y} &= \frac{\partial}{\partial y}\left(k\frac{\partial T}{\partial y}\right) + \mu\left(\frac{\partial u}{\partial y}\right)^2 && \text{energy}\end{aligned}\right\} \quad (1)$$

are applicable to flows with large temperature gradients in the x direction, provided

$$(\partial T/\partial x)_w \sim (T_w - T_\infty)/\delta \text{ or less} \quad (2)$$

Appendix B

Numerical Solution of the Functions $Y_n(\eta)$

The temperature distribution functions $Y_n(\eta)$, are determined by integrating Eq. (33),

$$Y_n'' + PrfY_n' - 2Prnf'Y_n = 0 \quad (33)$$

with the boundary conditions

$$Y_n(0) = 1$$

$$Y_n(\infty) = 0$$

Because the Blasius functions $f(\eta)$ and $f'(\eta)$ cannot be expressed in closed form, Eq. (33) is intractable by the ordinary analytical methods, and, hence, numerical integration is indicated. In order to start the usual methods of stepwise integration of a second-order differential equation, it is necessary to know the values of the dependent function and its first two derivatives at one of the boundaries. When the derivatives are not known at a boundary, it is necessary to estimate them and then check the validity by the degree to which the other boundary conditions are satisfied. Such a process usually reduces to one of trial and error, necessitating many tedious computations. Fortunately, this process can be avoided in the solution of Eq. (33) and similar boundary-layer equations where the asymptotic solution can be found. It will be noticed from Fig. 3 that the functions $f(\eta)$ and $f'(\eta)$ become linear and constant, respectively, for large values of η. Expressions for these functions accurate to four significant figures in the range $\eta > 4.1$ are:[16]

$$f'(\eta) = 2$$
$$f(\eta) = 2(\eta - 0.86038)$$

If these equations are introduced into Eq. (33) there results the asymptotic equation for Y_n,

$$Y_n'' + 2Pr(\eta - 0.86038)Y_n' - 4nPrY_n = 0 \quad \text{(B1)}$$

letting $x = \sqrt{Pr}(\eta - 0.86038)$, Eq. (B1) becomes*

$$Y_n'' + 2xY_n' - 4nY_n = 0 \quad \text{(B2)}$$

The general solution of the linear differential Eq. (B2) can be determined, if one particular solution (U) is known, by means of the expression

$$Y = U\left(C_1\int_0^x \frac{e^{-x^2}\,dx}{U^2} + C_2\right) \quad \text{(B3)}$$

where C_1 and C_2 are arbitrary constants. A particular solution U of Eq. (B2) is obtained readily when it is recognized that Eq. (B2) can be transformed to Hermite's differential equation. Letting $ix = \xi$ and $m = 2n$, Eq. (B2) is transformed to the Hermite equation

$$Y_m'' - 2\xi Y_m' + 2mY_m = 0 \quad \text{(B4)}$$

for which the following Hermite polynomial is a particular solution

$$U = H_m(\xi) = (2\xi)^m - \frac{m(m-1)}{1!}(2\xi)^{m-2} + \frac{m(m-1)(m-2)(m-3)}{2!}(2\xi)^{m-4} - \ldots \quad \text{(B5)}$$

Since $m(=2n)$ is always an even number in the present application, the polynomial is always real and can be

* The use of x as a dummy independent variable throughout the remainder of this appendix is not to be confused with the space coordinate x.

written

$$U = H_{2n}(ix) = (-1)^n(2x)^{2n} - \frac{2n(2n-1)}{1!} \times (-1)^{n-1}(2_n)^{2n-2} + \frac{2n(2n-1)(2n-2)(2n-3)}{2!} \times (-1)^{n-2}(2\xi)^{2n-4} - \ldots \quad \text{(B6)}$$

Substituting Eq. (B6) into Eq. (B3), there results

$$Y_n = H_{2n}(ix)\left[C_1\int_0^x \frac{e^{-x^2}\,dx}{H_{2n}^2(ix)} + C_2\right] \quad \text{(B7)}$$

Imposing the boundary condition $Y_n = 0$ as $\eta \to \infty$, it is found that

$$C_2 = -C_1\int_x^\infty \frac{e^{-x^2}dx}{H_{2n}^2(ix)} \quad \text{(B8)}$$

therefore,

$$Y_n = -C_1H_{2n}(ix)\int_x^\infty \frac{e^{-x^2}dx}{H_{2n}^2(ix)} \quad \text{(B9)}$$

is the asymptotic solution to Eq. (33). The first two derivatives needed in order to start the numerical integration are obtained from Eqs. (B9) and (B2),

$$Y_n' = -C_1\left[H_{2n}'(ix)\int_x^\infty \frac{e^{-x^2}\,dx}{H_{2n}^2(ix)} - \frac{e^{-x^2}}{H_{2n}^2(ix)}\right] = \frac{H_{2n}'(ix)}{H_{2n}(ix)}\,Y_n - C_1\frac{e^{-x^2}}{H_{2n}(ix)} \quad \text{(B10)}$$

$$Y_n'' = -2xY_n' + 4nY_n \quad \text{(B11)}$$

Eqs. (B9), (B10), and (B11) were evaluated numerically for values of x corresponding to $\eta = 4.1$ and $\eta = 4.2$. Once the functions Y_n, Y_n', and Y_n'' were obtained at these values of η, the stepwise numerical integration was started toward $\eta = 0$. The numerical integration method of Runge-Kutta was used in the calculations. The value of $Y_n(0)$ obtained at the end of a numerical integration process was never unity (the necessary boundary condition), since the correct C_1 was not known beforehand. This does not cause complications because Eq. (33) is homogeneous and the function obtained in the stepwise process can therefore be multiplied by that constant factor that makes $Y_n(0) = 1$.

References

[1] Lees, L., and Lin, C. C., *Investigation of the Stability of the Laminar Boundary Layer in a Compressible Fluid*, N.A.C.A. T.N. No. 1115, 1946.

[2] Lees, L., *The Stability of the Laminar Boundary Layer in a Compressible Fluid*, N.A.C.A. T.N. No. 1360, 1947.

[3] Crocco, L., *Sullo Strato Limite Laminare nei Gas Lunga una Parete Piana*, Rendiconti del Circolo Matematico di Palermo, Vol. LXIII, February, 1941.

[4] Crocco, L., *Lo Strato Limite Laminare nei Gas*, Monografie Scientifiche Di Aeronautica, Associazone Culturale Aeronautica Rome, No. 3, December, 1946.

[5] Hantzsche, W., and Wendt, H., *Die Laminare Grenzschicht der ebenen Platte mit und ohne Wärmeübergang unter Berücksichtigung der Kompressibilität*, Jahrbuch der Deutschen Luftfahrtforschung, 1942.

[6] Hantzsche, W., and Wendt, H., *Die Laminare Grenzschicht bei einem mit Ueberschallgeschwindigkeit angestroemten nichtangestellten Kreiskegel*, Jahrbuch der Deutschen Luftfahrtforschung, 1941.

[7] Fage, A., and Falkner, V. M., *Relation between Heat Transfer and Surface Friction for Laminar Fow*, A.R.C. R. & M. No. 1408, 1931.

[8] Schuh, H., *Boundary Layers of Temperature*, Reports and Translations, No. 1007 (MAP V6 307).

[9] Rubesin, M. W., *An Analytical Investigation of Convective Heat Transfer from a Flat Plate Having a Stepwise Discontinuous Surface Temperature*, Presented at A.S.M.E. Annual Meeting, November, 1948.

[10] Mangler, W., *Compressible Boundary Layers on Bodies of Revolution*, M. A. P. Volkenrode Ref., VG 83 No. 47T.

[11] von Mises, R., *Bemeukung zur Hydrodynamik*, Z.A.M.M., Vol. 7, 1927.

[12] von Kármán, T., and Tsien, H. S., *Boundary Layer in Compressible Fluids*, Journal of the Aeronautical Sciences, Vol. 5, No. 6, April, 1938.

[13] Chapman, Dean R., *Laminar Mixing of a Compresible Fluid with a Dead-Air Region*, N.A.C.A. T.N. No. 1800, 1948.

[14] Howarth, L., *Concerning the Effect of Compressibility on Laminar Boundary Layers and Their Separation*, Proc. Royal Society, Series A, No. 1036, Vol. 194, July 28, 1948.

[15] Pohlhausen, E., *Der Wärmeaustausch zwischen festen Körpern und Flüssigkeiten mit Kleiner Reibung und Kleiner Wärmeleitung*, Z.A.M.M., Bd. 1, p. 115, 1921.

[16] Howarth, L., *On the Solution of the Laminar Boundary Layer Equations*, Proc. Royal Society, Series A, Vol. 164, 1938.

Readers' Forum

BRIEF REPORTS of investigations in the aeronautical sciences and discussions of papers published in the JOURNAL *will be presented in this special department. The publication will be completed 6 to 8 weeks after receipt of the material. No proofs will be sent to the authors. The Editorial Committee does not hold itself responsible for the opinions expressed by the correspondents. Contributions should not exceed 800 words in length.*

Addition of Heat to a Gas Flowing in a Pipe at Sonic and Subsonic Speeds

Maurice Roy
Professor, École Polytechnique, Paris, France
April, 1949

IN THEIR PAPER "Addition of Heat to a Gas Flowing in a Pipe at Subsonic Speed" (JOURNAL OF THE AERONAUTICAL SCIENCES, Vol. 16, No. 2, p. 84, February, 1949), J. V. Foa and G. Rudinger contest, together with the opinions of many other authors, the one I expressed* when I stated that a *steady-flow process at sonic speed* is inconsistent with an external exchange of heat or with a change in the chemical state of the flow.

While developing an interesting conception, the authors, as a matter of fact, investigate a case quite different from the case of the *steady* flow that alone was considered by me. They contemplate, in fact, the transient conditions brought about by supplying heat locally to the initial flow, and then they discuss the final steady flow to which the disturbances thus produced would lead. But this conception of the final flow could not escape the inferences (and, in particular, the one above mentioned) that are directly drawn from the study of the final steady flow.

How is it then that there is a disagreement?

Concerning the physical hypotheses about the flow, I have assumed that the fluid was governed by the laws of perfect gases (C_P and γ constant) and that its viscosity and conductivity were negligible, assumptions that Foa and Rudinger seem also to admit.

In that case, the divergence between our results could be due to the method used in determining the permanent final flow. Perhaps, too, this divergence is at least partly to be explained by the fact that the authors localize the supply of heat in a cross section of the pipe—a conception difficult to realize.

As for me, I have assumed this supply to be permanent and distributed in the mass of the flow with an intensity per unit of mass and per unit of time varying along the pipe. It must be noted that a one-dimensional flow and an external supply of heat do not easily fit in with the supposed absence of internal conductivity. Moreover, as I have emphasized, this lack of conductivity excludes the so-called "deflagration" type of flame propagation.

I think today that my theory, published in 1946 when I did not know of other concordant studies, is far too schematic and should be completed, taking into account the internal conductivity, the turbulence, and also, of course, the viscosity of the fluid.

In addition, in the case of chemical reactions, more accurate physical data ought to be known concerning the speeds of the reactions.

For the sake of simplification, when considering the case of sufficiently large pipes, the assumptions of the flow being steady and one-dimensional could still be retained.

However, even so simplified, the problem raised remains a difficult one and calls for new studies.

* Reference 13 of the authors and previously a note "Théorie unidimensionnelle des tuyères-foyers" (*Comptes rendus de l'Académie des Sciences*, Paris, Vol. 222, p. 835, April 8, 1946.

Heat Addition to a Flowing Gas

J. V. Foa and G. Rudinger
Cornell Aeronautical Laboratory, Inc., Buffalo, N.Y.
June 21, 1949

OUR PAPER ON GAS FLOWS with heat addition[1] has been the subject of several comments[2–4] in the Readers' Forum. Some of these comments seem to imply that the disagreement between the conclusions of our paper and those of previous steady-state analyses is only apparent and essentially reducible to a matter of semantics. This implication is clearly expressed in Hall's comment,[2] where it is pointed out that we have used the phrase "initial condition" to describe the state *in time* preceding the addition of heat anywhere in the system, whereas other investigators have found it convenient to use it as referring to the state *in space* preceding heat addition.

One is, of course, at liberty to deal with a steady state where heat is being added at a constant rate and to refer to the upstream conditions as "initial" conditions. This is, as Hall points out, a widely established use of the term and indeed a valid one if it is adhered to consistently from the formulation of the propositions to that of the final inferences. When, however, the results of such a steady-state analysis are interpreted to mean that the heat-transfer coefficient becomes zero, or that combustion stops when the gas reaches sonic velocity, or that the upstream condition must be modified when the amount of heat added exceeds a certain "limiting value," then it is clear that in the final inference the word "initial" has come to refer to the state preceding the addition of heat *in time* at a fixed position in space and that the rules of valid inference have thus been violated.

The equations derived in previous steady-state analyses should, as we stated in our Introduction,[1] "only be interpreted to relate the conditions upstream and downstream of the heating region." These relations [which are restated in our paper as Eqs. (8), (9), and (10)] are well-established and have been plotted in various forms (such as the one presented by Barry and Fulton[3]). The three steady-state relations, together with three boundary conditions, are sufficient to determine all flow and state parameters in a steady régime of heat addition when the heating rate is known. Obviously, any change of this rate will result in a change of flow and/or state parameters, upstream and/or downstream of the heating region, and therefore in the establishment of a new steady state.

Of the three cases mentioned by Barry and Fulton,[3] the first two—(a) constant m, T_1, and also p_2 when $M_2 < 1.0$, and (b) constant P_1, T_1, and also p_2 when $M_2 < 1.0$—were discussed in our paper as illustrations of a treatment that is completely general within the framework of the assumptions that are listed there. The third case (constant M_1 and T_1) is not sufficiently defined and could not be applied to a physical system without specification of the missing boundary condition. Thus—e.g., in the systems considered in detail in our analysis (constant-area ducts discharging directly into the surrounding atmosphere)—the third boundary condition is $p_2 = \text{const.}$ for $M_2 < 1.0$, or $M_2 = 1.0$, and it can then be verified that when heat is added at $M \geq 1/\sqrt{\gamma}$ the downstream static temperature does indeed decrease, but the amount of heat that must be removed from the air supply system in order to maintain the prescribed upstream boundary

conditions is larger than that of the heat that is added to the flow. This mechanism is one of no interest and was for this reason specifically excluded in our study where it was concluded (page 90) that "except in the irrelevant case where the addition of heat is more than offset by a simultaneous heat removal, the addition of heat will always result in an increase of the static temperature of the gas above its initial value, regardless of the initial Mach Number."

More generally, it is true that, if the upstream conditions could be forced to remain constant when the rate of heat addition is changed, then the downstream static temperature would decrease when the heating rate is increased at $M \geq 1/\sqrt{\gamma}$. It must be noted, however, that in order to achieve such a situation, the control of the upstream conditions could not be effected directly but only through a special adjustment of the downstream boundary conditions, so that the latter would become functions of the amount of heat added. Since the boundary conditions are essential characteristics of any physical system, it is clear that any dependence of the boundary conditions on the heating rate would of necessity imply a continuous modification of the physical system itself as the heating rate is changed—a situation that is distinct from that treated in the problem under discussion. A system with automatically controlled boundary conditions could of course be made to behave in any desired manner.

Roy's statement[4] that a "steady flow process at sonic speed is inconsistent with an external exchange of heat or with a change of the chemical state of the flow" is correct and in full agreement with our own conclusions. On the other hand, his recommendation[5] that the Mach Number be kept as low as possible in the region of ignition because practically no combustion could take place in a mixture that is ignited at $M > 0.6$ reflects an erroneous interpretation of his results. Similarly, Barry and Fulton's recent discussion,[3] where they properly recognize the importance of the boundary conditions, can hardly be reconciled with Barry's previous statement[6] that "the amount of fuel which may be burned is limited by choking." In this connection, it may be pertinent to recall the cautionary note that was contained in our paper[1] (page 85), where it was explained that "when the inlet boundary conditions are assumed to be fixed, special care must be exercised in drawing conclusions from the results. For instance, the imaginary solutions obtained in certain cases must be understood to imply the physical impossibility of the assumed conditions rather than a limitation to the amount of heat that can be added."

Hall[2] and Roy[4] have also attempted to explain the disagreement between their own and our conclusions on the basis of arguments (heat transmission within the gas, localization of the heat source, consideration of transient phenomena, effects of viscosity and turbulence, mechanism of the chemical reactions) which are completely foreign to the problem as treated. Actually, this disagreement does not arise from the manner in which the relations governing flows with heat addition are derived and treated but only from their physical interpretation.

References

[1] Foa, J. V., and Rudinger, G., *On the Addition of Heat to a Gas Flowing in a Pipe at Subsonic Speed*, Journal of the Aeronautical Sciences, Vol. 16, No. 2, pp. 84–94 and 119, February, 1949.

[2] Hall, N. A., *Heat Addition to a Flowing Gas*, Readers' Forum, Journal of the Aeronautical Sciences, Vol. 16, No. 5, pp. 317–318, May, 1949.

[3] Barry, F. W., and Fulton, C. D., *Gas Flow in Ducts*, Readers' Forum, Journal of the Aeronautical Sciences, Vol. 16, No. 6, pp. 379–380, June, 1949.

[4] Roy, M., *Addition of Heat to a Gas Flowing in a Pipe at Sonic and Subsonic Speed*, Readers' Forum, Journal of the Aeronautical Sciences, Vol. 16, No. 9, p. 566, September, 1949.

[5] Roy, M., *Thermodynamique des Systèmes Propulsifs à Réaction et de la Turbine à Gaz.*, pp. 35–40; Dunod, Paris, 1947.

[6] Barry, F. W., Transactions of the A.S.M.E., Vol. 69, No. 7, p. 758, October, 1947.

A Discussion of the Theories of Plasticity

D. C. Drucker
Brown University, Providence, R. I.

March 1, 1949

THE EXCELLENT INDEPENDENT PAPERS by Dr. Batdorf (July JOURNAL) and Professor Bijlaard (this issue) deal with the same subject and come to essentially the same conclusion—a deformation theory of plasticity predicts the correct plastic buckling load for plates; a particular incremental, or flow, theory does not. Their conclusions are substantiated in all cases investigated experimentally. However, crucial direct tests as reported by Dr. Batdorf are just as conclusively against deformation and in favor of an incremental theory of plasticity. Dr. Batdorf therefore states that neither type of theory is proper. Professor Bijlaard adopts the point of view that the answer justifies the means.

Before analyzing the main issue, it seems desirable to attempt a clarification of some of the basic ideas and terminology of plasticity theory included in the papers. Deformation theory is the wording used to indicate that a relation exists between finite changes in stress and strain, usually between stress and strain themselves. Incremental, or flow, theory is used to emphasize the necessity for considering the history or path of loading. The stress-strain relation is in terms of the differentials of strain. Total strain or a finite strain increment is strongly dependent on the manner in which the final state of stress is reached. In all the forms written down to date, the two types of theory coincide only when all components of stress are increased in ratio, $\sigma_{ij} = K\sigma_{ij}^0$.

Deformation theory can be shown to be mathematically inconsistent in general and therefore, of necessity, often physically impossible. As theories either do or do not involve the history of loading, they must be of one type or the other and therefore must be incremental to be valid.

Some confusion seems to have arisen in this respect because of both authors' identification of incremental theory with its simplest possible form which they employ. In tensor notation, to save space,

$$d\epsilon_{ij} = d\epsilon_{ij}^e + d\epsilon_{ij}^p = d\epsilon_{ij}^e + FS_{ij}df$$

where $d\epsilon_{ij}$, the total strain increment, is composed of an elastic increment, $d\epsilon_{ij}^e$, and a plastic $d\epsilon_{ij}^p$. The criterion of loading or further plastic deformation, f, is $J_2 = {}^1/_2 S_{ij}S_{ij}$ or equally well the octahedral shearing stress. $F = F(f)$, and S_{ij} is the stress deviation, $S_{ij} = \sigma_{ij} - {}^1/_3\sigma_{kk}\delta_{ij}$, the stress with the average normal stress taken away. Such a theory is the easiest to handle of all incremental work-hardening types, but it is of the class termed isotropic stress hardening. As it is isotropic, it implicitly assumes that if the yield point is raised by tension in one direction it is raised equally for tension in any other direction. Much worse, it assumes a rise in the compressive yield point of the same amount as for the tensile and so is by no means in good agreement with experiment.

Far more general incremental theories have been formulated, the most general at present may be written in the form

$$d\epsilon_{ij} = d\epsilon_{ij}^e + G\frac{\partial f}{\partial \sigma_{ij}}\left(\frac{\partial f}{\partial \sigma_{kl}}\,d\sigma_{kl}\right)$$

where the criterion of loading, f, may be as anisotropic as desired and may depend upon stress, strain, and their history, as may G. Such dependence obviously makes for tremendous mathematical complication, but simple experiments such as alternating plastic tension and compression show beyond doubt that it does exist. It is likely that simple forms will be adequate for most problems.

In particular, the choice of

$$f = (S_x - m\epsilon_x^p)^2 + (S_y - m\epsilon_y^p)^2 + (S_z - m\epsilon_z^p)^2 + \ldots$$

where S is the stress deviation, ϵ^p is the plastic strain, and m is a

constant, gives both a Bauschinger effect and a lower yield point for tension in the y-direction than in the x-direction, following tension in the x-direction. The major objection of Dr. Batdorf to incremental theory is thus seen to be an objection to the particular isotropic stress theory $f = J_2$. Nevertheless, the theory proposed by Dr. Batdorf apparently does differ basically from the $G(\partial f/\partial\sigma_{ij})[\partial f/\partial\sigma_{kl}d\sigma_{kl}]$ form, which assumes a linear relation between differentials of stress and of strain. Such an assumption is by no means a necessary one, but the great difficulties now encountered indicate that the possibility of ever solving stress analysis problems in plasticity with a nonlinear theory is certainly remote.

The assumption of linearity can be given direct physical meaning. In the case of shear imposed on an initial tension or compression which is held fixed, line A on Dr. Batdorf's Fig. 3, incremental theory predicts, and experiments confirm, that the first increment of shear strain is purely elastic. Unlike Dr. Batdorf's theory, linearity further assumes that this will be true when the normal stress is increased, line B of Dr. Batdorf's Fig. 3. This is an extremely important point, and tests will soon be under way at Brown University (Contract N7onr-358, Office of Naval Research and Bureau of Ships) to check or disprove linearity by direct measurement.

Now to return to the basic question. Why do the authors find that deformation theory (which is invalid in general) gives correct plastic buckling loads while incremental, or flow, theory (which agrees with many physical facts) does not? In the first place, the comparison that has been made is not entirely fair. The deformation theory results are based on the Shanley idea of buckling proceeding as the load increases and so should correspond to the start of lateral displacement and not quite the measured buckling load. Secondly, if the Shanley effect is taken into account, answers obtained with incremental theory for initially perfectly flat rectangular plates supported on all sides become reasonable. Bending of plates with a slight initial bow would lead to similar results.

On the other hand, the Shanley effect alone is not sufficient to account for the present discrepancy in the start of twisting of a long cruciform section or rectangular plate hinged on one edge parallel to the compression direction and free on the other. This is the case of shear added to compression, and, as described previously, according to linear theory the initial modulus in shear is the elastic modulus whether the compression increases or remains constant.

Two possibilities exist. Linear theory may be incorrect, which in a sense corresponds to Professor Bijlaard's suggestion that deformation theory may be admissible for the small strain increments considered in buckling, as well as to Dr. Batdorf's theory. If not, another factor must be taken into account in the unexplained case. For example, an extremely small initial deflection or twist will greatly lower the effective shear modulus under increasing axial load and may well provide the explanation.

Both possibilities should be explored, but even if linear incremental theory is found to be an oversimplification and if deformation theory should prove adequate for buckling, the conclusion cannot, and should not, be extended to general plasticity problems. Direct experimentation only can establish the proper incremental theory.

On Nonsteady Motion of Delta Wings

John W. Miles
Department of Engineering, University of California at Los Angeles
May 27, 1949

WE CONSIDER HERE the nonsteady motion of a pointed wing in a supersonic stream directed along the positive x axis. Let the port and starboard edges be $y_p(x)$ and $y_s(x)$, respectively, where

$$\left.\begin{aligned} y_p(0) &= y_s(0) = 0 \\ y_s'(x) &> \tan\theta \\ y_p'(x) &< -\tan\theta \end{aligned}\right\} \tag{1}$$

$$\theta = \sin^{-1}(c/U) \tag{2}$$

which is to say that the wing is a "simple" plan form and the problem is "purely supersonic." θ is the Mach angle, U is the free-stream velocity, and c is the velocity of sound. For an isosceles, delta wing $y_s(x) = x\tan\mu$, $y_p(x) = -x\tan\mu$, $\mu > \theta$. We are interested primarily in two problems, corresponding to the response of this wing to downwash distributions exhibiting harmonic and step function time dependences, respectively.

If the prescribed downwash velocity normal to the plane of the wing ($z = 0+$) is $w(x, y)\exp(i\omega t)$, positive *down*, the resulting (linearized) velocity potential at the wing is given by[1]

$$\phi(x, y, 0+) = \int_0^x d\xi \int_{y_p(\xi)}^{y_s(\xi)} d\eta\, g(x-\xi, y-\eta)\, w(\xi, \eta)\tan\theta$$

$$g(x, y) = \frac{1}{\pi}(x^2\tan^2\theta - y^2)^{-1/2}\exp(-i\lambda x) \times \cos[\lambda\sin\theta(x^2\tan^2\theta - y^2)^{1/2}]\cdot 1(x\tan\theta - |y|) \tag{3}$$

$$\lambda = (\omega b/U)\sec^2\theta \tag{4}$$

where b is a characteristic length. Unfortunately, the integrations demanded by Eq. (3) have successfully resisted reduction to known (i.e., tabulated) functions, even for the simplest $w(x, y)$. However, it is possible to reduce spanwise, weighted integrals of this potential to integrals arising in the two-dimensional problem. Thus, we introduce

$$\psi(x) = \int_{y_p(x)}^{y_s(x)} \phi(x, y, 0+)\, f(y)dy \tag{5}$$

where $f(y)$ is an appropriate weighting function. Introducing ϕ from Eq. (3) and making certain transformations, we obtain the result

$$\psi(x) = \tan\theta\int_0^x d\xi\int_{y_p(\xi)}^{y_s(\xi)} d\eta\, G(x-\xi, \eta)w(\xi, \eta) \tag{6}$$

$$G(x, y) = \exp(-i\lambda x)1(x)\cdot\frac{1}{\pi}\int_0^\pi \cos(\lambda x\sin\theta\sin\varphi) \times f(x\cos\varphi + y)d\varphi \tag{7}$$

The (dimensionless) weighted force on a spanwise strip is given by

$$\gamma(x) = \left[4\tan\theta\left(\frac{\rho U^2}{2}\right)\right]^{-1}\int_{y_p(x)}^{y_s(x)} [p(x, y, 0-) - p(x, y, 0+)]f(y)dy \tag{8a}$$

$$= \left(\frac{\partial}{\partial x} + \frac{i\omega}{U}\right)\psi(x)\cot\theta \tag{8b}$$

The most important cases in practice are $f_0(y) = 1$ and $f_1(y) = y$, corresponding to the calculation of the force and rolling moment, respectively, on a spanwise strip. Making these substitutions in Eq. (7), we find that Eq. (6) may be rewritten

$$\psi_n(x) = \tan\theta\int_0^x G_0(x-\xi)w_n(\xi)d\xi, \quad n = 0, 1 \tag{9}$$

$$G_0(x) = \exp(-i\lambda x)J_0(\lambda x\sin\theta) \tag{10}$$

$$w_n(x) = \int_{y_p(x)}^{y_s(x)} w(x, y)\, y^n dy \tag{11}$$

Since $G_0(x)$ is essentially the two-dimensional Green's function,[2] the calculation of the lift and moments on our wing is reduced to an equivalent two-dimensional problem. Similarly, the problem of finding the wing loads due to the deflection of a delta control

surface with inboard end $y = a$ may be reduced to an equivalent two-dimensional problem, it being necessary only to assume $w(x, y) = w(x)1(y - a)$ in Eq. (11). In essence, Eq. (9) states that "strip" theory is exact for $n = 0, 1$.

In the case of step function loading, we assume the downwash in the form $w(x, y)1[t - t_0(x)]$. The result is expressed as in Eq. (6), but $G(x, y)$ is replaced by its Bromwich integral, viz.,

$$\psi(x, t) = \tan\theta \int_0^x d\xi \int_{y_p(\xi)}^{y_s(\xi)} d\eta A[x - \xi, \eta, t - t_0(\xi)]w(\xi, \eta) \tag{12}$$

$$A(x, y, t) = \frac{1}{2\pi} \lim_{\epsilon \to 0} \int_{-\infty}^{\infty} \frac{d\omega \exp(i\omega t)G(x, y)}{\epsilon + i\omega} \tag{13a}$$

$$= \frac{1}{2\pi} \int_0^{\pi} d\varphi f(x\cos\varphi + y)\{1[Ut - x\sec^2\theta \times (1 + \sin\theta\sin\varphi)] + 1[Ut - x\sec^2\theta(1 - \sin\theta\sin\varphi)]\} \tag{13b}$$

For the cases $f_0(y) = 1$ and $f_1(y) = y$, we find

$$\psi_n(x) = \tan\theta \int_0^x A_0\left[\frac{x - \xi}{Ut - Ut_0(\xi)}\right] w_n(\xi)d\xi, \quad n = 0, 1 \tag{14}$$

$$A_0(w) = 1[(1 - \sin\theta) - w] + \frac{1}{\pi} 1[w - (1 - \sin\theta)]1[(1 + \sin\theta) - w]\cos^{-1}\left[\frac{w - \cos^2\theta}{w\sin\theta}\right] \tag{15}$$

For a uniform gust entry (at $t = 0$), $Ut_0(x) = x$, while for a sudden change in angle of attack (at $t = 0$), $t_0(x) \equiv 0$. Either symmetric or asymmetric gusts may be considered, and we can also find the response of the wing to sudden symmetric or asymmetric deflections of the control surfaces.

As an interesting special case, we remark that if we take $\lambda = n = 0$ in Eqs. (9)–(11), corresponding to steady symmetric flow, the lift coefficient for the wing is

$$C_L = 4\tan\theta[w(x, y)]_{\text{avg.}} \tag{16}$$

a result previously obtained by Professor Lagerstrom of GALCIT.[3]

References

[1] Garrick, I. E., and Rubinow, S. I., *Theoretical Study of Air Forces on an Oscillating or Steady Thin Wing in a Supersonic Main Stream*, N.A.C.A. T.N. No. 1383, 1947.

[2] Miles, J. W., *The Aerodynamic Forces on an Oscillating Airfoil at Supersonic Speeds*, Journal of the Aeronautical Sciences, Vol. 14, No. 10, pp. 351–358, October, 1947.

[3] Verbal communication.

On Transient Two-Dimensional Flows at Supersonic Speeds

Charles E. Watkins

Research Scientist, Langley Aeronautical Laboratory, N.A.C.A., Langley Air Force Base, Va.

May 31, 1949

In the May, 1949, issue of the Journal of Aeronautical Sciences, Biot[1] treats the chordwise lift distribution on a two-dimensional supersonic wing penetrating a sharp-edged gust by two methods: one based on a surface distribution of sources in the fluid at rest and the other by considerations of conical flow. In the present note it is shown, with the aid of the Laplace transformation, that this lift distribution, as well as that due to a two-dimensional wing undergoing a sudden change in angle of attack, follows directly from the moving source solution given by Garrick and Rubinow.[2] This approach is of particular interest in that the different phases of the time histories of the lift

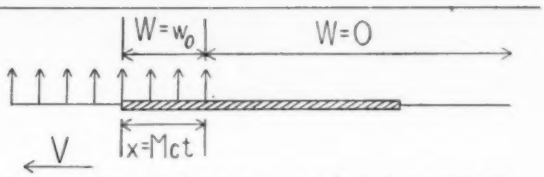

Fig. 1. Shape functions in terms of boundary conditions for sudden change in angle of attack.

distributions automatically present themselves as mathematical limitations in the inversions of the Laplace transformation. Furthermore, more general transient problems follow directly.

Before proceeding with the analysis it may be pointed out that Heaslet and Lomax[3] have used the source distribution method employed by Biot and independently obtained the lift distribution for both gust problems.

Analysis

Consider the velocity potential due to a distribution of moving sources which satisfies the boundary conditions for a thin oscillating wing in supersonic flow referred to a uniformly moving coordinate system as given in[2]

$$\varphi(x, z, t) = -\frac{1}{2\beta\pi} \int_0^x \int_0^{\pi} W(\xi, \theta)w(t)d\theta\, d\xi \tag{1}$$

where $W(\xi, \theta)$ and $w(t) = [W(t - \tau_1) + W(t - \tau_2)]$ are, respectively, spatial and time functions of airfoil shape to be chosen so as to satisfy given boundary conditions. The variables x, z, ξ, θ refer to rectangular coordinates, t is time, τ_1 and τ_2 are time-lag functions associated with the physical mechanism of a moving supersonic source and defined by

$$\tau_1 = \frac{x - \xi}{c\beta^2}(M - \sin\theta), \quad \tau_2 = \frac{x - \xi}{c\beta^2}(M + \sin\theta)$$

M is Mach Number, c is velocity of sound, and $\beta = \sqrt{M^2 - 1}$. Eq. (1) is by no means limited to an oscillating airfoil. In other words, the time function need not be sinusoidal but may be chosen in such forms that Eq. (1) will represent the velocity potential for a two-dimensional wing in other types of time-varying supersonic flow. In particular, the velocity potential for a two-dimensional wing undergoing a sudden change in angle of attack or upon penetrating a sharp edged gust may be readily obtained from this equation:

(1) *Sudden Change in Angle of Attack*—Consider first a wing undergoing a sudden change in angle of attack. The shape function in terms of the boundary conditions for this case may be expressed as follows (see Fig. 1)

$$\left.\begin{aligned} W(\xi, \theta) &= -V\alpha \text{ over the range occupied by the wing} \\ &= 0 \text{ outside the range occupied by the wing} \end{aligned}\right\} \tag{2}$$

where V is the velocity in free stream direction and α is the change in angle of attack.

The corresponding time function $w(t)$ is the unit step function; hence,

$$\left.\begin{aligned} [w(t - \tau_1) + w(t - \tau_2)] &= 0, \quad \text{when} \quad t < \tau_1 \\ &= 1, \quad \text{when} \quad \tau_1 < t < \tau_2 \\ &= 2, \quad \text{when} \quad t > \tau_2 \end{aligned}\right\} \tag{3}$$

The integration with respect to θ in Eq. (1) can be performed with the aid of the Laplace transformation. The Laplace transform of Eq. (3) is

$$\bar{w}(s) = (1/s)(e^{-s\tau_1} + e^{-s\tau_2}) \tag{4}$$

where s denotes the variable or operator in the Laplace transformation. Making use of Eqs. (2), (3), and (4) and the definitions of τ_1 and τ_2, the Laplace transformation of Eq. (1) (considered independent of z) is

$$\varphi(s) = \frac{V\alpha}{\beta\pi}\int_0^x\int_0^\pi e^{-\frac{x-\xi}{c\beta^2}Ms}\cosh\left(s\,\frac{x-\xi}{c\beta^2}\sin\theta\right)d\theta d\xi \quad (5)$$

Making use of the known Bessel function relation

$$(1/\pi)\int_0^\pi \cosh(\lambda\sin\theta)d\theta = I_0(\lambda) \quad (6)$$

the integration with respect to θ yields

$$\bar{\varphi}(s) = \frac{v\alpha}{\beta}\int_0^x e^{-\frac{x-\xi}{c\beta^2}Ms} I_0\left(s\,\frac{x-\xi}{c\beta^2}\right)d\xi \quad (7)$$

For the integration with respect to ξ, it is convenient to revert to the inverse of the transform of Eq. (7), which may be found in tables of Laplace transforms.[4] Reverting to the direct function and performing the integration yields

$$\varphi(x, t) =$$

$$\frac{v\alpha}{\beta\pi}\left[x\cos^{-1}\left(\frac{Mx - C\beta^2t}{x}\right) + c\beta t\left(\pi - \cos^{-1}\frac{x - Mct}{ct}\right)\right] \quad (8)$$

where the inverse trigonometric terms in Eq. (8) must be interpreted to be: 0 when the arguments are ≥ 1, and π when the arguments are ≤ -1.

The expression for the ratio of superstream pressure to dynamic pressure is

$$\frac{\Delta p}{q} = -\frac{4}{V}\left[\frac{1}{V}\frac{\partial\varphi}{\partial t} + \frac{\partial\varphi}{\partial x}\right] \quad (9)$$

from which Eq. (8) gives

$$\frac{\Delta p}{q} = -\frac{4\alpha}{\beta\pi}\left[\cos^{-1}\frac{Mx - C\beta^2t}{x} + \frac{\beta}{M}\left(\pi - \cos^{-1}\frac{x - Mct}{ct}\right)\right] \quad (10)$$

where the interpretations of (or limitations on) the inverse trigonometric terms in Eq. (8) apply. From the considerations of the arguments, three distinct time phases discussed physically in a subsequent paragraph, can be established:

Phase 1.—If

$$(Mx - c\beta^2t)/x \geq 1$$

then

$$(x - Mct)/ct \geq 1$$

and the pressure coefficient reduces to

$$\Delta p/q = -4\alpha/M \quad (11)$$

Phase 2.—If

$$-1 < (Mx - c\beta^2t)/x < 1$$

then

$$-1 < (x - Mct)/ct < 1$$

and the pressure coefficient is given by Eq. (10) directly.

Phase 3.—If

$$(Mx - C\beta^2t)/x \leq -1$$

then

$$(x - Mct)/ct \leq -1$$

and the pressure coefficient reduces to

$$\Delta p/q = -4\alpha/\beta \quad (12)$$

Physically, Phase 1 is bounded by $t = 0$ and $t = x/(V + c)$, the latter value denoting the time required for a point x on the wing to meet an oncoming disturbance originating at the leading edge. Phase 2 is bounded by $t = x/(V + c)$ and $t = x/(V - c)$, the latter value denoting the time required for a point x on the wing to overtake the outgoing disturbance originating at the leading edge. Phase 3 refers to values of $t > x/(V - c)$ and corresponds to the steady Ackeret results.

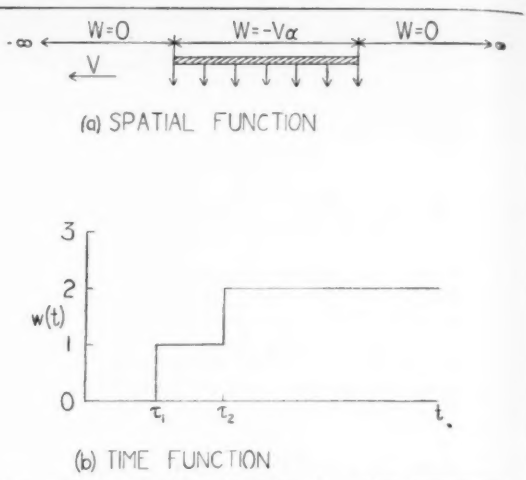

FIG. 2. Spatial shape function for wing-penetrating sharp-edged gust.

TABLE 1

Present note	Biot	Heaslet & Lomax
x	$x + Mct$	$x + Mt$
z	z	z
t	t	t/c

(2) *Wing Penetrating a Sharp Vertical Gust.*—For a wing passing into a sharp vertical gust of vertical velocity w_0, the spatial shape function in terms of the boundary conditions may be written (see Fig. 2)

$$W(\xi, \theta) = w_0, \text{ for the portion of the wing within the gust} \\ = 0, \text{ for the portion of the wing outside the gust} \quad (13)$$

The time function $\omega(t)$ is used as given in Eq. (3). Derivation of the velocity potential follows directly from the preceding discussion. The corresponding pressure coefficient is

$$\frac{\Delta p}{q} = \frac{4w_0}{\pi\beta V}\cos^{-1}\left(\frac{Mx - C\beta^2t}{x}\right) \quad (14)$$

The pressure coefficients in the three time phases previously discussed are:

Phase 1.—The pressure coefficient is zero.

Phase 2.—The pressure coefficient is given by Eq. (14) directly.

Phase 3.—The pressure coefficient reduces to that of the steady state condition for constant vertical motion

$$\Delta p/q = 4w_0/\beta V \quad (15)$$

For convenience to the reader the relations between the coordinates used herein, those used by Biot,[1] and those used by Heaslet and Lomax are given in Table 1.

By direct substitution it is easily shown that all the results are in agreement.

REFERENCES

[1] Biot, M. A., *Loads on a Supersonic Wing Striking a Sharp-Edged Gust*, Journal of the Aeronautical Sciences, Vol. 12, No. 5, p. 296, May, 1949.

[2] Garrick, I. E., and Rubinow, S. I., *Theoretical Study of Air Forces on an Oscillating or Steady Thin Wing in Supersonic Main Stream*, N.A.C.A. T.N. No. 1383, 1947.

[3] Heaslet, M. A., and Lomax, Harvard, *Two-dimensional Unsteady Lift Problems in Supersonic Flight*, N.A.C.A. T.N. No. 1621, 1948.

[4] Campbell, G. A., and Foster, R. M., *Fourier Integrals for Practical Applications*; D. Van Nostrand Co., Inc., 1948.

On Unsteady One-Dimensional Flows with Heat Addition

William Swartz
Department of Mathematics, Massachusetts Institute of Technology, Cambridge, Mass.
May, 1949

AN INTERESTING PAPER of Kahane and Lees[1] treated, by the method of characteristics, the problem of addition of heat to an initially isentropic flow through a tube. They have utilized a form of the characteristic equations containing more than two dependent variables, necessitating approximation other than those involved in taking finite differences. This has been pointed out by Lin,[2] who also derives a simple form of the characteristic equations permitting the numerical integration to proceed in a straightforward manner. At his suggestion, the present writer has derived these same equations in a manner analogous to that of Meyer.[3] For a perfect gas, these equations are

$$ds/dt = q^* \text{ along } dx/dt = u \tag{1}$$

$$\frac{dp}{\gamma p} \mp \frac{du}{a} = \frac{q^*}{\gamma}\,dt \text{ along } \frac{dx}{dt} = u \mp a \tag{2}$$

where s is the entropy divided by the specific heat c_v and q^* is the rate of increase of entropy—i.e., the heat generated per unit mass divided by c_vT. Other symbols are those used by Kahane and Lees.

In view of the additional approximations used by Kahane and Lees, it was deemed interesting to solve the same problem with the simplified method. The relationship between the notations Q^* and K of reference 1 and q^* is

$$q^* = (1/c_vT)\,(dQ^*/dt) = K/c_v \tag{3}$$

It is convenient to work with all quantities in dimensionless form. The value of K employed by Kahane and Lees gives q^* (dimensionless) $= 0.36\gamma$. Dimensionless forms of the variables a, p, and ρ are obtained by dividing by their respective initial values; the velocity is to be divided by a_0, the initial value of a. The distance and time parameters are taken as x/L and a_0t/L, respectively, where L is the length of the section of the tube which is subjected to heating. In terms of dimensionless quantities, the Eqs. (1) and (2) remain unchanged, but the equation of state becomes

$$p = \rho^\gamma e^s \tag{4}$$

and the velocity of sound is

$$a = \sqrt{p/\rho} \tag{5}$$

Since the calculations are exceedingly laborious, it seems worth while to point out that the solution may be explicitly integrated in the region bounded by the x-axis and the Mach lines passing through (0, 0) and (1, 0) (Fig. 2 of reference 1). It can be shown that ρ and u are constants throughout the region, and that the entropy and pressure are given by

$$s = q^*t \tag{6}$$

and

$$p = e^{q^*t} \tag{7}$$

The Mach lines are

$$x = 0.8t \mp (2/q^*)e^{(1/2q^*t)} + \text{const.} \tag{8}$$

and the path lines are the straight lines

$$x = 0.8t + \text{const.} \tag{9}$$

The calculations are also materially shortened by noting that, in the region to the right of $x/L = 1$, the pressure and velocity are constant along each of the family of Mach lines characterized by the plus sign. Likewise, they are constants along each member of the minus family of Mach lines in the area to the left of $x/L = 0$. This is easily shown, remembering that $q^* = 0$ in these regions.

The characteristic and path line diagrams obtained agree well, in general, with those of Kahane and Lees. Several Mach lines of the minus family at the left of the disturbed area were extended until they nearly intersect with the straight Mach line through (0, 0). An estimate of the coordinates of the beginning of the upstream-moving shock wave was thus found to be in the neighborhood of $a_0t/L = 1.2$ (presumably more accurate than Fig. 3 of reference 1, which shows no shock at $a_0t/L = 1.5$). Qualitatively, of course, there is general agreement.

Of interest is the behavior of temperature along the path lines. Using the equation of state and Eq. (5), the absolute temperature in dimensionless form is merely

$$T = a^2$$

The temperature was calculated along three path lines originating at $x/L = 0$, 0.5, and 1. Although the last path line is in a region of no heat addition, a slow steady increase in temperature is found. This is associated with the compression indicated by the density calculations. Along the other path lines, temperature increases at a more rapid rate within the area of heat addition, with a slight drop in temperature upon crossing the boundary $x/L = 1$. This drop of temperature *after* an addition of heat *to a fluid element* is not contradictory to the Second Law of Thermodynamics. It has been mentioned before—e.g., in reference 4. Foa and Rudinger[5] emphasized the change of temperature associated with a *flow field* and raised objections against statements not made by previous authors.

REFERENCES

[1] Kahane, A., and Lees, L., *Unsteady One-Dimensional Flows With Heat Addition or Entropy Gradients*, Journal of the Aeronautical Sciences, Vol. 15, No. 11, pp. 665–670, November, 1948.

[2] To appear in the *Quarterly of Applied Mathematics*.

[3] Meyer, R. E., *The Method of Characteristics for Problems of Compressible Flow Involving Two Independent Variables*, Quarterly Journal of Mechanics and App. Math., Vol. I, Part 2, pp. 196–219, June, 1948.

[4] Chambré, P., and Lin, C. C., *On the Steady Flow of a Gas Through a Tube With Heat Exchange or Chemical Reaction*, Journal of the Aeronautical Sciences, Vol. 13, No. 10, pp. 537–542, October, 1946.

[5] Foa, J. V., and Rudinger, G., *On the Addition of Heat to a Gas Flowing in a Pipe at Subsonic Speeds*, Journal of the Aeronautical Sciences, Vol. 16, No. 2, pp. 84–94, February, 1949.

The Problem of Stringer Roll

Paul E. Sandorff
Group Engineer, Research, Lockheed Aircraft Corporation, Burbank, Calif.
May 23, 1949

WITH REGARD TO THE PROBLEM OF stringer roll treated by G. C. Best in his paper in the May, 1949, issue of the JOURNAL (Vol. 16, No. 5, p. 289), the writer wishes to direct attention to the article "Bending Rigidity and Column Strength of Thin Sections," *A.S.M.E. Transactions*, November, 1947.

The reader will find there a ready-to-use method for treating rolling tendencies of unsymmetrical flanges, together with substantiating test data and charts that facilitate solution. The mathematics begin from the same basis as that used by Mr. Best, but they are developed to show that flanges act with an efficiency determined only by geometrical considerations. Revised or effective section properties may therefore be computed which indicate directly the behavior of the structure under column or bending load.

It is believed that the stress analyst will find this approach better suited to his purposes, though Mr. Best's treatment does make available certain information otherwise not obtainable.

Note on Life Expectancy Analysis of Structures

George Gerard
Guggenheim School of Aeronautics, New York University, New York, N. Y.
June 17, 1949

THE CUMULATIVE DAMAGE CONCEPT [1] has received rather wide attention because it provides a simple method of analysis in which the effects of loading at various stress levels can be accounted for. Experimental evidence as to the validity of the cumulative damage concept, however, is somewhat contradictory. Fatigue test data obtained by loading at only two stress levels indicate that metals may be appreciably damaged by overstressing and strengthened by understressing. On the other hand, experiments by Miner[1] at a number of stress levels offer data in support of the cumulative damage concept.

It is to be noted that relatively little attention has been given to the frequency distribution of loads imposed on an airplane in considering the validity of the cumulative damage concept. It was found that, by considering both the loading spectrum and the fatigue properties of the material, the distribution of damage increments was of the nature of a probability curve. Hence, it is proposed that the validity of the cumulative damage concept may be established for life-expectancy analyses by using a similar loading spectrum in laboratory tests.

Life-Expectancy Analysis

For particular airplane characteristics, the loading spectrum usually specified in the form of load relative frequency as a function of load factor can be assumed to be a load relative frequency-stress level relationship for the structure. The fatigue property spectrum may also be represented as a single curve when drawn for a mean stress corresponding to the pertinent load factor. Methods for constructing such curves are presented in reference 2.

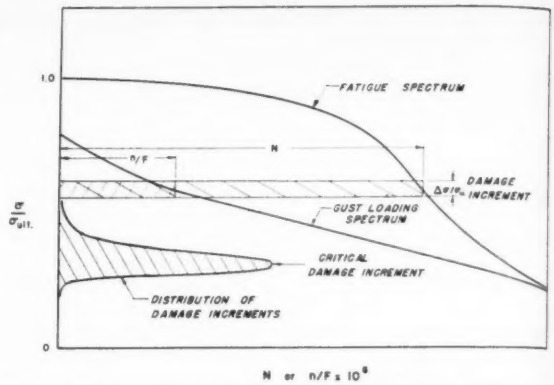

FIG. 1. Life expectancy analysis using cumulative damage concept.

The analysis of life-expectancy proceeds from the loading and fatigue property spectra. The criterion for fatigue life according to the cumulative damage concept[1] is

$$\Sigma n/N = 1.0 \tag{1}$$

In the analysis, the loading spectrum is given in terms of relative frequency and contains the fatigue life, F, as a factor. Hence, from Fig. 2, the per cent of fatigue life used at various stress levels contains the F term which when summated has the following form

$$(1/F)\,\Sigma\,(n/N) = \delta \tag{2}$$

In general, $\delta \neq 1.0$, as required by the cumulative damage concept and, hence, by adjusting the value of F, the condition imposed by Eq. (1) can be satisfied. Thus, the fatigue life, F, in number of repeated loads encountered is obtained as

$$F = 1/\delta \tag{3}$$

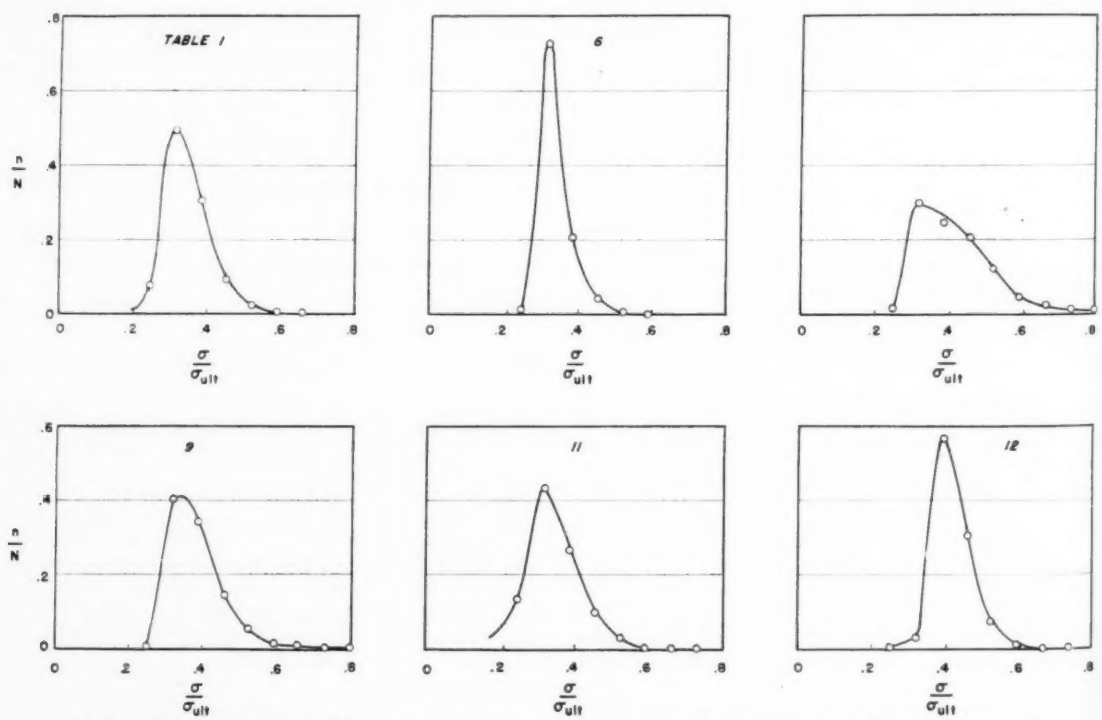

FIG. 2. Distribution of damage increments for analysis of reference 2. Table numbers are those of reference 2.

Damage Increment Distribution

From fatigue analyses that utilize the cumulative damage concept, the increments of damage, n/N, which are attributed to each stress level, can be plotted to obtain a damage curve such as shown in Fig. 1. Damage curves plotted from the gust analyses conducted on an hypothetical airplane in reference 2 are shown in Figs. 2. Analyses on several other airplanes indicated curves of a similar nature and, consequently, those shown in Figs. 2 may possibly be representative of this type of analysis.

It is significant to note that the curves all peak sharply, indicating that the fatigue life is strongly influenced by a particular stress increment referred to herein as the "critical damage increment." In fact, analysis of the data used to construct Figs. 2 indicated that, in all cases analyzed except one, over 70 per cent of the fatigue life could be attributed to the two increments at the peak of the distribution curve. This trend remains to be established for many more cases, but, if it is correct, it indicates that almost all damage can be attributed to a rather narrow band of stress, the critical damage increment. This trend approaches the type of fatigue analysis in which only one stress level is assumed responsible for fatigue failure.

Of greater significance than the critical damage increment is the fact that the distribution of damage increments closely approaches a class of curves known as probability curves. A distribution of this nature tends to minimize the effects of damaging and strengthening at high and low stress levels, respectively, since the various stresses are disposed about the critical damage increment and of a low magnitude relative to the critical increment.

It appears that, because of the probability distribution of the damage increments, laboratory tests should be run using a loading spectrum of this nature. Tests run in this manner may establish the validity of the cumulative damage concept for the particular type of life-expectancy analysis discussed herein, although it is probable that its validity cannot be established in general.

References

[1] Miner, M. A. *Cumulative Damage in Fatigue*, Journal of Applied Mechanics, Vol. 67, No. 9, pp. A-159–A-164, September, 1945.

[2] Jackson, L. R., and Grover, H. J., *The Application of Data on Strength Under Repeated Stresses to the Design of Aircraft*, N.A.C.A. A.R.R 5H27 (Wartime Report W-91), October, 1945.

End-Fixity of Columns

George Winter
Professor and Head, Department of Structural Engineering, Cornell University, Ithaca, N.Y.
May 13, 1949

In their papers on end-fixity of columns in the February, 1949, Journal of the Aeronautical Sciences (Vol. 16, No. 12, pp. 116, 117–119), N. M. Newmark and G. C. Best have given attractive approximate formulas for determining the effective length coefficient of columns with known rotational end restraints.

It may be of interest, in this connection, to note that simple charts for the determination of this same quantity were published in the following: "Elastically Encastred Struts," by N. J. Hoff (*J. Royal Aero. Soc.*, Vol. 40, p. 663, November, 1936), and "Buckling of Trusses and Rigid Frames," by George Winter, P. T. Hsu, B. Koo, and M. H. Loh, (*Bulletin No. 36*, Cornell University Eng. Exp. Station, April, 1948). These charts allow the determination of c directly on the basis of the rotational spring constants at both ends—i.e., Dr. Newmark's k_1 and k_2 or Mr. Best's K_1 and K_2—without the necessity of first computing from them auxiliary quantities, such as in Mr. Best's method. Ways of accounting for the influence on these spring constants of axial forces acting in the restraining members are simplified by additional charts in the second of the above publications. The main chart of that paper for determining c accounts not only for positive but also for negative restraints. The latter feature is important because a complete stability analysis of a framework is frequently impossible without accounting for negative restraints of which Mr. Best notes that "they are not considered to actually occur."

Indeed, in the simplest truss, consisting of two compression members rigidly joined at their intersection and for simplicity's sake hinged at their other ends to the third, tension member negative restraint does occur for the compression bar with the smaller L/r at the end joined to the one with larger slenderness if axial forces are equal in both of them. In other words, the more slender bar, tending to buckle, induces an end moment into the more rigid bar rather than to provide a restraining moment.

The importance of this factor is brought out in Mr. Best's papers, in which is shown the application of these charts to an exact solution, by successive approximation, of the stability of a rigid framework composed of any number of bars.

Errata—The Rolling and Yawing Moments Due to Yaw of Unswept Wings

R. F. Anderson
Northrop Aircraft, Inc., Hawthorne, Calif.
July 14, 1949

Two errors appeared in my Readers' Forum item on pages 445–447 of the July issue of the Journal of the Aeronautical Sciences:

(1) Page 447, first paragraph after Eq. (5). The last sentence of this paragraph should read: "Values of m were obtained from reference 4 using $m_0 = 2\pi$."

(2) Page 447, third paragraph after Eq. (5), fourth and fifth lines. The corrected sentence should read: "For example, the relation $\partial C_{n_\psi}/\partial C_L{}^2 = -0.125/A$ could be used."

Stability of Sandwich Plates

P. P. Bijlaard
Professor, Institute of Technology, Delft, Holland, on leave; Associate Professor, Cornell University, Ithaca, N.Y.
June 15, 1949

In an interesting paper, Seide[1] calculated the compressive, buckling stress of sandwich plates with clamped unloaded edges, assuming the faces to act as membranes. His computations may be used as a check on a method the present writer developed some time ago.[2, 3] In order to do this the thickness of the faces has to be taken into account in Seide's calculations too, since, apart from disregarding the flexural rigidity of the faces, its neglect underestimates the shearing rigidity of the core. With a thickness ratio $t_f/h_c = 1/20$ of faces and core, it already results in a 9 per cent smaller shearing rigidity.

The thickness of the faces may be taken into account by inserting other values for the shearing stiffnesses D_{Qx} and D_{Qy} in Eqs. (6) of reference 4. As was derived in references 2 and 3, thinking all other deformations to be zero and considering the faces to have no flexural rigidity, as in reference 4, but having their

actual thickness, with the notations of reference 1 the shearing force per unit width is

$$Q_x = G_c[(h_c + t_f)^2/h_c](\partial w/\partial x) \tag{1}$$

so that

$$D_{Q_x} = \frac{Q_x}{\partial w/\partial x} = G_c \frac{(h_c + t_f)^2}{h_c} = D_{Q_y} \tag{2}$$

This leads for example in the elastic range to the differential equation

$$\nabla^4 w + \left(1 - \frac{h_c}{(h_c + t_f)^2} \frac{D}{G_c} \nabla^2\right) \frac{2t_f\sigma_{cr}'}{D} \frac{\partial^2 w}{\partial x^2} = 0 \tag{3}$$

instead of Eq. (A5) of reference 5. In these formulas, G_c is the shear modulus of the core material and D and σ_{cr}' are the flexural stiffness and buckling stress of the sandwich plate, both under the assumption of zero flexural rigidity of the faces. In the plastic range, the more exact differential equations are also obtained by replacing value h_c by $(h_c + t_f)^2/h_c$.

The total critical thrust $2t_f\sigma_{cr}$ is equal to the sum of the thrust $2t_f\sigma_{cr}'$ from Eq. (3) and that of the single faces, $2t_f\sigma_0$, calculated for the same wave length, analogous to what was done in references 2 and 3, and has to be minimized.

In references 2 and 3, the present writer proved that the critical load for a sandwich plate may be written as follows:

$$P_{cr} = P_0 + (P_m^{-1} + P_s^{-1})^{-1} \tag{4}$$

in which P_0 is the joint critical load for the single faces; P_m is the critical load for the sandwich plate, if G_c with respect to the shearing stresses τ_{xz} and τ_{yz} is assumed to be infinite, and P_s is obtained by assuming only G_c to have a finite value. In calculating P_m and P_s, the proper flexural rigidity of the faces is neglected. All loads are calculated for the same wave length, which has to be chosen such as to make P_{cr} a minimum.

This method can be considered as exact if the deflection surfaces applying for the computation of P_0, P_m, and P_s are identical, as for example for cylindrical buckling of a simply supported sandwich plate under end thrust and for buckling of a rectangular sandwich plate with simply supported edges, subjected to compression in both directions.[2, 3] If the deflection surfaces have not the same form, the method yields conservative results, because in reality they have to coincide everywhere, giving an excess restraint and so increasing P_{cr}. The latter case obtains for the case considered by Seide in reference 1, so that, taking into account the changes proposed above here, Seide's paper provides a possibility to check how much the present writer's method is conservative here. Even for this case, where the deflection surfaces for computing P_m and P_s differ greatly,[3] it proves to be only conservative by, at most, 4 per cent. Thus it may be advised to use it also in other cases, since the calculations involved are much less than those based on the differential equations of the plate as a whole.

With the notations of reference 1 the method gives an example for a rectangular plate under pure compression or pure shear

$$(P_{cr} \text{ or } S_{cr}) = \eta k_0 \pi^2 D_e/b^2 \tag{5}$$

in which η is the reduction coefficient for plasticity of the faces, k_0 is the elastic buckling stress coefficient for a plate with infinite shearing rigidity as far as stresses τ_{xz} and τ_{yz} are concerned, and b is the plate width. In Eq. (5),

$$D_e = (D_f/D_t + \varphi)D_t \tag{6}$$

in which

$$\left.\begin{aligned} D_t &= E_f t_f (h_c + t_f)^2/2(1 - \mu_f^2) \\ D_f &= E_f t_f^3/6(1 - \mu_f^2) \\ \varphi &= \alpha/(\alpha + \eta r k_0) \\ r &= (\pi^2 D_t/b^2 G_c)/[h_c/(h_c + t_f)^2] \end{aligned}\right\} \tag{7}$$

while E_f and μ_f are Young's modulus and Poisson's ratio for the faces. For loading by pure compression and with simply supported or clamped edges

$$\alpha = 1 + (\beta^2/m^2) \tag{8}$$

in which β is the plate aspect ratio a/b and m is the number of half wave lengths in the direction of loading. For pure shear in a long plate with simply supported or clamped edges

$$\alpha = [1 + (L^2/b^2)]^{1/2} \tag{9}$$

in which L is the half wave length in the long direction. The expression $(D_f/D_t + \varphi)$ in Eq. (6) has to be minimized by variation of the wave length.

References

[1] Seide, P., *Compressive Buckling of Flat Rectangular Metalite Type Sandwich Plates with Simply Supported Loaded Edges and Clamped Unloaded Edges*, N.A.C.A. T.N. No. 1886, May, 1949.

[2] Bijlaard, P. P., *On the elastic stability of thin plates, supported by a continuous medium*, Proc. Ned. Akad. v. Wet., Vol. 49, No. 10, 1946.

[3] Bijlaard, P. P., *On the elastic stability of sandwich plates I–II*, Proc. Kon. Ned. Akad. v. Wet., Vol. 50, Nos. 1 and 2, 1947.

[4] Libove, C., and Batdorf, S. B., *A General Small Deflection Theory for Flat Sandwich Plates*, N.A.C.A. T.N. No. 1526, April, 1948.

[5] Seide, P., and Stowell, E. Z., *Elastic and Plastic Buckling of Simply Supported Metalite Type Sandwich Plate in Compression*, N.A.C.A. T.N. No. 1822, February, 1949.

On Damping in Pitch for Delta Wings

John W. Miles

Department of Engineering, University of California at Los Angeles

May 24, 1949

ROBINSON HAS RECENTLY CALCULATED the damping in pitch for thin triangular wings on the assumption of an equivalent steady flow over a parabolically cambered wing.[1] Using his results, we have obtained a quasi-stationary solution including all first order terms (in frequency). This solution is based on the following relation: If Φ is a linear operator for a given supersonic plan form which gives the potential (Φ) at the wing due to the downwash (w) there [viz. $\Phi(x, y) = \Phi\{w(x, y)\}$], on the assumption of linearized steady flow, the quasi-stationary solution is given by[2]

$$\Phi(x, y, t) = \Phi\{wcx, y, t\} - \sec^2\theta[\partial/\partial(Ut)][x\Phi\{w(x, y, t)\} - \Phi\{xw(x, y, t)\}] + 0[(\omega b/U)^2] \tag{1}$$

where U is the free-stream velocity, directed along the positive x axis; θ is the Mach angle; and ω is the angular frequency. (This result may require modification in those configurations where a Kutta condition must be invoked.)

If we consider a pitching oscillation of a delta wing about the centroidal axis [$x = (2/3)c$, where c is the maximum chord], the downwash distribution is given by

$$w(x, y, t) = U\alpha\left[1 + \left(\frac{i\omega c}{2U}\right)\left(x - \frac{2}{3}\right)\right] \exp(i\omega t) \tag{2}$$

where we choose the average chord $(c/2)$ as our characteristic length. The lift and moment [about $x = (2/3)c$] coefficients due to this distribution are found to be

$$C_{L_\alpha} = \left[\left(\frac{\rho U^2}{2}\right)S\right]^{-1} \frac{\partial L}{\partial \alpha} = m, \quad \sigma \geq 1 \tag{3a}$$

$$= mf_0, \quad \sigma \leq 1 \tag{3b}$$

$$= 2\pi \tan\gamma + 0(\sigma^3), \quad \sigma \ll 1 \tag{3c}$$

$$C_{L_{\dot\alpha}} = \left[\left(\frac{\sigma U^2}{2}\right)S\right]^{-1} \frac{\partial L}{\partial\left(\frac{i\omega c\alpha}{2U}\right)} = -\frac{2}{3} m \tan^2\theta, \quad \sigma \geq 1 \tag{4a}$$

$$= -\frac{2}{3} m[(3f_0 - 2f_1)\tan^2\theta - 4(f_1 - f_0)], \quad \sigma \leq 1 \tag{4b}$$

$$C_{L_\alpha} = \frac{8\pi}{3}\tan\gamma + 0(\sigma^2\log\sigma), \quad \sigma \ll 1 \tag{4c}$$

$$C_{M_\alpha} = 0 \tag{5}$$

$$C_{M_{\dot\alpha}} = \left[\left(\frac{\sigma U^2}{2}\right)S\frac{c}{2}\right]^{-1}\frac{\partial M}{\partial\left(\frac{i\omega c\alpha}{2U}\right)} = -\frac{m}{9}(2-\tan^2\theta), \quad \sigma \geq 1 \tag{6a}$$

$$= -\frac{m}{9}[2(2f_1 - f_0) - (3f_0 - 2f_1)\tan^2\theta], \quad \sigma \leq 1 \tag{6b}$$

$$= -\frac{8\pi}{9}\tan\gamma + 0(\sigma^2\log\sigma), \quad \sigma \ll 1 \tag{6c}$$

$$m = 4\tan\theta \tag{7}$$

$$f_0 = f_0(\sigma) = \frac{(\pi/2)\sigma}{E'(\sigma)} \tag{8}$$

$$f_1 = f_1(\sigma) = \frac{(3\pi/4)\sigma(1-\sigma^2)}{(1-2\sigma^2)E'(\sigma) + \sigma^2K'(\sigma)} \tag{9}$$

$$\sigma = (\tan\gamma/\tan\theta) \tag{10}$$

where 2γ is the apex angle, m is the two-dimensional lift curve slope, and K' and E' are the *complementary* complete elliptic integrals of the first and second kind, respectively. The cases $\sigma \geq 1$, $\sigma \leq 1$, and $\sigma \ll 1$ correspond to the cases where the leading edges are outside, inside, and close to the axis of the Mach cone, respectively.

If the axis of rotation is at $x = ac/2$, we have

$$C_{L_{\dot\alpha}}(a) = C_{L_{\dot\alpha}}(4/3) - [a - (4/3)]C_{L_\alpha} \tag{11}$$

$$C_{M_{\dot\alpha}}(a) = C_{M_{\dot\alpha}}(4/3) + [a - (4/3)]C_{L_{\dot\alpha}}(4/3) - [a - (4/3)]C_{L_\alpha} \tag{12}$$

Upon examination, we find that below a certain critical Mach Number $C_{M_{\dot\alpha}}$ will be positive (i.e., "negative" damping) for axes located between two points lying fore and aft of mid-chord ($a = 1$). At the Mach Number specified by

$$\tan\theta = 1, \quad M = \sqrt{2}, \quad \sigma \geq 1 \tag{13a}$$

$$\tan\theta = \left(\frac{4f_1 - 3f_0}{3f_0 - 2f_1}\right)^{1/2}, \quad M = \left(\frac{2f_1}{4f_1 - 3f_0}\right)^{1/2}, \quad \sigma \leq 1 \tag{13b}$$

these two points coincide at $a = 1$, and for greater Mach Numbers, $C_{M_{\dot\alpha}}$ remains negative. The maximum value of this critical Mach Number is $\sqrt{2}(\sigma \geq 1)$. We also find that $C_{M_{\dot\alpha}}$ is negative for all axes aft of $a = 3/2$, regardless of apex angle.

In the limiting case of the extremely slender wing, ($\sigma \ll 1$), we find

$$C_{M_{\dot\alpha}}(a) = -2\pi(2-a)^2\tan\gamma + 0(\sigma^2\log\sigma) \tag{14}$$

so that we have the rather interesting anomaly that the damping vanishes for rotation of an extremely slender delta about the base. We remark that this same situation holds for any slender body.

The functions f_1 and f_0 are given by the curves $mg[\partial C_L/\partial(\bar{c}q/V)]$ and $(\partial C_L/\partial\alpha)$, respectively, in Fig. 5 of Robinson's paper,[1] where λ represents σ.

References

[1] Robinson, A., *Rotary Derivatives of a Flat Delta Wing at Supersonic Speeds*, J. Roy. Aero. Soc., Vol. 52, pp. 735–752, November, 1948.

[2] Miles, J. W., *On Harmonic Motion at Supersonic Speeds*, Journal of the Aeronautical Sciences, Vol. 16, No. 6, pp. 378–379, June, 1949.

Changes of Address

Since the Post Office Department does not as a rule forward magazines to forwarding addresses it is important that the Institute be notified of changes in address 30 days in advance of publishing date to ensure receipt of every issue of the JOURNAL and REVIEW.

Notices should be sent directly to:

Institute of the Aeronautical Sciences, Inc.
2 East 64th Street, New York 21, New York

SUGGESTIONS *for* CONTRIBUTORS

to the Publications of the

INSTITUTE *of the* AERONAUTICAL SCIENCES

The Institute of the Aeronautical Sciences invites both members and nonmembers from any country to submit papers for publication in the JOURNAL OF THE AERONAUTICAL SCIENCES and the AERONAUTICAL ENGINEERING REVIEW. The Institute, following the practice of other societies, does not pay for contributions.

The following directions for the preparation of papers, if followed by authors, will save correspondence, avoid the return of papers for changes, minimize the work of preparation for the printer, and save the expense due to the charges made for "author's corrections."

MANUSCRIPTS: The original typewritten copy of the paper desired, double or triple spaced on one side of white paper sheets, consecutively numbered. There should be wide margins to allow for the marking of directions to the printer. Correcting, changing, or adding to papers after they are in type is costly. It is, therefore, imperative that papers submitted be in final form. Typographical errors may be corrected on proofs, but if authors wish to add material, they may do so at their own expense. In mailing, drawings may be rolled, but manuscripts should be sent flat. Send by first class mail (register, if you wish, for your own protection) to the Editorial Office, Institute of the Aeronautical Sciences, 2 East 64th Street, New York 21, N.Y. All manuscripts will be examined by the Editorial Committee and by the Editor. Authors will be advised as promptly as possible whether the paper is acceptable for publication.

TITLES: The title of the paper should be brief. The name and initials of the author should be written as he prefers. The use of the full name of an author is advocated because of the frequent duplication of initials and surnames which sometimes makes it difficult to establish the identity of the author. This is particularly important for large annual indexing and abstracting services. All titles and degrees or honors are omitted. The name of the organization with which the author is associated should be placed after his name on a separate line. The date on which the paper is received will be inserted by the Editor. The author's title should be indicated in a footnote.

SUMMARIES OR ABSTRACTS: An abstract to be printed at the beginning should accompany each article. It should be adequate as an *index* and as a *summary*. It should contain a statement of major conclusions reached, since summaries in many cases constitute the only source of information used in compiling scientific reference indexes. Abstracts printed in other journals, especially foreign, in most cases, consist of summaries from printed papers. The summary should explain as adequately as possible the major conclusions to a nonspecialist in the subject and should contain from 100 to 300 words, depending on the length of the paper.

SUBHEADINGS: Subheadings should be inserted by the author at frequent intervals. The work of editorial preparation will be simplified by the author providing many subheadings.

MATTER USUALLY DELETED: Photographs or illustrations of little technical interest and not showing advances in general practice. Too detailed tabular matter (general results of such tables may be included in the text). Lengthy descriptions of materials or processes or of preliminary experiments or theories that preceded final results; salient features only are of interest.

REFERENCES AND FOOTNOTES: References should appear as footnotes only, numbered consecutively, grouped together at the end of the manuscript. The arrangement should be as follows: (for books)—[1] Durand, W. F., *Aerodynamic Theory*, 1st Ed., Vol. 1, p. 23; Julius Springer, Berlin, 1934. (For magazines)—[1] Englund, C. R., Crawford, A. B., and Mumford, W. W. *Some Results of a Study of Ultra-Short-Wave Transmission Phenomenon*, Proc. I. R. E., Vol. 20, No. 12, pp. 481 and 482, March, 1933. Please give author, title, edition, volume, page, publisher, and date of publication as indicated. Omission of one required fact causes much extra editorial work and possible inaccuracies.

ILLUSTRATIONS: Illustrations should accompany manuscripts and each should always be referred to in the text, by number. Drawings or graphs should not be larger than 12 × 16 inches, and must be made with jet black India Ink on white paper or tracing cloth, the latter being preferred. *Do not use typewriter for lettering.* The smallest lettering on 8 × 10 inch figures should be no less than 1/4 inch high. Cross-section paper (white with black lines) may be used, but should not have more than 4 lines per inch. If finer ruled paper is used, the major division lines should be drawn in with black ink, omitting the finer divisions. In the case of finely ruled paper, only blue-lined paper can be accepted. *Tracing paper and blueprints* are not acceptable. Lettering and all markings must be large enough to be readable after reduction. Mail rolled or flat, never fold. Drawings that cannot be reproduced (including pencil drawings) will be returned to the author for redrawing, thus delaying publication of the paper. Photographs should be distinct and show clear black and white contrasts. They must be on glossy white paper. Avoid round and oval photographs.

CAPTIONS AND LEGENDS: Legends or captions must accompany each drawing or photograph submitted. If written on the drawing or photograph, they should be placed below and well outside the part to be reproduced. Each table should have a caption such as Table 1, Table 2, Table 3, etc. Captions should be complete in themselves so as to make the data intelligible to the reader without reference to the text. A duplicate list of captions for figures should be included as the last page of the manuscript. Use "Fig. 1" (not Figure 1), Figs. 3 and 4, etc., in both the text and the numbering of illustrations. In the text, "Eq. (1)," or "Eqs. (1) and (2)" are preferable to "Equation (1)." In captions and legends, except for "Fig." and "Eq.," and in table headings, write all words in full; do not abbreviate.

MATHEMATICAL WORK: Only the simplest formulas should be typewritten, all others should be carefully written in pen and ink, the writing to be large enough so that ample room is provided to mark mathematical matter for the printer. A considerable space for marking should be allowed above and below all equations. All complicated equations should be repeated on separate sheets with plenty of space left for marking. The solidus should be used for simple fractions appearing within the text. Make all expressions clear to the typesetter. Greek letters used in formulas should be clearly designated by name on the margin of the manuscript. All symbols should be clearly written and carefully checked. The difference between capital and lowercase letters should be clearly distinguished and care taken to avoid confusion between zero (0) and the letter (o), between the numeral (one) and the letter (ell) and the prime (′), between alpha and a, kappa and k, u and mu, v and nu, n and eta. All subscripts and exponents should be clearly marked and dots and bars over letters or mathematical expressions should be avoided. Avoid complicated exponents and subscripts. When it is necessary to repeat a complicated expression, it should be represented by some convenient symbol.

NOMENCLATURE AND ABBREVIATIONS: Standard abbreviations should be used, and it should be noted that most abbreviations are lower case such as m.p.h., b.m.e.p., i.hp., b.hp., hp., . . . etc.